2021

Petrogenesis and tectonic implications of cordierite-orthoamphibole gneisses (COG) in the NW Wyoming Province

Brianna K. Crenshaw ms
University of Montana

PETROGENESIS AND TECTONIC IMPLICATIONS OF CORDIERITE-

ORTHOAMPHIBOLE GNEISSES (COG) IN THE NW WYOMING PROVINCE

By

BRIANNA KATHLEEN CRENSHAW

B.S. Geology & Geophysics, Louisiana State University, Baton Rouge, LA, 2018

Thesis

presented in partial fulfillment of the requirements
for the degree of

Master of Science
in Geoscience

The University of Montana
Missoula, MT

May 2021

Approved by:

Scott Whittenburg,
Graduate School Dean

Julia Baldwin, Committee Chair
Geosciences

Rebecca Bendick, Committee Co-Chair
Geosciences

Christopher Palmer, Committee Co-Chair
Chemistry

Crenshaw, Brianna, M.S., May 2021   *Geosciences*

Petrogenesis and tectonic implications of cordierite-orthoamphibole gneisses (COG) in the NW Wyoming Province

Chairperson: Julia Baldwin

Studying cordierite orthoamphibole gneisses (COG) from five different mountain ranges across the Montana Metasedimentary Terrane (MMT) of the Wyoming Province offers a unique opportunity to elucidate the enigmatic origins and petrogenesis of the lithology in addition to gaining a further understanding of Precambrian crustal assembly processes. Geochemical analyses suggest that COG originates from a basalt that underwent metasomatic alteration, likely via seawater, prior to metamorphism. Moreover, COG is considered to represent oceanic crust that was part of the epicontinental sea adjacent to the Wyoming Province before collision with the Medicine Hat Block. Field observations of associated lithologies such as marbles, quartzites, and amphibolites provide context for the interpretation of the geologic environment which coincides with the proposed petrogenetic model. Petrography and phase equilibria models show that COG retains a robust geologic record that includes ocean basin closure prior to collision, the tectonics of the Big Sky Orogeny (ca. 1.78-1.72 Ga), and the regional tectonic unroofing and orogenic collapse that followed. Phase equilibria models from across the MMT depict an overall trend of thermotectonic conditions in the Big Sky Orogeny being the highest in the Tobacco Root Mountains and decreasing in grade as you increase in proximity to Giletti's Line. However, the Highland Mountains are considered the exception to this trend, as they are interpreted to be island arc terrane that was accreted onto the margin of the Province during basin closure.

TABLE OF CONTENTS

List of figures

List of tables

Acknowledgments

1. Introduction

The dynamic processes involved in the assembly and stabilization of cratons have long been enigmatic and poorly understood. Laurentia is an amalgamation of terranes that is considered to be the geologic core of North America. It was formed through a series of micro-continental collisions from 2.0-1.8 Ga, and as such preserves one of the most extensive records of crustal assembly processes. Studying the Archean rocks of the middle-lower crust of Laurentia thus serves as a paragon to gain insight into the processes of crustal assembly. The Wyoming Province in southwest Montana is considered a key natural laboratory to study these interactions.

Of particular interest, is the Montana Metasedimentary Terrane (MMT) which lies at the northwest margin of the Wyoming Province. It is an area of exposed cratonic margin material distinguished by the presence of metasupracrustal sequences intercalated with metavolcanics and quartzofeldspathic gneisses (Mogk et al., 1992). The rocks here record two major metamorphic events. Isotopic dating has identified an older event at ~2.45 Ga, which is poorly defined and enigmatic, primarily due to complete to near-complete overprinting by a subsequent metamorphic event, which is believed to have occurred from 1.78-1.72 Ga (Harms et al., 2004). This younger event has been termed the Big Sky Orogeny. Evidence for the Big Sky Orogeny indicates extensive reworking took place at amphibolite to granulite facies conditions that was followed by regional tectonic unroofing during cooling. The timing of the Big Sky Orogeny is notable, as it is occurs synchronously with other periods of active tectonism recorded along other margins of the Wyoming Province, including within the Trans-Hudson Orogeny along the eastern side of the Province and the Cheyenne belt to the south (Mueller et al., 2005). The remarkable synchronicity of these events raises profound but unanswered questions about the

1

processes by which the Wyoming Province was assembled relative to the rest of the ancestral North American craton. Furthermore, unraveling the thermotectonic history documented here provides a key opportunity to gain a better understanding of continental crustal amalgamation and Precambrian orogenesis.

This study focuses on a distinctive mafic lithology that occurs throughout the MMT that is hypothesized to preserve a record of ocean basin closure between the Wyoming Province and Medicine Hat Block. Garnet-bearing cordierite orthoamphibole gneisses (COG) occur in the MMT as lenses and boudinaged layers within metasedimentary rocks such as marbles, quartzites, and metapelites. These rocks contain intricate and complex reaction textures, including symplectites and coronas involving cordierite, spinel, sapphirine, staurolite, and kyanite (Cheney et al., 2004; Goodsmith, 2015; Hamelin, 2015). These metamorphic rocks, which also contain the orthoamphibole minerals gedrite and anthophyllite co-existing with cordierite, reflect a Ca-poor and Mg- and Al-rich bulk composition. Various genetic models have been proposed for this unusual bulk composition, which include partial melting of a residuum of a metapelite or metavolcanic that experienced melt loss in a prior metamorphic event (Grant, 1968; Beeson, 1978; Hoffer and Grant, 1980), metamorphism of a paleosol horizon (Gable et al., 1970; Young, 1973; Reinhardt and Cook, 1987), or metamorphism of a hydrothermally-altered basalt (Vallance, 1967; Schumacher, 1988; Smith et al., 1992; Peck and Smith, 2005; Hinchey and Carr, 2007). This study hypothesizes that the COG gneisses of the MMT represent a hydrothermally-altered basaltic protolith that may preserve a record of accretion of oceanic crust during the Paleoproterozoic.

The primary objectives of this project are to combine field observations, petrography, geochemical analysis, and Pressure-Temperature (P-T) thermodynamic modeling to identify the

protolith of COG and to extrapolate a comprehensive geologic history that yields insight into the crustal dynamics recorded along this cratonic margin. The results of this study will result in a better understanding of how metamorphic conditions vary across the ranges of the MMT and allow for subsequent implications to be made about the spatial dynamics of the Big Sky Orogeny. By extension, this project will ultimately improve our understanding of the processes involved in continental assembly and the long-term stability of cratons.

2. Geologic Setting

2.1 Regional Geology

The Wyoming Province is a thick (15-20 km), geologically distinct unit of Archean rocks that exists underneath portions of Montana, Wyoming, and southern Canada (Figure 1). It is one of seven cratons that are considered to comprise Laurentia, alongside the Hearne, Rae, Slave, Nain, Superior, and Burwell Provinces (Hoffman, 1988; Mueller and Frost, 2006).

Detrital zircon ages from the Beartooth Mountains, Tobacco Root Mountains, and the Ruby Range (Figure 1) suggest the Wyoming Province formed between 3.4 and 3.2 Ga during a period of significant crustal growth (Mueller et al., 1998). This was followed by continental arc magmatism and terrane accretion which was then followed by a second period of crustal growth from 2.68-2.50 Ga (Mueller et al., 1998; Mueller and Frost, 2006)

Collisional orogenesis is known to have occurred along each of the margins of the craton during the Proterozoic, which produced the three boundaries that now serve to define the aerial extent of the province. These boundaries are the Black Hills orogen to the east, the Cheyenne Belt to the south, and the Great Falls Tectonic Zone to the northwest (Figure 1) (Harms et al., 2004; Mueller et al., 2005; Mueller and Frost, 2006). The Black Hills orogen represents the

3
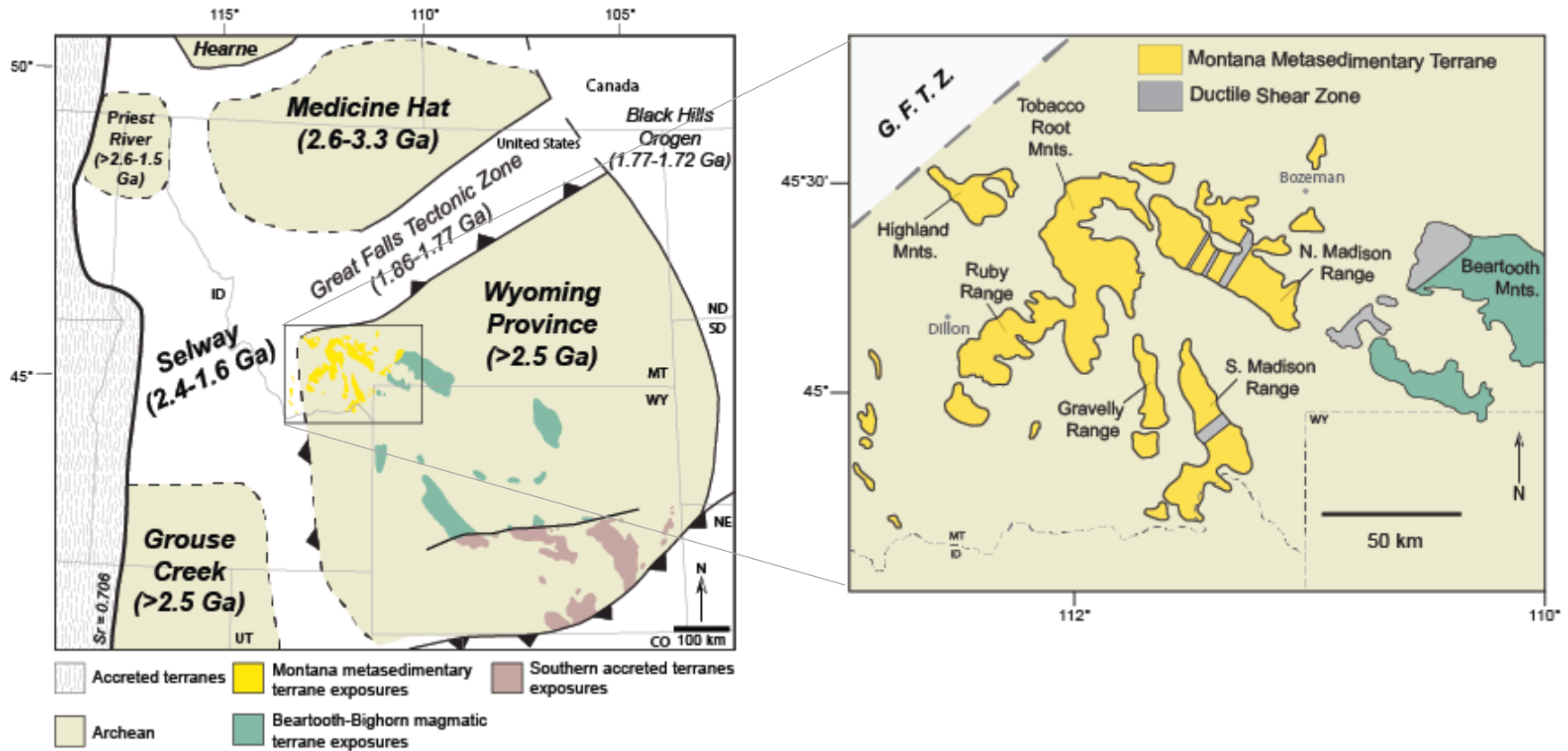
Figure 1. Overview map (left), after Foster et al., 2006, showing the Wyoming Province and nearby cratons. This study focuses on one of the three metamorphic terranes within the Wyoming Province, the Montana Metasedimentary Terrane (yellow). The various mountain ranges encompassed by the MMT can be seen on the map to the right (after Mogk et al., 1992) alongside key geographic features related to the regional setting, such as the GFTZ and the ductile shear zone to the southeast.

collision between the Wyoming Province and Superior Province from 1.77 to 1.72 Ga. Notably, this is not to be confused with the collision between the Hearne and Superior Province to the north, an event termed the Trans-Hudson orogeny that occurred from 1.86 to 1.79 Ga (Dahl et al., 1999). The southern boundary, termed the Cheyenne Belt, is believed to represent the suture zone from the collision of the Wyoming Craton and Yavapai Province from 1.78-1.72 Ga (Chamberlain, 1998; Whitmeyer and Karlstrom, 2007). Lastly, the northwestern margin has been interpreted to record the collision between the Medicine Hat Block and the Wyoming Province, resulting in the suture zone which has been termed the Great Falls Tectonic Zone (GFTZ).

The interpretation of the GFTZ as the suture zone is supported by geophysical evidence indicating the presence of a north-dipping subducted slab below the Medicine Hat Block (Gorman et al., 2002). In addition to this, a unique trace element and Nd-isotopic signature has been found in the Precambrian rocks of the Little Belt Mountains which reflects juvenile lithosphere being subducted in a convergent environment (Foster et al., 2006). However, the metamorphic record documented within in the GFTZ reflects a far more extensive tectonothermal history as compared to the Little Belt Mountains. U-Pb zircon and monazite ages obtained from gneisses within the Tobacco Root Mountains and Highland Mountains show that these areas experienced granulite facies metamorphism and partial melting around 1.77 Ga (Harms et al., 2004), which is approximately 100 Ma after the peak metamorphic conditions of the Little Belt Mountains.

Three different metamorphic terranes have been identified within the Wyoming Province: the Beartooth-Bighorn Magmatic Terrane (BBMT), the Southern Accreted Terranes (SAT), and

the Montana Metasedimentary Terrane (MMT) (Figure 1). The youngest of the terranes is the SAT and it is an amalgamation of Late Archean supracrustal sequences comprised of metavolcanics, metasediments, and a minor volume of metamorphosed banded iron formation. The lithologies of the SAT are thought to have been deposited and metamorphosed via continental arc magmatism and terrane accretion ca. 2.68-2.67 Ga and then eventually cratonized by 2.50 Ga (Chamberlain et al., 2003; Mueller and Frost, 2006).

The BBMT and MMT are believed to represent the older portions of the Province and thus the earliest to be cratonized (ca. 2.80 Ga) (Mueller and Frost, 2006). The boundary separating them is referred to as the Madison Mylonite Zone, which is a prominent southwest to northeast-trending shear zone that extends from the middle of the Madison Range to the uppermost parts of the Beartooth Range (Figure 1). The juxtaposition of the two terranes is thought to have occurred along the northeastern end of the Madison Mylonite Zone ca. 2.6-2.5 Ga (Mogk et al., 1992; Mueller et al., 1993).

The BBMT is dominated by 3.0-2.8 Ga metaplutonic rocks of the trondhjemite-tonalite-granodiorite association alongside lesser amounts of granite and high-K granodiorite (Mogk et al., 1992; Mueller and Frost, 2006).

The MMT is comprised of Archean metasedimentary rocks such as quartzites, pelitic schists, and marbles that are intercalated with older (3.2-3.0 Ga) quartzofeldspathic gneisses. The crust of the MMT is believed to be geochemically distinct from the crust of other parts of the Wyoming Province as well as other Archean terranes within Laurentia. The set of characteristics that distinguishes rocks of the MMT from adjacent, younger terranes includes their age range from 3.5-2.5 Ga, detrital zircon and Sm-Nd ages of up to 4.0 Ga, and uniquely enriched Pb isotope signatures (Foster et al., 2006).

2.2 The Montana Metasedimentary Terrane

The MMT is located in southwest Montana where it lies within the GFTZ, along the NW margin of the Wyoming Province. The Precambrian rocks of the MMT preserve a rich record of Paleoproterozoic tectonism which documents the final stages of crustal assembly for this part of Laurentia. Moreover, they provide an excellent opportunity to study the dynamics of crustal accretion, metamorphism, anataxis, and exhumation.

The terrane of the MMT encompasses five major mountain ranges, including the Tobacco Root Mountains, Highland Mountains, Ruby Range, Northern and Southern Madison Ranges, and Gravelly Range. The primarily lithologies consist of middle Archean quartzofeldspathic gneisses and late Archean metasedimentary lithologies such as pelites, marbles, and various quartzites.

The rocks of the MMT have experienced several episodes of high-grade metamorphism whose spatio-temporal effects and tectonothermal significance are a subject of ongoing research.

Zircon and monazite geochronology have identified the presence of two dominant metamorphic age populations represented throughout the MMT. The older population has been dated at 2.55-2.45 Ga and has been identified in the Madison Range, Tobacco Root, Gallatin Range, Tendoy Mountains, and the Black Hills of South Dakota (Mogk et al., 1992). It has been hypothesized to reflect either a time of contraction induced crustal accretion, or a period of extension related to mantle plume activity (Jones, 2008). This event has been termed the Tendoy Orogeny, however it remains relatively ill-defined and has not been identified in the BBMT or SAT (Kellogg et al., 2003; Dahl et al., 2004).

The younger metamorphic age population identified within the MMT is from 1.8-1.7 Ga and is considerably more pronounced in nature. It has been interpreted as recording the collision

of the Medicine Hat Block and Wyoming Province, a tectonothermal event which has been

named the Big Sky orogeny (Harms et al., 2004). Previous work in the Tobacco Root Mountains

characterizes the metamorphic conditions of the Big Sky orogeny to be upper amphibolite to

lower granulite facies conditions around 700-800 C° at >10 kbar (Cheney et al., 2004). Peak

metamorphism was followed by subsequent cooling and decompression at roughly 700 C° and

~7 kbar, followed by near isothermal decompression to ~5 kbar, which has been attributed to

post-collisional regional unroofing.

   The overall goal of this study is to use a less common but distinctive lithology found within

the MMT to examine how the conditions of the Big Sky orogeny varied spatially across the

terrane, and what this implies about the kinematics and subsurface architecture involved in the

collisional regime.

2.3 Cordierite-orthoamphibole gneisses (COG) and proposed petrogenetic models

This study focuses on a single lithology, cordierite-orthoamphibole gneisses (COG),

which has been of particular interest to petrologists around the world due to its highly debated

protolith and petrogenesis, the fact that they are commonly associated with large, economic

deposits of sulphide minerals, and their complex assemblages and textures that are important for

obtaining accurate P-T paths (Heimann et al., 2006; Diener et al., 2008). In the MMT, COG has

provided some of the most elucidating evidence that yields important insights into the complex

metamorphic history of the region. In addition to occurring along the Proterozoic suture zone,

referred to as the GFTZ, complex reaction textures and diagnostic mineral assemblages

preserved in COG have been vital for constraining peak metamorphic conditions. Overall, this

lithology poses a unique opportunity to examine both the chemical and mechanical nature of the Proterozoic collision margin.

Gedrite-anthophyllite-cordierite gneisses occur as lenses and discontinuous layers within metasedimentary sequences as well as other, more fine-grained amphibolites throughout the MMT. Outcrop thickness varies considerably, with thinner lenses (1-5 meters) often found interlayered with pelitic schists. The typical assemblage for this lithology is gedrite/anthophyllite (35%), garnet (30%), plagioclase (15%), quartz (10%), cordierite (5%), and biotite (5%) (Burger et al., 2004). However, the precise mineralogy is highly variable between locations. Spectacular coarse-grained localities have been found that preserve almandine-rich garnets up to 10 centimeters in diameter and laths of orthoamphibole up to 10 centimeters in length. The dominant species of orthoamphibole present is typically gedrite ($Mg/(Mg + Ca) \approx 0.6$), which frequently displays a characteristic play of colors due to the exsolution lamellae of anthophyllite (Figure 4). Cordierite and orthopyroxene are also commonly observed in outcrop as either partially replacing garnet or forming complete coronas around garnet.

The efficacy of this lithology to yield valuable geologic information is principally due to its diverse mineral assemblage, as well as its unusual bulk composition. Additionally, several COG localities preserve intricate and complex reaction textures such as symplectites and coronas of cordierite, spinel, sapphirine, staurolite, and kyanite. Aluminosilicate polymorphs and other replacement reactions are also observed which commonly involve garnet, cordierite, and gedrite. The complexity of this lithology has led to it being widely used by petrologists for obtaining peak *P-T* conditions and *P-T* paths (Smith et al., 1992; Qian et al., 2015). Additionally, orthoamphibole minerals coexisting with cordierite reflect an Mg- and Al-rich, Ca-poor bulk

composition, which is unusual for a mafic protolith, which is typically high Ca, with relatively

lower Mg and Al.
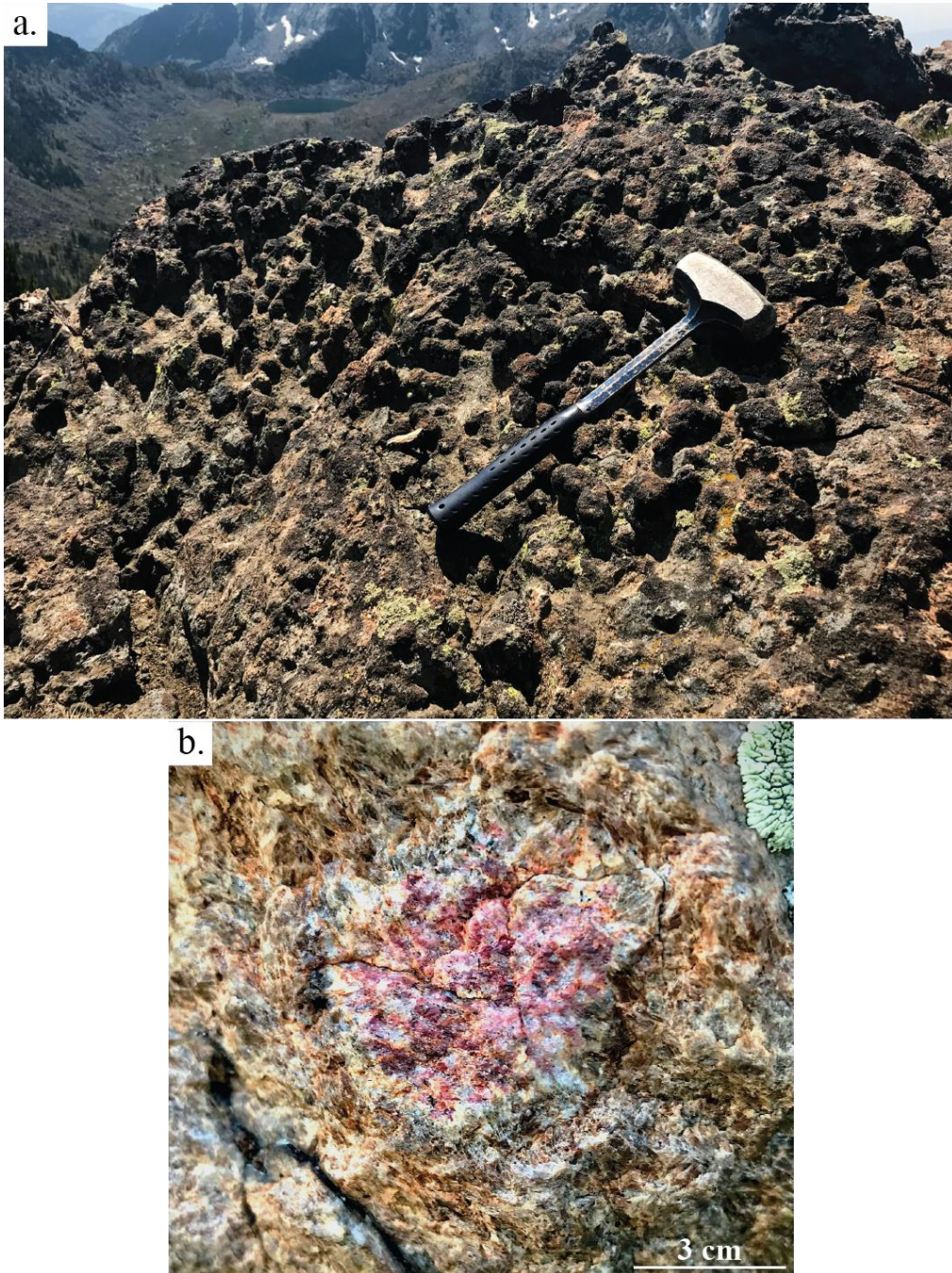
Figure 2. Examples of spectacular outcrop textures seen in the gedrite-gneisses, such as golf ball sized garnets at Thompsons Peak in the Tobacco Roots (a) and large garnets with coronas of orthopyroxene and cordierite in the Highland Mountains (b).

Previous studies of COG have led to the emergence of 4 possible petrogenetic models, respectively, which all involve various degrees of chemical alteration involving metasomatism and, in some cases, partial melting. These models can be separated into two categories based on whether or not metasomatic alteration is believed to occur during, or prior to, metamorphism. In the first model, syn-metamorphic metasomatism occurs by introducing Fe and Mg via diffusion or infiltration of a hydrothermal fluid into a range of rock types (Eskola, 1914; Irving and Ashley, 1976). The second model proposes partial melting of a metavolcanic in which COG represents the residuum after extraction of granitic melt (Grant, 1968; Hoffer and Grant, 1980). In the third model, COG is created through the metamorphism of a particular sedimentary facies, such as a pelitic evaporite or paleosol horizon (Gable et al., 1970; Young, 1973; Reinhardt and Cook, 1987). Then in the last model, COG represents a volcanic rock that was hydrothermally altered prior to metamorphism (Vallance, 1967; Schumacher, 1988; Smith et al., 1992; Pamić et al., 2002; Peck and Smith, 2005; Qian et al., 2015).

Given the widely accepted cratonic margin setting for these rocks, this study hypothesizes that the protolith material of COG is likely hydrothermally altered basalt which might reflect accretion of Paleoproterozoic oceanic crust that represents volcanic arc material that was situated between the Medicine Hat Block and Wyoming craton, and that the preservation of this material provides evidence for ocean basin closure and accretion of arc material to the margin of the Wyoming Province during the Big Sky orogeny.

Ultimately, this investigation aims to integrate detailed field studies with geochemical data, petrography, and Pressure-Temperature (*P-T*) models of COG in order to better define their petrogenesis and to place firmer constraints on the variation in metamorphic conditions across the Big Sky orogeny. Unraveling the tectonics of this collisional zone via utilizing the COG

petrology and geochemistry will not only elucidate our understanding of how this previously

poorly understood lithology developed, but will by extension, also yield a better understanding

regarding the long-term evolution and stability of cratons.

3. Methods

3.1 Fieldwork

During the summer of 2018, a sampling expedition was conducted in the Tobacco Root

Mountains, Ruby Range, and Highland Mountains at known outcrops of COG. This was

followed by a thorough field investigation in the summer of 2019 where more samples were

collected from all three mountain ranges in addition to the Madison Range and Gravelly Range.

Detailed field observations and generalized outcrop maps were created in order to gain an

understanding of the context that COG occurs in. The relationship COG has with other

lithologies and major structural features was an aspect of particular interest given the relevance it

has to the petrogenetic origins of the lithology.

3.2 Petrography and SEM imaging

A total of 44 new thin sections were made by Spectrum Petrographics, Inc., which were

supplemented by an additional 22 thin sections that had been gathered from previous studies.

The majority of the thin sections that were made were from COG samples collected from the

Ruby Range, Tobacco Root Mountains, Highland Mountains, Gravelly Range, and Madison

Range. However, a portion of the samples were fashioned from contextual lithologies such as garnet-amphibolites and pelitic gneisses.

Using a petrographic microscope, detailed reports were compiled that characterized the assemblages and reaction textures. Further petrographic analysis was also done by using a Tecscan Vega-3 LM Scanning Electron Microscope (SEM) in conjunction with an Oxford Instruments 80 mm^2 X-Max SDD energy-dispersive spectroscopy (EDS) detector that is housed at the University of Montana. This allowed for the collection of both backscattered electron images (BSE) and energy dispersive x-ray spectroscopy (EDS) elemental compositional maps.

3.3 Bulk rock chemistry

Twenty-two samples were selected for bulk geochemical analysis based on the spatial distribution of localities and the range of representative lithologies and mineral assemblages. Individual samples were hand selected to promote the most accurate and homogenous representation of the outcrop. Blocks were cut and trimmed to remove all weathered surfaces and analyzed at by XRF at Washington State University's GeoAnalytical Lab.

The samples were ground into a fine powder using a swing mill with a tungsten carbide surface. Then for each sample, 3.5 grams of the powder was mixed with 7.0 grams of a dilithium tetraborate (Li_2B_4O7) flux and put into graphite crucibles to be fused in a muffle oven at 1000°C. Once cooled, the individual glass beads were reground, refused, and polished on diamond laps to provide a smooth flat analysis surface. The beads were then analyzed by a ThermoARL X-ray fluorescence (XRF) Spectrometer. XRF analyses measured 10 major and minor elements and 19 trace elements.

Inductively coupled plasma-mass spectrometry (ICP-MS) was also conducted on the samples in order to analyze 14 REE's and 13 additional trace elements. Sample preparation for this began by taking the allocated portion of sample and grinding it into a fine powder and then mixing it with a proportional amount of dilithium tetraborate flux. The mixture was then placed into a graphite crucible and fused into a glass bead in the muffle oven at 1000 C°. After cooling, the bead was reground into a powder and a 250 mg portion is set aside to undergo evaporation. The first evaporation was done using HNO_3, HF, and $HClO_4$ at 110 C°. After drying the sample was rinsed with a small amount of water before undergoing the second evaporation using $HClO_4$ at 160 C°. Following this, the sample was brought into a solution with water, HNO_3, H_2O_3, and HF. Finally, this solution was warmed on a hot plate until becoming transparent in color and then diluted with de-ionized water.

3.4 Mineral chemistry

Mineral compositions were measured by calibrating the EDS detector to a range of natural mineral standards. Spot analyses were conducted on polished thin sections with an accelerating voltage of 20kV, a beam current of 1.4 nA, and live counting time set to 75 seconds. Mineral compositions were measured for garnet, orthoamphibole, orthopyroxene, cordierite, plagioclase, and biotite. In particular, garnet, orthoamphibole, biotite, and plagioclase were frequently found in several different modes within a single section; they occurred in the matrix, as porphyroblastic inclusions, as well as in coronas or symplectite textures. In such cases, representative spot analyses were collected on all varieties and petrographic settings of that mineral that were present.

3.5 Thermodynamic modeling

The bulk rock chemistry was used as input for the Theriak-Domino program (De Capitani and Petrakakis, 2010). This thermodynamic modeling program models the equilibrium mineral stability fields, based on minimization of Gibbs Free Energy, using the bulk composition of the rock as the input and thus it is able to generate a representative pseudosection (isochemical phase diagram) for any given sample. The version of Theriak-Domino used was 09.03.2019 and it was run on Windows. Representative pseudosections for the Ruby Range, Highland Mountains, Tobacco Roots, and Madison Range COGs were calculated with varying water content. The thermodynamic database used was generated by Doug Tinkham (*https://dtinkham.net/peq.html*) and configured using pyroxene and amphibole models (White et al., 2002; Green et al., 2007; Diener and Powell, 2012) as well as garnet and biotite models (White et al., 2007). The stable mineral assemblages for each pseudosection were selected based on petrographic and SEM observations of that sample. H_2O and Fe_2O_3 content was determined for each sample by constructing T-X (H_2O and Fe_2O_3) diagrams to see which values corresponded to the observed hydrous and oxide mineral assemblages.

4. Results

4.1 Structural and field relationships

The various field sites cumulatively cover an area of approximately 2000 mi2 and span across Madison and Beaverhead counties in southwest Montana (Figure 3). Although each of the

mountain ranges in this study expressed unique geological characteristics, there were some core lithologic suites that were common to all field locations. This suite was comprised of quartzofeldspathic gneisses interlayered with amphibolite, which was commonly juxtaposed by cross-cutting mafic dike and sills. Relatively small packages of heterogeneous metasupracrustal rocks would then be found in close proximity, one of which being COG. For each COG sample in this study, the mineral assemblage, reaction textures, and UTM coordinates are listed in Table 1.
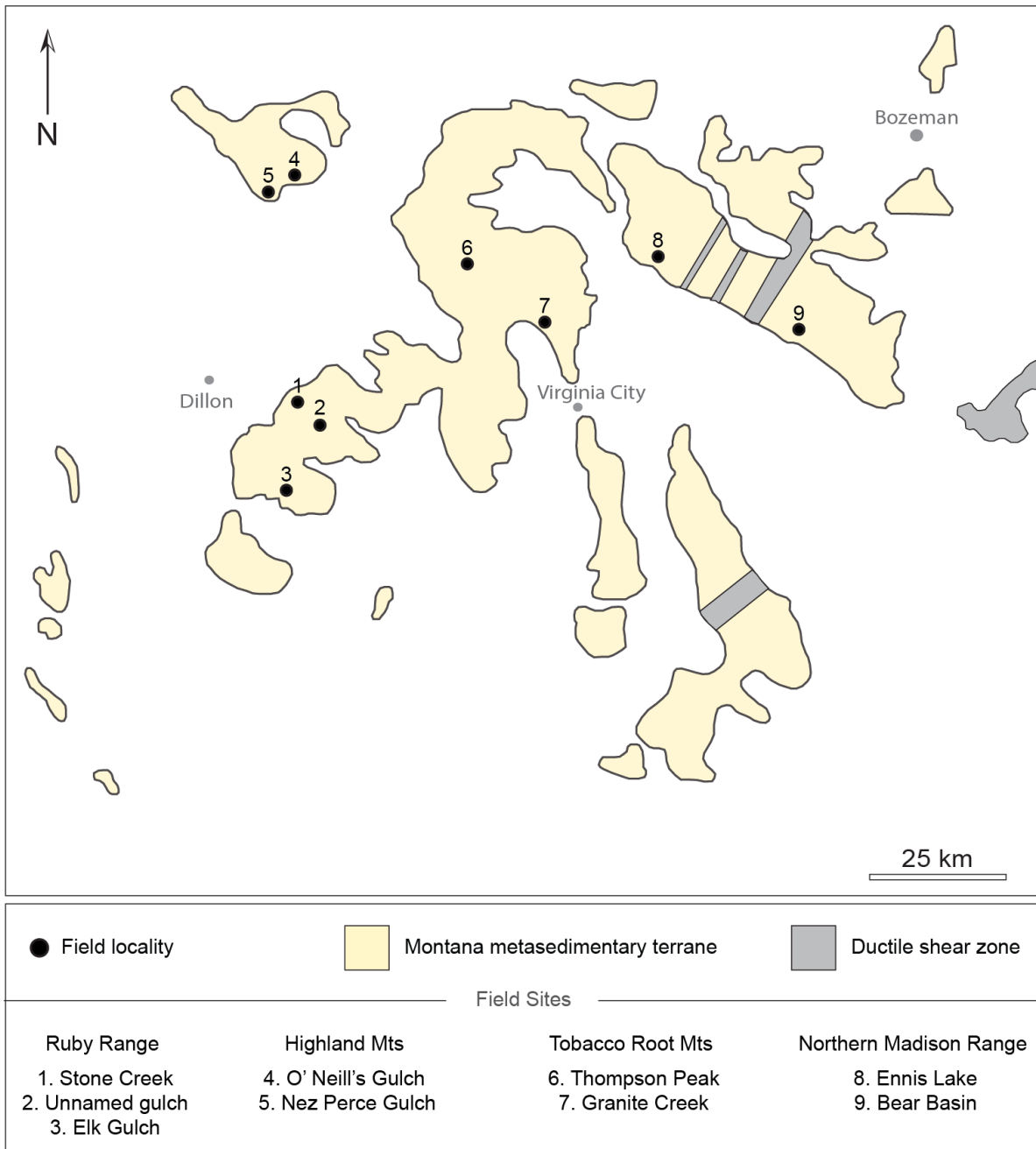
Figure 3. Location map of the different field sites referenced throughout the text.

Mtn. Range	COG Sample	GPS Coordinates UTM Zone 12 (WGS 84)		Mineral Assemblage											Reaction Textures		
				Oam	Grt	Opx	Ky	Crd	Bt	Pl	Qtz	Rt	Ilm	Etc.	C	S	O
Ruby Range	RR-BC-03a	392988	5008135	x	x	x	x	x			x	x	tr		x		x
	17-JB-1	392988	5008135	x	x	x	x	x		x	x	x	x		x	x	
	14-MG-06b	391901	5008753	x	x	tr	x	x	x	x	x	x	tr	Spl, Sph, Crn	x	x	
Highland Mountains	HM-BC-01a	389493	5048161	x	x	x		x	tr	x	x	x	x	Sil	x		x
	18-HM-01	389493	5048161	x	x	x	x	x		x	x	x		Sil	x		x
	NP04	384544	5045456	x	x	tr				x	x	x	tr	Chl, Zrn, Ap			
Tobacco Root Mountains	18-TR-03	420328	5042227	x	x	x		x	x	x	x	x	x		x		x
	18-TR-06	431750	5029182	x	x	x		x	x	x	x						
	TB2	431750	5029182	x	x	x	x	x		tr	x	x			x	x	
N. Madison Range	MR-BC-03a	448966	5033483	x	x	x	x		x	x	x	x	x	Crn, Ap, Ms	x		
Gravelly Range	20-JB-14	440488	5000740	x	x					x	x						

Table 1. Sample coordinates and assemblages. Mineral abbreviations after Kretz, 1983. Reaction texture abbreviations are as follows: C= coronas, S= symplectites, and O= other.

Ruby Range

The three primary locations where COG can be found in the Ruby Range are Stone Creek, Elk Gulch and what is referred to as "unnamed gulch" (Figure 3). Despite being relatively close in spatial proximity, there are key textural, mineralogical, and contextual differences that exist between each site.

The rocks of the Stone Creek locality belong to a group known as the Christensen Ranch Metasedimentary Suite (CRMS). The outcrop of COG here is extremely limited, confined to a ~30 cm-thick layer, however sample of COG can be found in abundance as large chunks in float along the slope. The most notable feature of COG at this locality were observed in hand sample. The samples are weakly foliated schists, dominated by prismatic blades of anthophyllite (2-6 mm) (Figure 4). Magenta-colored garnets of varying sizes (2 mm-2 cm) are also scattered throughout the matrix alongside the less abundant grains of biotite, plagioclase, staurolite, and cordierite.

The COG outcrop at the "unnamed gulch" locality was approximately 6 meters thick and considerably weathered, making surfaces that weren't fresh ruddy orange in color. However, the increased amounts of quartz and plagioclase cause COG at this locality to have a more leucocratic color scheme overall. In hand sample, the orthoamphiboles present were less prismatic and finer-grained (1-4 mm) than the Stone Creek locality. Abundant pods of garnet were found associated with the orthoamphiboles separating them from the matrix. Along strike, there were several zones that were notably quartzofeldspathic in character. COG here is bounded to the west with a thick sequence of ridge-forming amphibolite and to the east by a large quartz vein.

Figure 4. Hand sample images from the Stone Creek locality in the Ruby Range. Blades of anthophyllite intermixed with pods of garnet can be observed with the naked eye exhibiting their characteristic play of colors resulting from the presence of their exsolution lamellae (c).

The rocks at the Elk Gulch locality are bounded by two normal faults on either side and they collectively belong to a group known as the Older Gneiss and Schist (OGS). The various lithologies found at this location include amphibolite, gedrite gneisses and schists, amphibole schists, garnet-bearing migmatitic gneisses, migmatitic granitic gneisses, and large bodies of meta-ultramafic rocks (Figure 5). COG itself is found interbedded with amphibolite. There are two outcrop types of COG at this locality that have distinct differences. Although within the same unit, COG at this locality changes along strike. The first outcrop sampled lies towards the south. It's slightly finer grained and also contains lesser amounts of garnet overall as compared to the other localities. Small (~3 mm) white grains of plagioclase can be observed forming the "turkey tracks" texture across the surface (Figure 5c). Notably, there is a sequence of labradorite

schists directly to the southwest of this which are juxtaposed by large veins which contain

megacrysts of gedrite. The second outcrop of COG is located ~75 m to the northeast. It has a

more schist like character overall and is coarse grained with abundant magenta garnets (Figure

5d).

Figure 5. Outcrop and hand sample images from Elk Gulch including migmatitic gneisses (a and b) alongside two representative hand samples of the different expressions of COG observed at this locality. The outcrop to the south (c) is fine grained with no garnet present, and exhibits laths of plagioclase oriented in the "turkey tracks" texture. The outcrop to the north (d) is coarse grained and has distinct layering. Leucosomes filled with garnet, quartz, and plagioclase reside between layers of orthoamphibole schist.

Highland Mountains

The two localities of COG in the Highlands are found along O'Neill's Gulch and the Nez Perce Creek area. Both were considerably coarse-grained, with megacrysts of gedrite up to 5 cm in length (Figure 6) and garnet porphyroblasts up to 5 cm in diameter.

O'Neill's Gulch is dominated by prominent outcrops of ridge-forming amphibolite, which trend to the northeast and can be traced for over 50 meters along strike. The amphibolite is fine-grained and approximately 2-meters-thick with discrete, individual beds that range from 3-10 cm in thickness. It's primarily composed of hornblende and plagioclase, which make it range
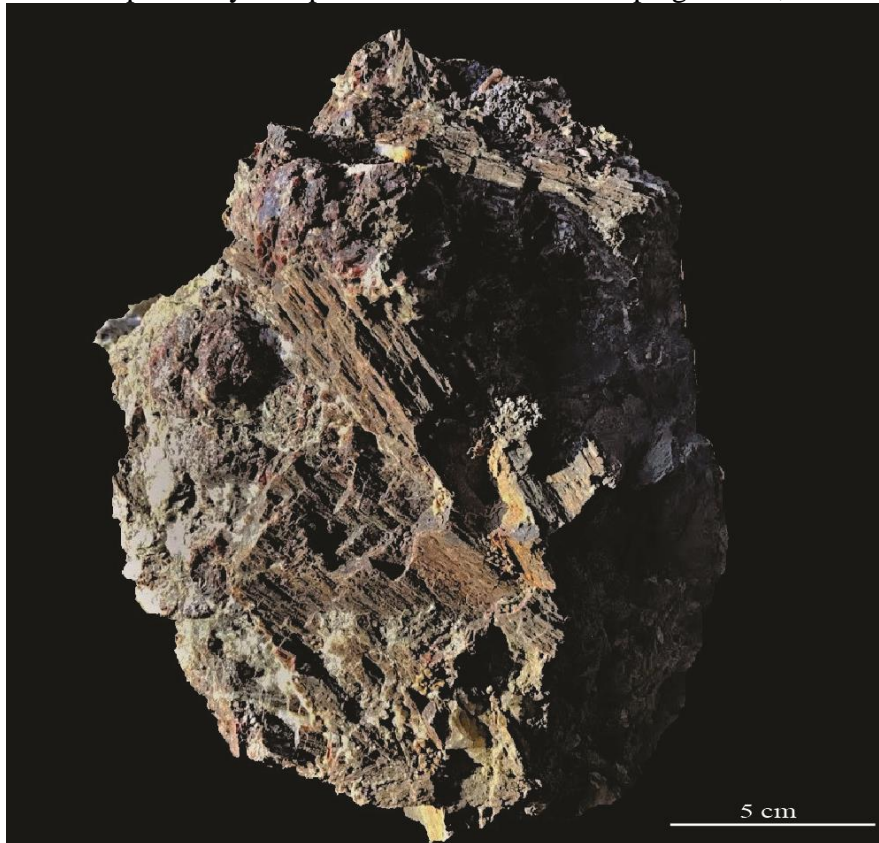
Figure 6. Hand sample of HM-BC-01a. Extremely coarse grained COG sample from O' Neil's Gulch in the Highland Mountains, MT.

from dark grey to black in color. COG is found in discontinuous lenses amongst the amphibolite

22

and has a weathered surface that is orange-brown in color. Both the amphibolite and COG have localized zones enriched with megacrystic garnets that frequently exhibit remarkable reaction coronas of cordierite that can be seen with the naked eye (Figure 7d). Quartzofeldspathic gneiss with large garnets up to 3 cm in diameter are found above the amphibolite, at the stratigraphic top of this section (Figure 7b).

The Nez Perce Creek area contains a diverse variety of lithologies, including: garnetiferous gneiss, biotite schist, mylonitic biotite gneiss, quartzofeldspathic gneiss, garnet amphibolite, and COG. Similar to O'Neills gulch, fine-grained amphibolite comprises almost all of the localized ridges, making prominent outcrops which were used to measure strike for the area. The same quartzofeldspathic gneiss is also found at the stratigraphic top of this section. Outcrops of COG at this locality are smaller and roughly 2 meters along strike, on average. COG is primarily interbedded within amphibolite however it is also found as a transitional lithology from the amphibolite to adjacent schists.
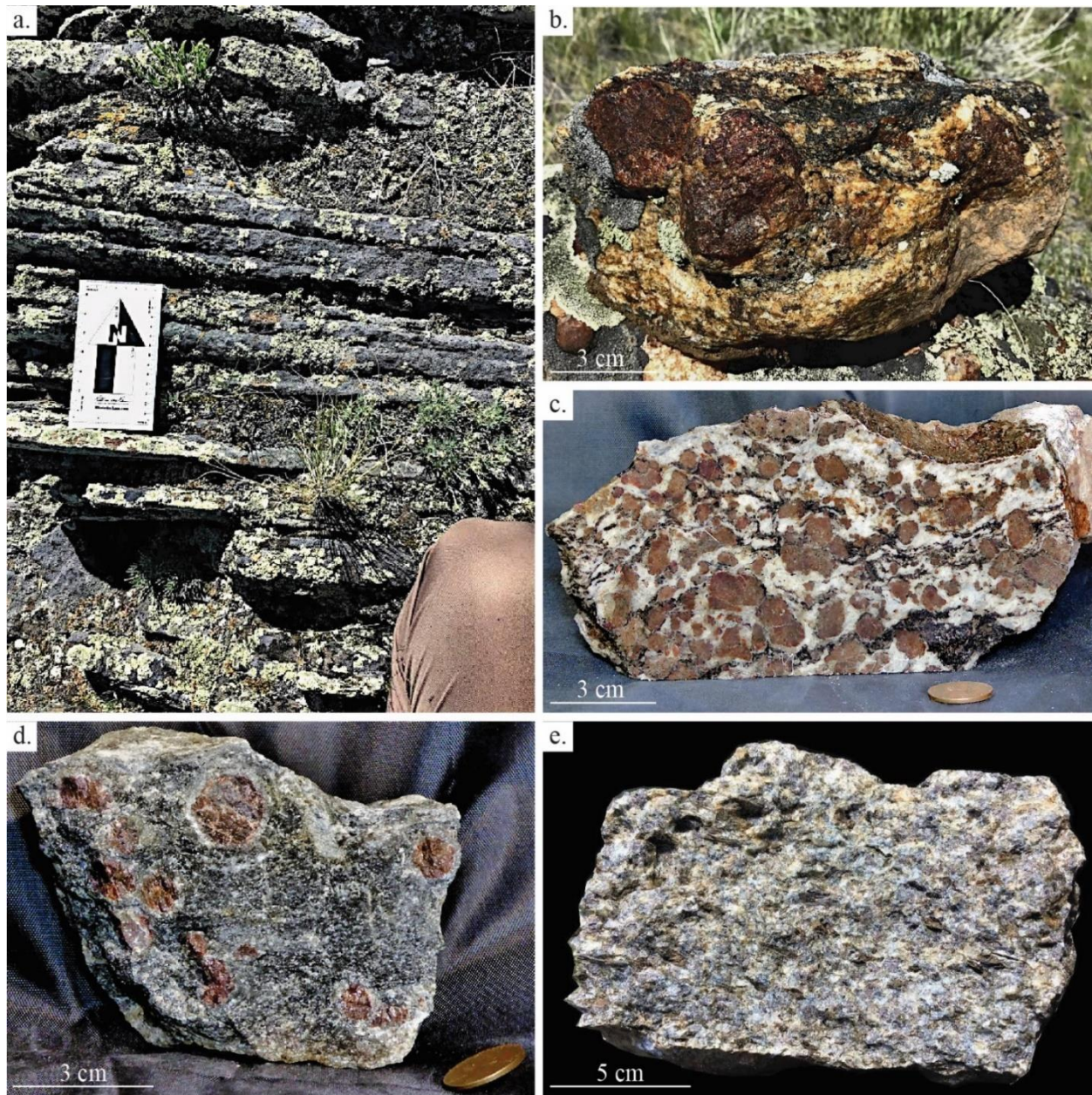
Figure 7. Outcrop and hand samples images from O'Neill's Gulch including amphibolite (a) showing distinct coronas of cordierite around garnet porphyroblasts. Other lithologies found associated with COG in the Highlands include: garnetiferous-quartzofeldspathic gneiss (b), garnet-biotite migmatitic leuco-schist (c), amphibolite with cordierite coronas around garnet (d.), and gedrite-bearing cordierite schist (e.).

Tobacco Root Mountains

Although numerous exposures of COG have been identified in the Tobacco Roots, this study focuses on those at the Thompson Peak and the Granite Creek locations.

The Thompson Peak area preserves one of the widest, best-studied exposures of the Spuhler Peak Metamorphic Suites (SPMS) (Cheney et al., 2004). The lithologies found here include: amphibolite, hornblende gneiss, COG, quartzite, aluminous gneiss, and lesser amounts of quartzofeldspathic gneiss. There are also a few localized zones of garnetite that exhibit surfaces covered in garnets the approximate size of golf balls (Figure 2a). This locality has little evidence of any fabric, if there is any at all, and additionally has an abundance of extremely coarse grain sizes that can be found across all lithologies.

COG is found both intercalated with amphibolite as well as within sequences of aluminous gneiss and schist. Outcrops range in thickness from <1 meter to >30 meters. The variety of COG found within the amphibolite is non-foliated and considerably coarse-grained, with clove-colored tabular blades of gedrite up to 15 cm in length that often exhibit a characteristic play of colors from exsolution lamellae of anthophyllite. Almandine-rich garnets up to 10 cm in diameter can be found within the COG of this variety that show light blue rims of cordierite. The variety of COG interbedded with the aluminous gneiss and schists is distinctly more fine-grained, with blades of gedrite that are on average a few millimeters in length. This expression of COG often has weak foliation present as well.

To the south, the Granite Creek locality has a much smaller and less diversified exposure of COG. However, the dramatic textures and overall coarse grain size remains consistent with the Thompson Peak outcrops. COG at Granite Creek contains coarse grained,

melty leucosomes that are distinctly partitioned from the darkly colored schistose areas. The leucosomes are comprised of quartz, garnet, and plagioclase that are all roughly 0.5 cm in diameter. The purple-red garnet at this locality is not as coarse grained as the Thompson Peak section, at roughly 2-5 cm in diameter, and it is solely found as porphyroblasts within the pods of leucocratic material. The remaining melanocratic portions of the lithology, observed with the naked eye, are foliated blades of clove-colored gedrite (0.3-1 cm) and biotite.

Madison Range

There are two main study sites within the Madison Range are within Bear Basin and near Ennis Lake, Montana.

The location of the COG exposure within Bear Basin lies directly adjacent to the main trail within a group of lithologies collectively called the Bear Basin Schist. The lithologies here consist of aluminous schists, amphibolites, and quartzites that all highly vary along strike both compositionally and texturally. The unit is about 50 feet thick and can be traced for roughly 150 feet along strike. COG is found here as a medium to coarse grained biotite or hornblende schist with occasional lenses of quartz. This dark-colored schist is most often intercalated within what is referred to as albitite (Condit et al., 2018). Large blades of gedrite, hornblende, and kyanite can be found within the schistose portions of this exposure that are up to 5 cm in length. However, acicular blades of orthoamphibole also occur within portions of the albitite as large, radial sprays. This gives particular portions of the albitite lithology an overall garbenschiefer texture. There are areas of slightly less abundance within this unit that are more fine-grained, respectively, and exhibit strongly folded quartzofeldspathic layering. Notably, this overall unit is

bound to the northwest by a large kyanite-biotite pegmatite. Then on the opposite side of the main trail, directly to the east, there is a large section of medium-grained biotite-gneiss with thick and distinct compositional layering.

The second locality within the Madison Range lies directly north of Ennis Lake, along the eastern side of the gorge in Bear Trap Canyon. COG has a limited amount of exposure here, occurring as small isolated outcrops on the steep slopes of the valley wall. The characteristics of COG here closely resemble those of the Granite Creek location to the north. There is a distinct partitioning between pods of "melty", coarse-grained leucosomes and dark colored schistose areas (Figure 8). The leucosomes are dominated by quartz, plagioclase, and garnet, while the dark schist is comprised mostly of gedrite, biotite, and hornblende. This exposure is bound to the southwest by garnetiferous quartzofeldspathic gneiss. It has an overall light orange color that is similar to the quartzofeldspathic gneiss found in the Highlands, although this locality has much smaller garnets. To the east of COG, is a large exposure of the quartzofeldspathic gneiss except it is intimately intercalated with layers of biotite schist that are, on average, 3-4 cm thick.
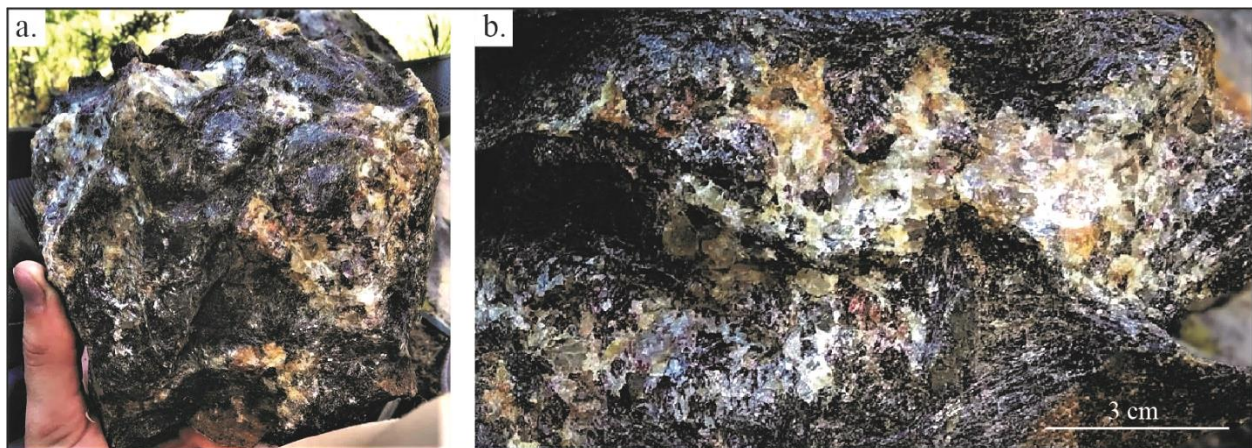
Figure 8. Representative COG sample (MR-BC-03a) from the northern Madison Range near Ennis Lake, MT.

Gravelly Range

Due to the minimal exposure of COG in the Gravelly Range, the outcrop locality here is considerably localized and inconspicuous. The primary lithology associated with this exposure of COG is an amphibolite that is comparable to the kind identified in the Highland Mountains. The variety of COG found here is a fine-grained gneiss, which could allow it to be easily overlooked in the field as amphibolite (Figure 22a and 22b). Orange-brown blades of orthoamphibole, 1-2.5 mm in length, define foliation. Small layers (<2 mm thick) containing plagioclase, quartz, and garnet are found interspersed parallel to foliation.

4.2 Petrography

In order to document the diverse assemblages and textures represented by this lithology across the region, samples of COG were collected from each study site for petrographic analysis.

Tobacco Roots

TB2: Granite Creek

TB2 is medium to coarse grained with a mineral assemblage of orthoamphibole, orthopyroxene, garnet, kyanite, cordierite, rutile, quartz, and trace amounts of plagioclase. Blades of gedrite (<4 cm) are oriented parallel to foliation alongside banded aggregates of garnet grains that are each about ~0.5 cm in diameter. There is an abundance of intricate textures exhibited in this section including polymineralic partial, and complete, coronas as well as a multitude of symplectite textures between orthopyroxene, quartz, and cordierite (Figure 9).

Anhedral garnets show partial polymineralic coronas of first cordierite and then orthopyroxene, which additionally exhibit symplectitic intergrowth. Grains of kyanite are observed within the core regions of several garnet porphyroblasts, alongside enclaves of the garnet which are rimmed with plagioclase (Figure 10).
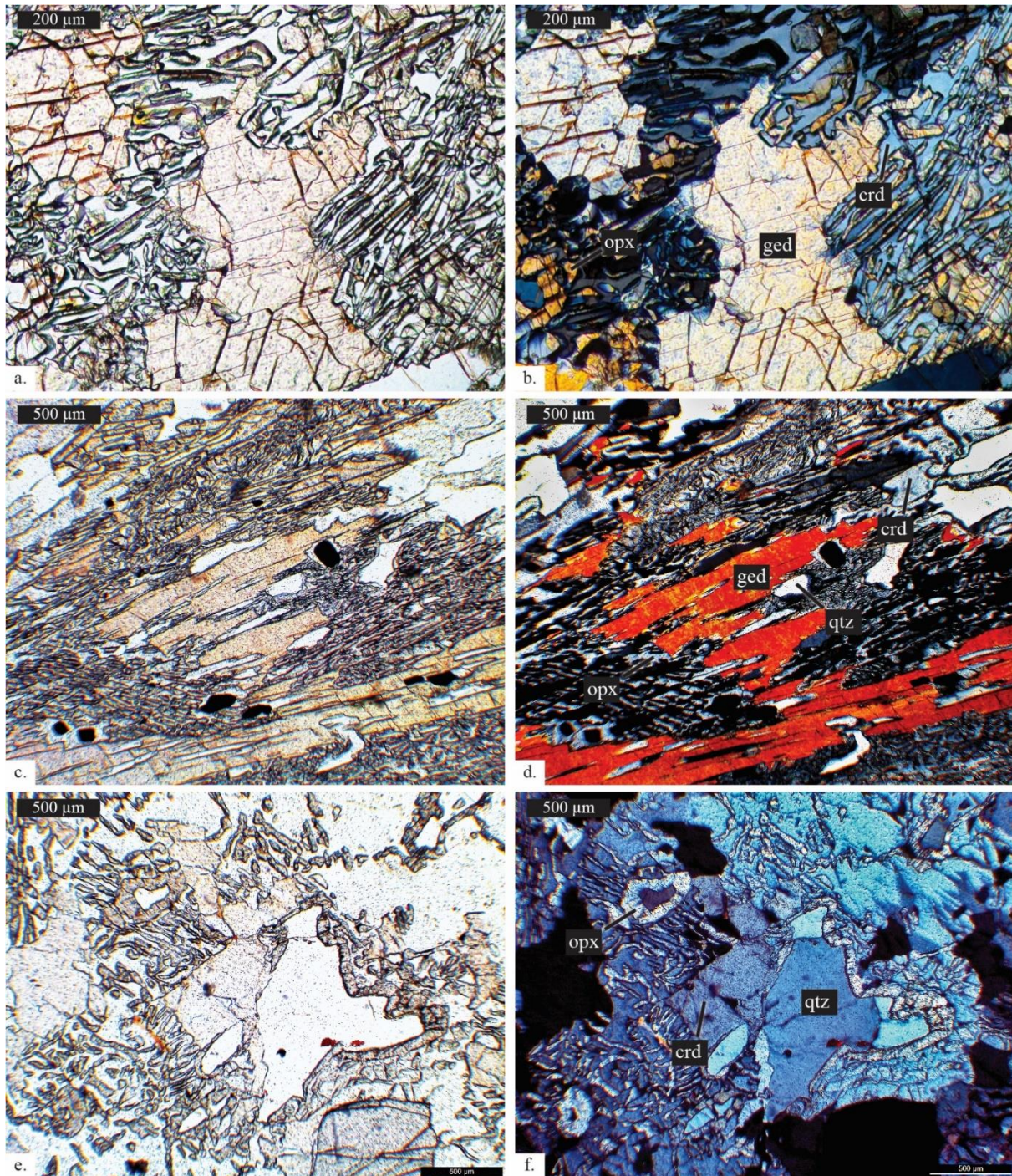
Figure 9. Photomicrographs of TB2 showing cordierite and orthopyroxene symplectites associated with orthoamphibole grains (a/b/c/d) and moats of orthopyroxene forming around quartz grains, which are also involved in adjacent symplectites (e and f).
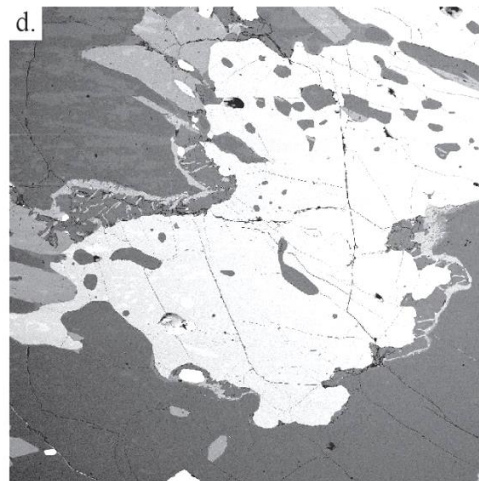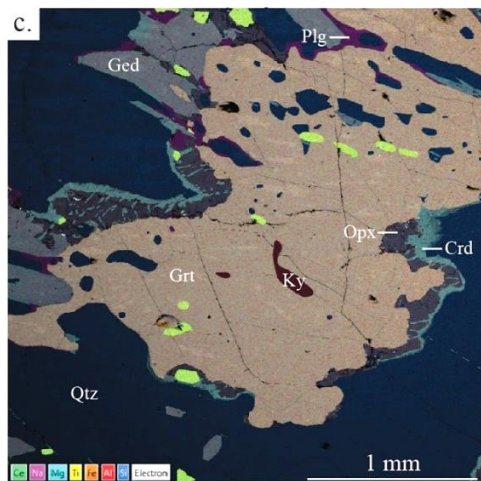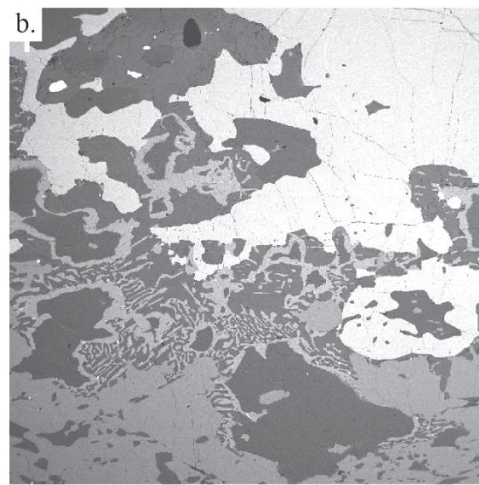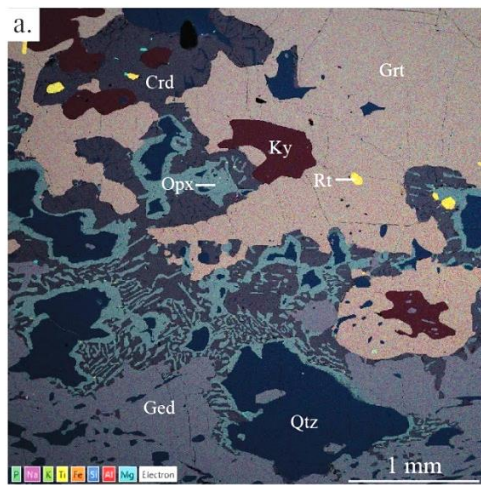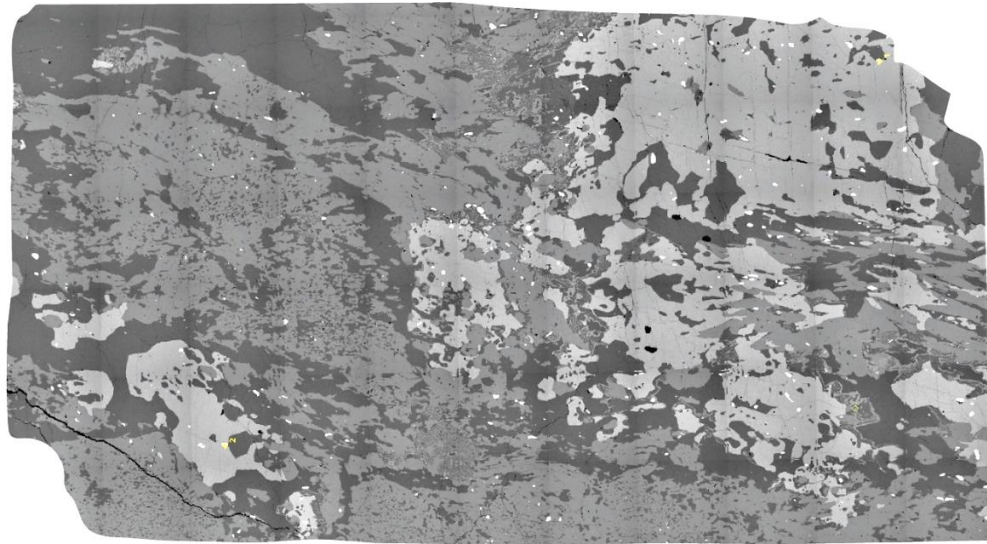
Figure 10. SEM-EDS and BSE images of TB2 showing enclaves of cordierite around garnet and kyanite that form coronas and symplectites with orthopyroxene and quartz (a and b). Partial coronas around garnet of cordierite and orthopyroxene form symplectites within the coronas while can be seen partially surrounding blades of gedrite (c and d).

31

18-TR-06: Granite Creek

18-TR-06 is a coarse-grained schist with a mineral assemblage of gedrite, garnet, plagioclase, quartz, biotite, kyanite, cordierite, orthopyroxene. Leucosomes that also contain garnet and cordierite are intercalated as lenses within the dark colored schist, which is predominantly gedrite and biotite. There are cordierite coronas around garnet porphyroblasts, and plagioclase is found as an interstitial material that specifically separates garnet from biotite and quartz grains.

18-TR-03: Thompson Peak

18-TR-03 is a coarse-grained garnet orthoamphibolite. Subhedral garnet porphyroblasts (0.5-1.5 cm in diameter) have an abundance of cracks and fissures which have moats of cordierite surrounded by acicular blades of pyroxene (Figure 11b). The overall assemblage is gedrite, garnet, hornblende, quartz, cordierite, plagioclase, pyroxene, and ilmenite, with trace amounts of rutile and apatite. Quartz and plagioclase co-occur and are only found as coronas or partial replacements of garnet porphyroblasts. Ilmenite is the primary oxide and is found throughout the section in both the groundmass and as inclusions within garnet. However small grains of rutile exist only as inclusions within garnet.
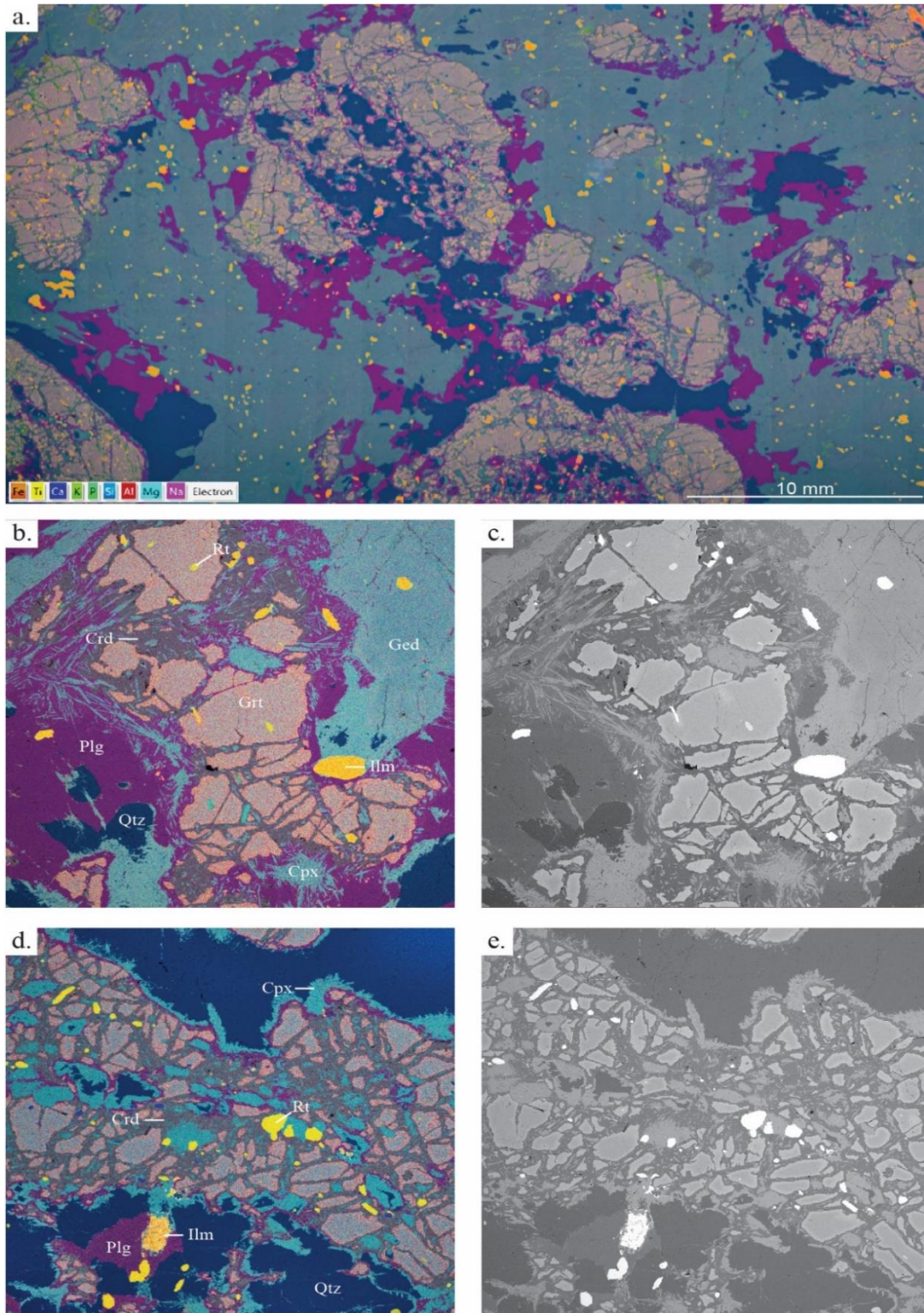
Figure 11. SEM-EDS and BSE images of 18-TR-03. Rims of plagioclase and quartz surround the garnets (a) which have large cracks filled with enclaves of cordierite (b and d). Splintery blades of pyroxene form secondary coronas around the garnet after plagioclase (b and d).

Ruby Range

RR-BC-06a: Elk Gulch

RR-BC-06a is a fine grained orthoamphibolite with an overall assemblage of garnet, gedrite, orthopyroxene, plagioclase, quartz, cordierite, rutile, and ilmenite. The dark brown color of the orthoamphibole alongside the abundance of orthopyroxene give the groundmass an overall light black color in hand sample, which strongly contrasts abundant lenses of fuchsia colored garnets. The garnets are smaller, approximately 2-3 mm in diameter, however they comprise roughly 40% of the overall assemblage. In thin section, intergrowth textures exist between orthoamphibole, plagioclase, orthopyroxene, and garnet. Inclusions of synkinematically grown rutile are observed within the garnet porphyroblasts, as well as partial coronas of cordierite.

17-JB-1: Stone Creek

17-JB-1 is a clove-colored schist with gedrite defining the foliation. Garnet porphyroblasts (up to 1 cm in diameter) have partial to complete coronas of cordierite that form symplectites with the surrounding gedrite (Figure 12a). The overall assemblage includes gedrite, garnet, quartz, kyanite, cordierite, and rutile. Anhedral kyanite can be found as inclusions within the core regions of the garnets showing preferring orientation, suggesting synkinematic growth. Quartz grains also showing preferential orientation are then found as inclusions closer to the rim of the porphyroblasts (Figure 12b).
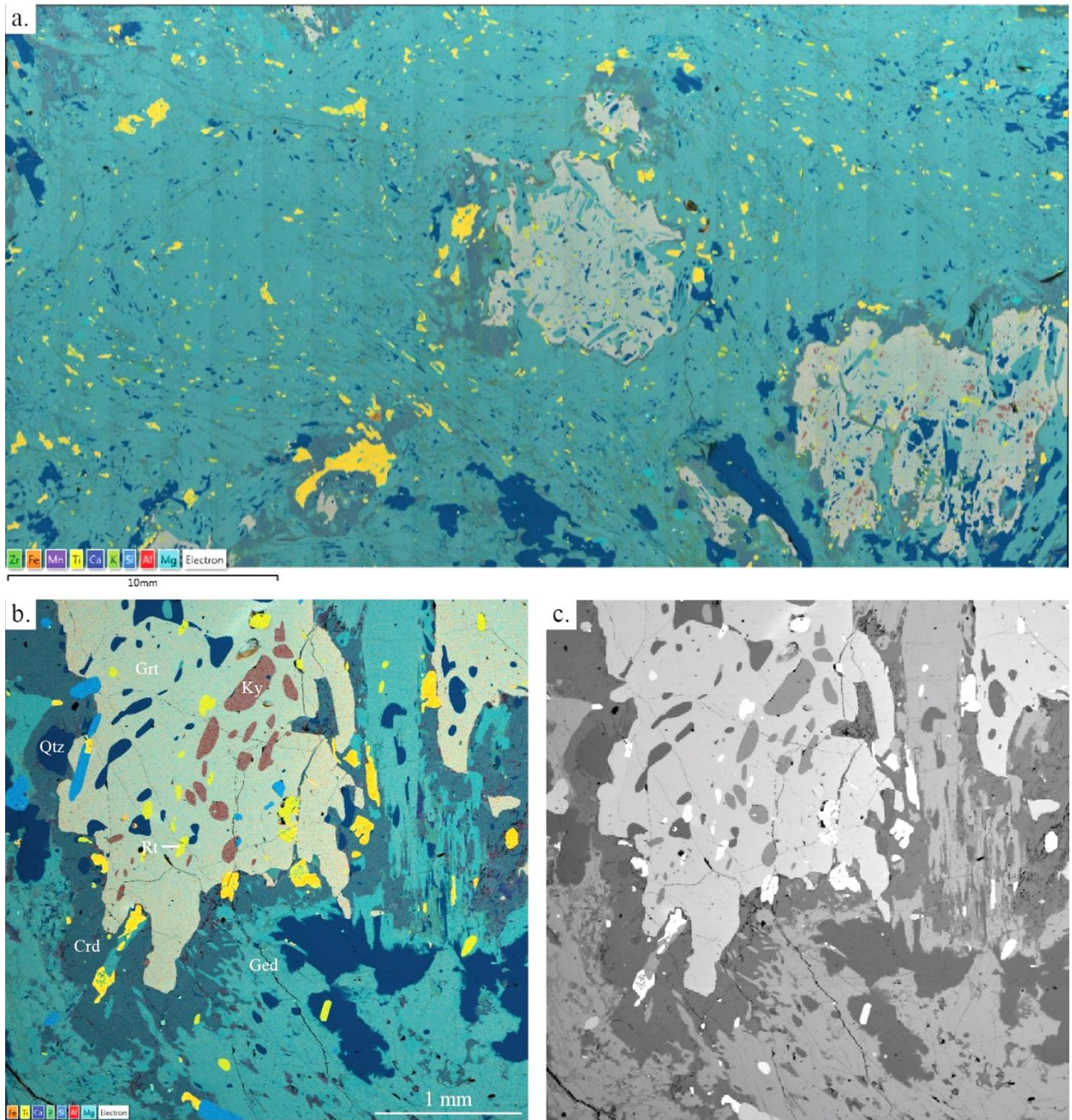
Figure 12. SEM-EDS and BSE images of 17-JB-1 with the overall section scan (a) showing the groundmass of orthoamphibole and quartz and the large porphyroblasts of garnet, which have coronas and symplectites of cordierite and gedrite alongside inclusions of kyanite, rutile, and apatite (b and c).

RR-BC-03a: Unnamed Gulch

RR-BC-03a is a clove-colored gedrite schist with an assemblage of gedrite, garnet, orthopyroxene, cordierite, kyanite, staurolite, quartz, and rutile, with trace amounts of graphite and apatite. In hand sample, tan blades of gedrite (2- 15 mm) can show a play of color due to anthophyllite exsolution lamellae. The groundmass is predominantly gedrite, orthopyroxene, and rutile with localized zones enriched in quartz. Garnet porphyroblasts have symplectitic coronas of orthopyroxene and cordierite. Anhedral kyanite (> 100 µm) is found lining some boundaries of where the opx-crd symplectitic coronas border gedrite (Figures 13 and 14). The inclusions found within the garnets include orthopyroxene, staurolite, graphite, rutile, and quartz (Figure 14).

14-MG-06b: Stone Creek

14-MG-06b is an anthophyllite schist with a mineral assemblage that contains anthophyllite, biotite, plagioclase, orthopyroxene, quartz, garnet, cordierite, staurolite, kyanite, corundum, spinel, sapphirine, muscovite, rutile, and ilmenite. The hand sample is dominated by radial sprays of prismatic anthophyllite blades (2-6 mm) which are dark brown to black. Flakes of biotite (<1 mm) are associated with the garnets in the sample. The garnets vary in size from approximately 2-4 mm in diameter, but some are found up to 2 cm. They are light fuchsia colored and found scattered throughout the matrix Anthophyllite and biotite define a weak foliation. There are anhedral cordierite grains (~1-3 mm) that are grey-blue in color
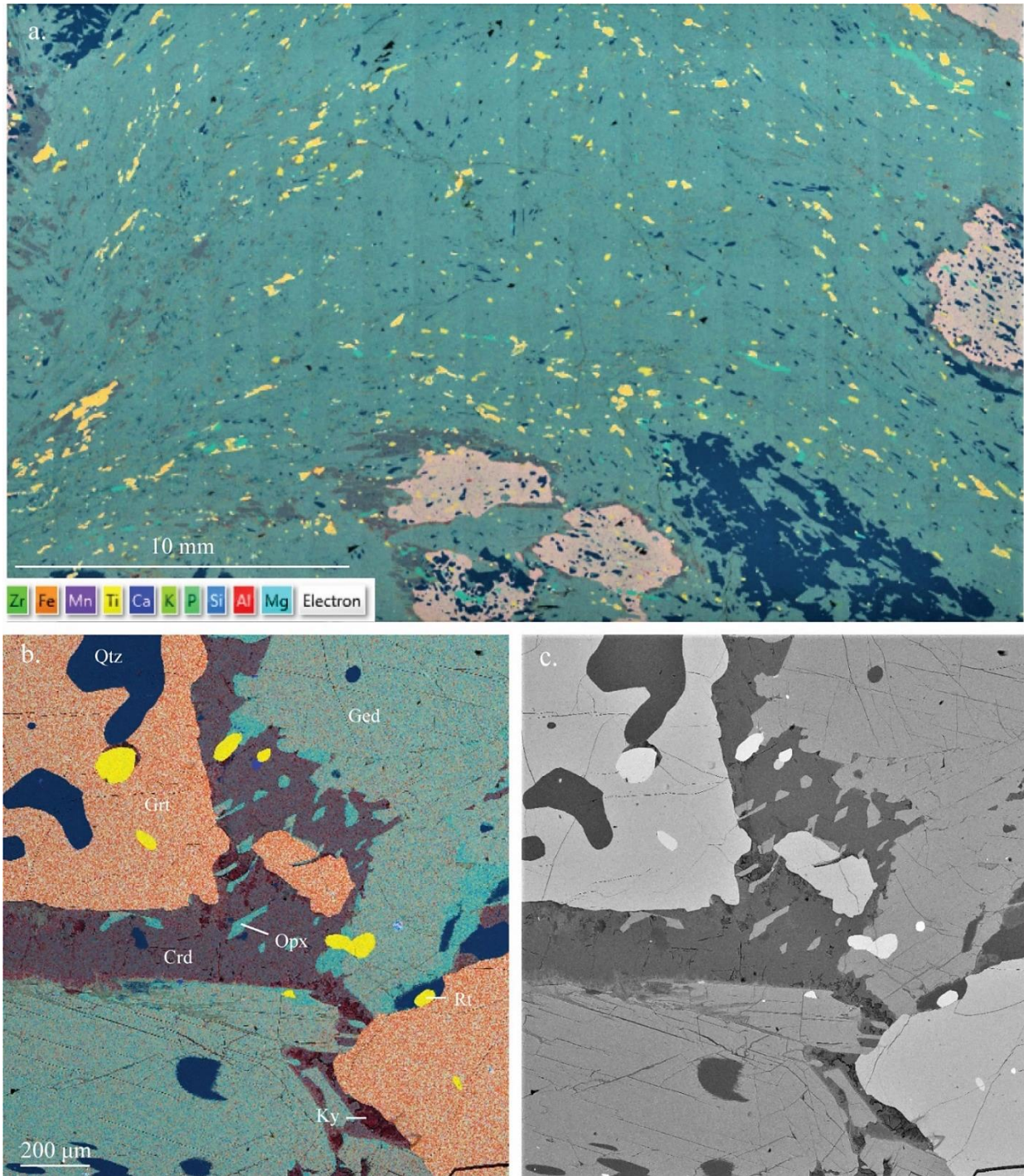
Figure 13. SEM-EDS thin section maps of RR-BC-03a. In the full section SEM-EDS scan (a), cordierite coronas can be seen around the garnet poikioblasts that reside in a groundmass of gedrite, orthopyroxene, quartz, and rutile. Closer EDS (b) and BSE (c) images reveal the symplectitic texture of some of the coronas that involve orthopyroxene, cordierite, and kyanite.
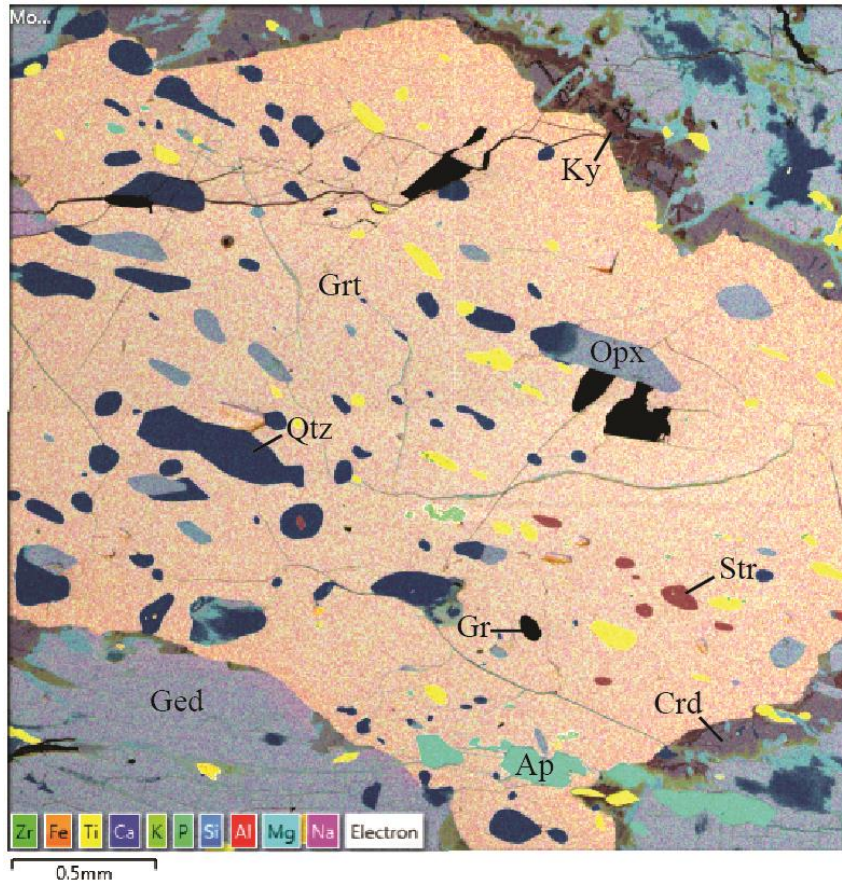
Figure 14. Additional SEM-EDS thin section image of RR-BC-03a showing the various inclusions and textures around a garnet porphyroblast involving kyanite (ky), orthopyroxene (opx), quartz (qtz), staurolite (str), cordierite (crd), apatite (ap), and graphite (gr).

alongside shapeless, white grains of plagioclase found interstitially between grains of anthophyllite, especially in areas proximal to garnets. In thin section, there is an abundance of remarkable textures involving moat phases, enclaves, polymineralic coronas, and symplectites (Figure 15). Generally speaking, the archetype of the symplectites observed is with kyanite at the "core" of the grain and either spinel, sapphirine, or corundum forming wormy intergrowths around it. The primary minerals found to be acting as a corona are plagioclase, cordierite, and

muscovite. The coronas of plagioclase typically lie closer to the interior of the reaction as the

"first" corona that formed and then coronas of cordierite typically surround the plagioclase.
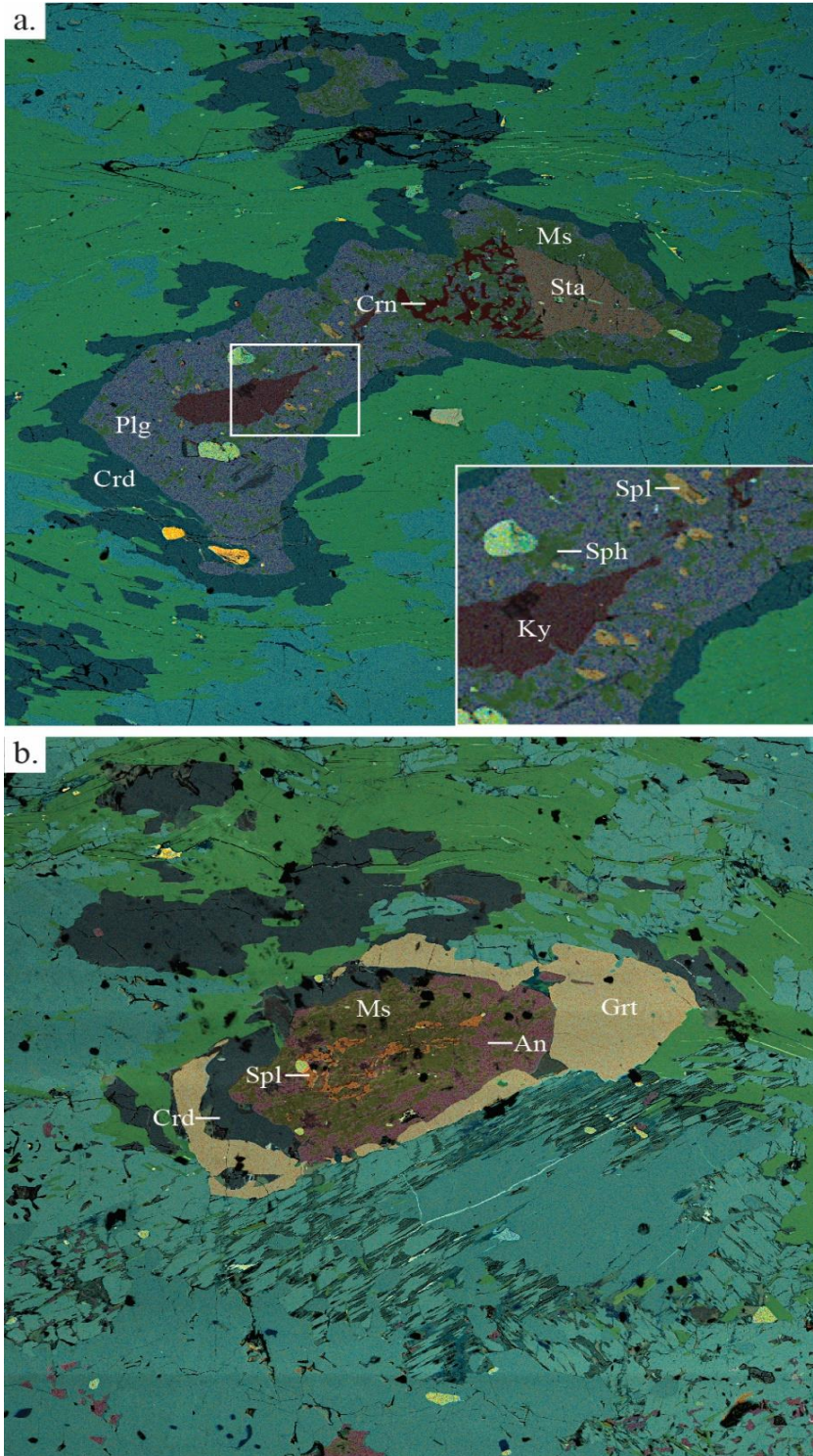
Figure 15. SEM-EDS thin section images of 14-MG-06b from the Stone Creek locality in the Ruby Range showing the polymineralic coronas and symplectite textures.

Highlands

HM-BC-01a: O' Neill's Gulch

HM-BC-01a is a coarse-grained schist dominated by light brown blades of gedrite (0.5-3.5 cm) and subhedral garnets (1-2 cm) that are light pink in color. Oxidation of the gedrite blades from weathering can give the sample an overall orange-brown color. The total assemblage includes gedrite, garnet, plagioclase, quartz, sillimanite, biotite, orthopyroxene, rutile, ilmenite, and apatite. In thin section, the poikiloblastic garnet grains are highly fractured and contain an amalgamation of small blades of orthopyroxene and gedrite surrounded by cordierite (Figures 16-18). Plagioclase is found in the areas around garnets filling the *interstitial spaces between*
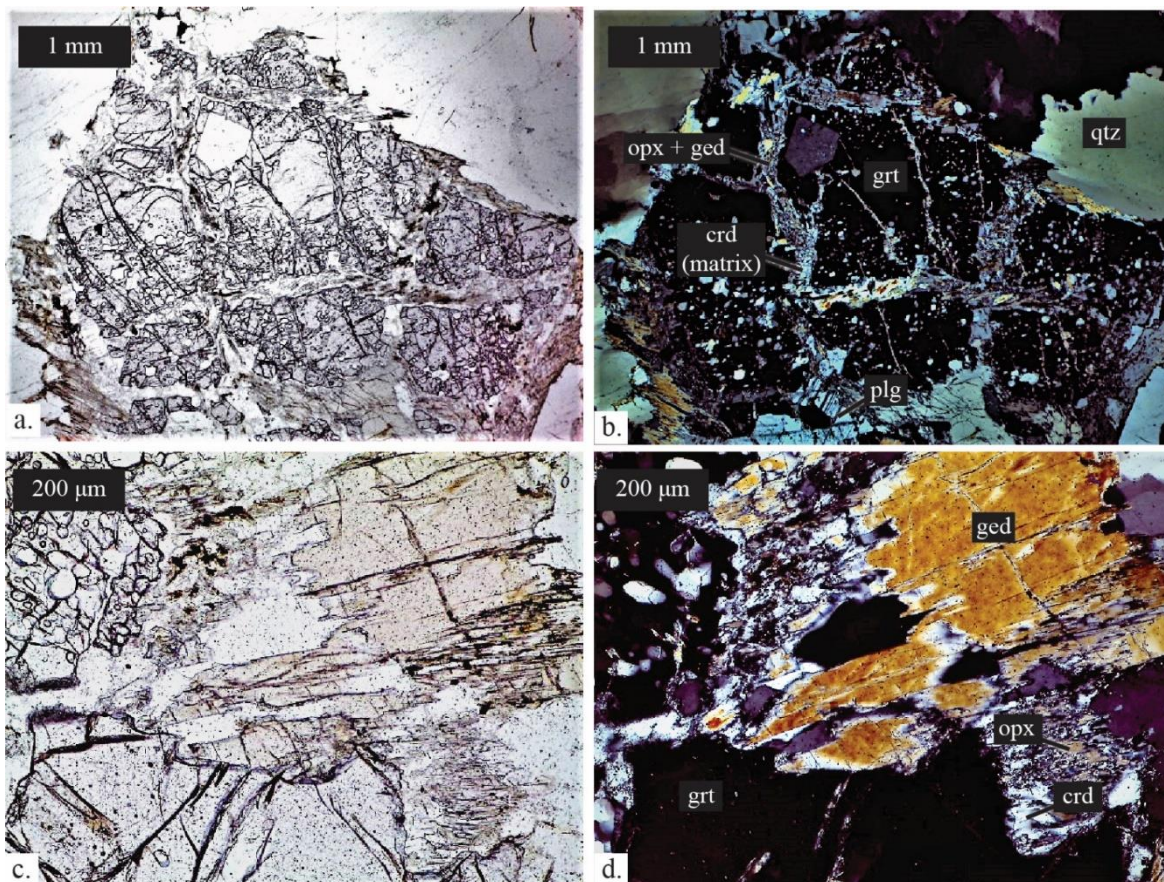
Figure 16. Photomicrographs of HM-BC-01a from O'Neill's Gulch in the Highland Mountains.

orthoamphibole, orthopyroxene, and cordierite. Plagioclase also forms abundant coronas around all the sillimanite grains in the section (Figures 17 and 18b).
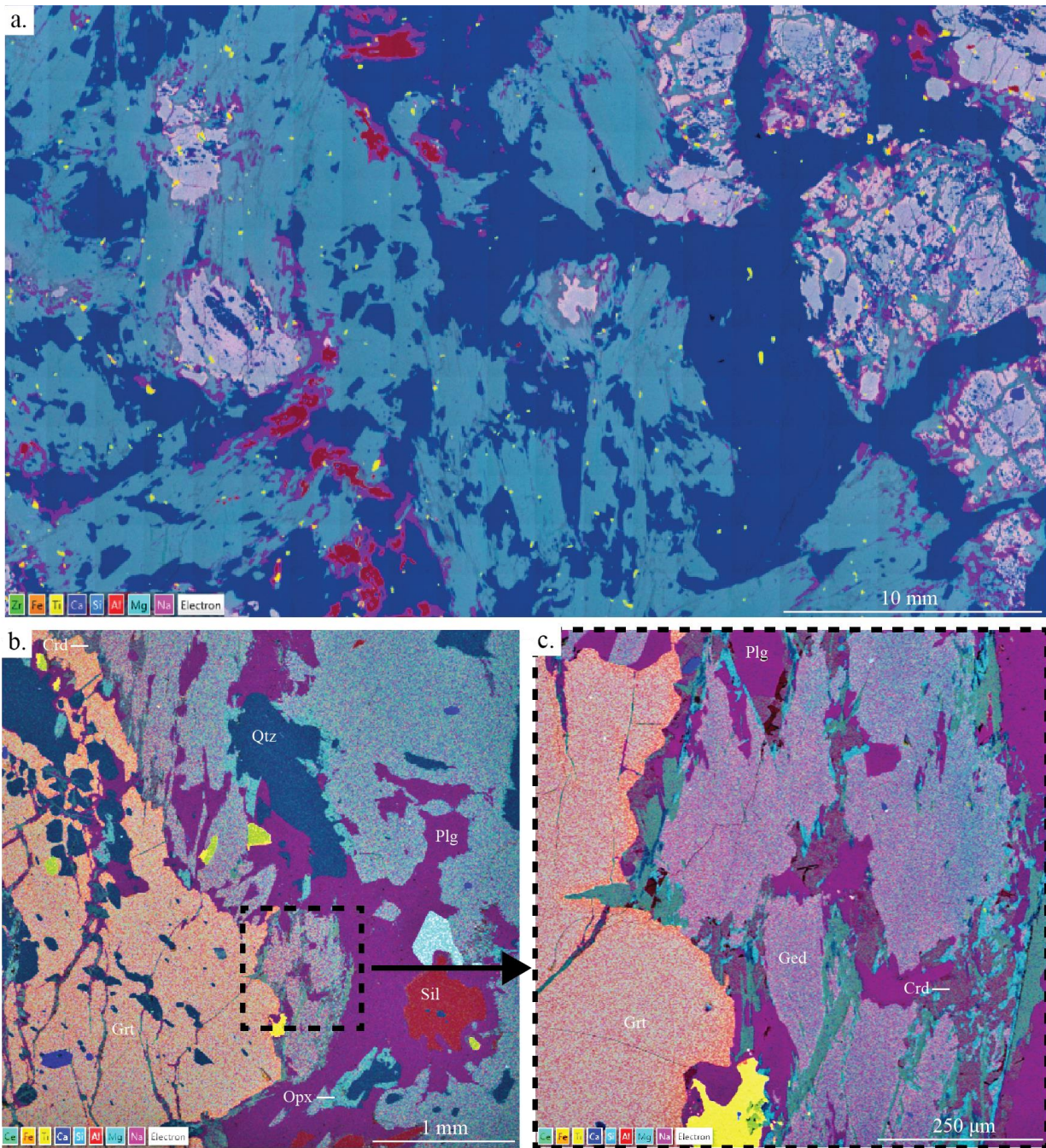
Figure 17. HM-BC-01a SEM and EDS images showing the full section scan (a) with coronas of plagioclase (purple) around sillimanite grains (red). Moat textures involving gedrite, cordierite, and plagioclase exist around the garnets (b and c).
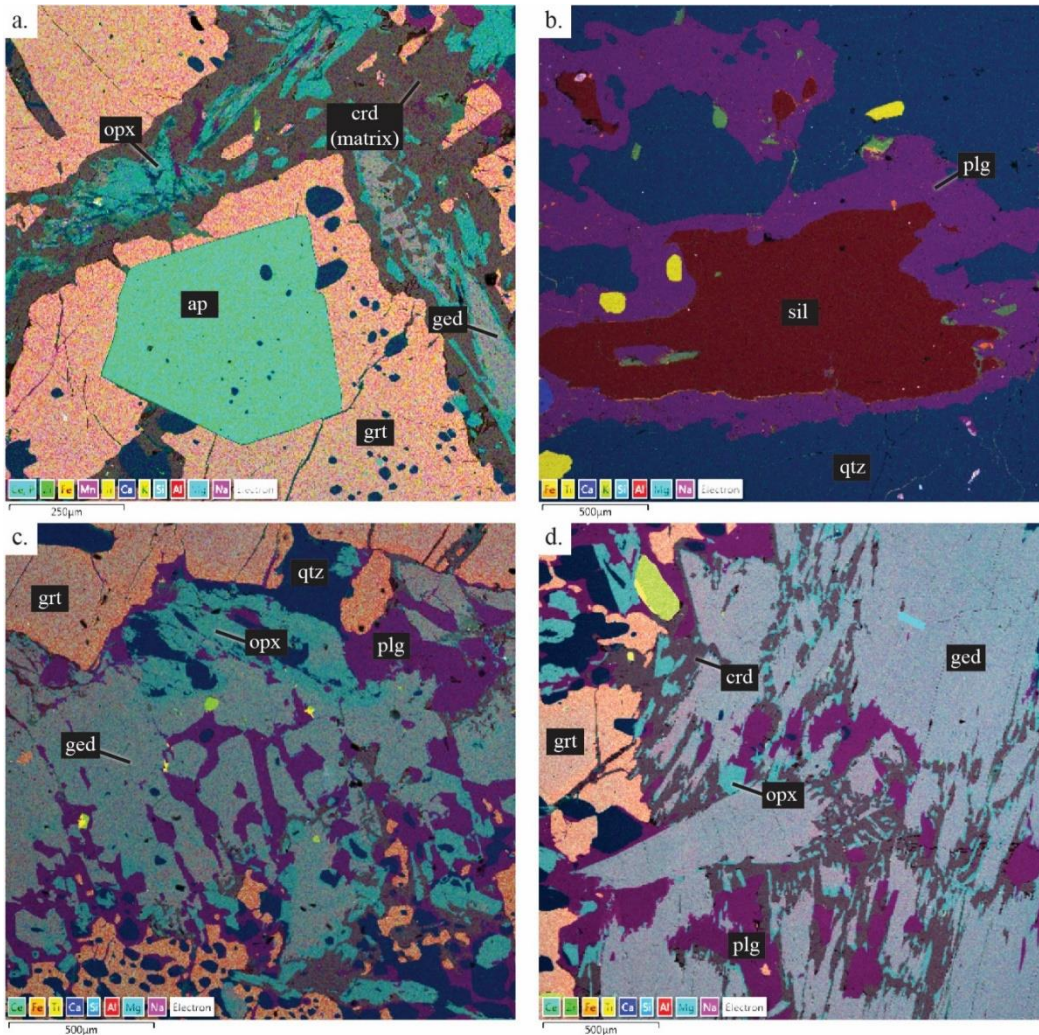
Figure 18. Additional HM-BC-01a SEM-EDS images displaying observed textures in the section including the moat phases within garnet fissures (a), plagioclase coronas around sillimanite (b), and intergrowth textures between gedrite, orthopyroxene, quartz, and cordierite (b and c).

18-HM-01: O' Neill's Gulch

18-HM-01 is a very similar in character to HM-BC-01a with the primary

exceptions being the lack of sillimanite, comparably, and it not having the same "microcosms"

within the fractures of the garnets. However, plagioclase forms coronas around garnet that display symplectitic intergrowth with the gedrite in the groundmass (Figure 19).
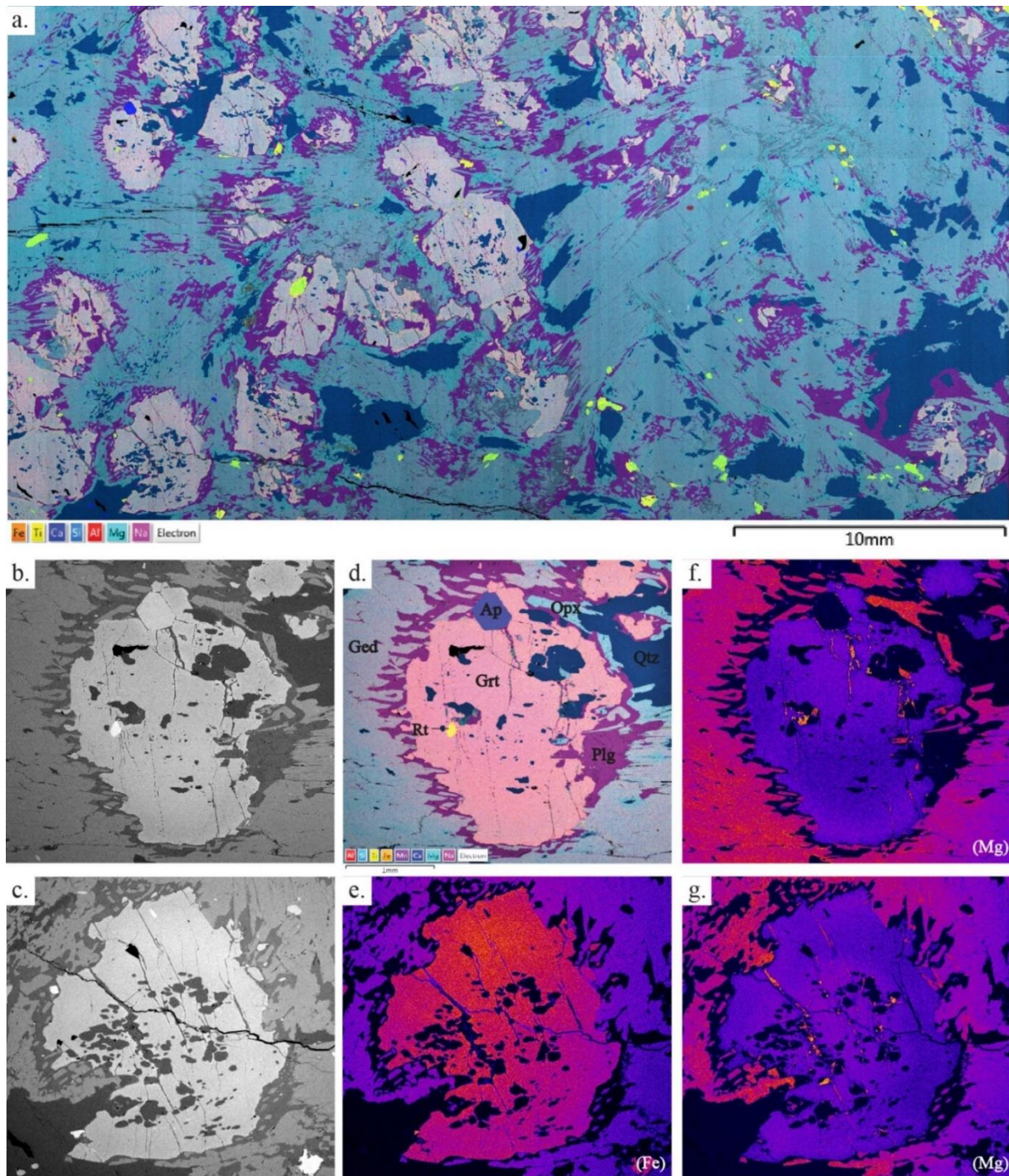
Figure 19. SEM-EDS maps of 18-HM-01 (a), with BSE and SEM-EDS images of notable textures associated with garnet (b,c,d), and Mg-Fe garnet maps showing any preferential zoning (f and g).

NP04: Nez Perce Gulch

NP04 is a very coarse-grained gedrite schist with blades of gedrite up to 4.5 cm. There are distinct leucocratic layers of garnet and quartz that are separated from the groundmass that is mainly gedrite. The total assemblage is comprised of gedrite, garnet, plagioclase, rutile, and ilmenite with minor amounts of apatite, chlorite, and orthopyroxene, and trace amounts of corundum. Plagioclase is found interstitially and associated with gedrite and garnet. Garnet porphyroblasts (<1.5 cm) contain an abundance of quartz inclusions and are surrounded by moats of plagioclase and partial to complete coronas of orthopyroxene.

Madison Range

MR-BC-03a: Ennis Lake

MR-BC-03a is a coarse-grained orthoamphibole schist with distinct lenses of leucosomes that contain garnet, quartz, and plagioclase (Figure 8). Dark brown to black blades of prismatic gedrite define foliation in the schistose parts of the sample. Garnets range from 3 mm – 2 cm in diameter. The distinct leucosomes pods can also be seen in thin section (Figure 20). The mineral assemblage includes gedrite, garnet, plagioclase, orthopyroxene, kyanite, quartz, rutile, biotite, and apatite, with trace amounts of corundum. The groundmass, or *schistose areas of the*

sample, is dominantly gedrite with minor amounts of rutile and apatite. In the leucosome areas of
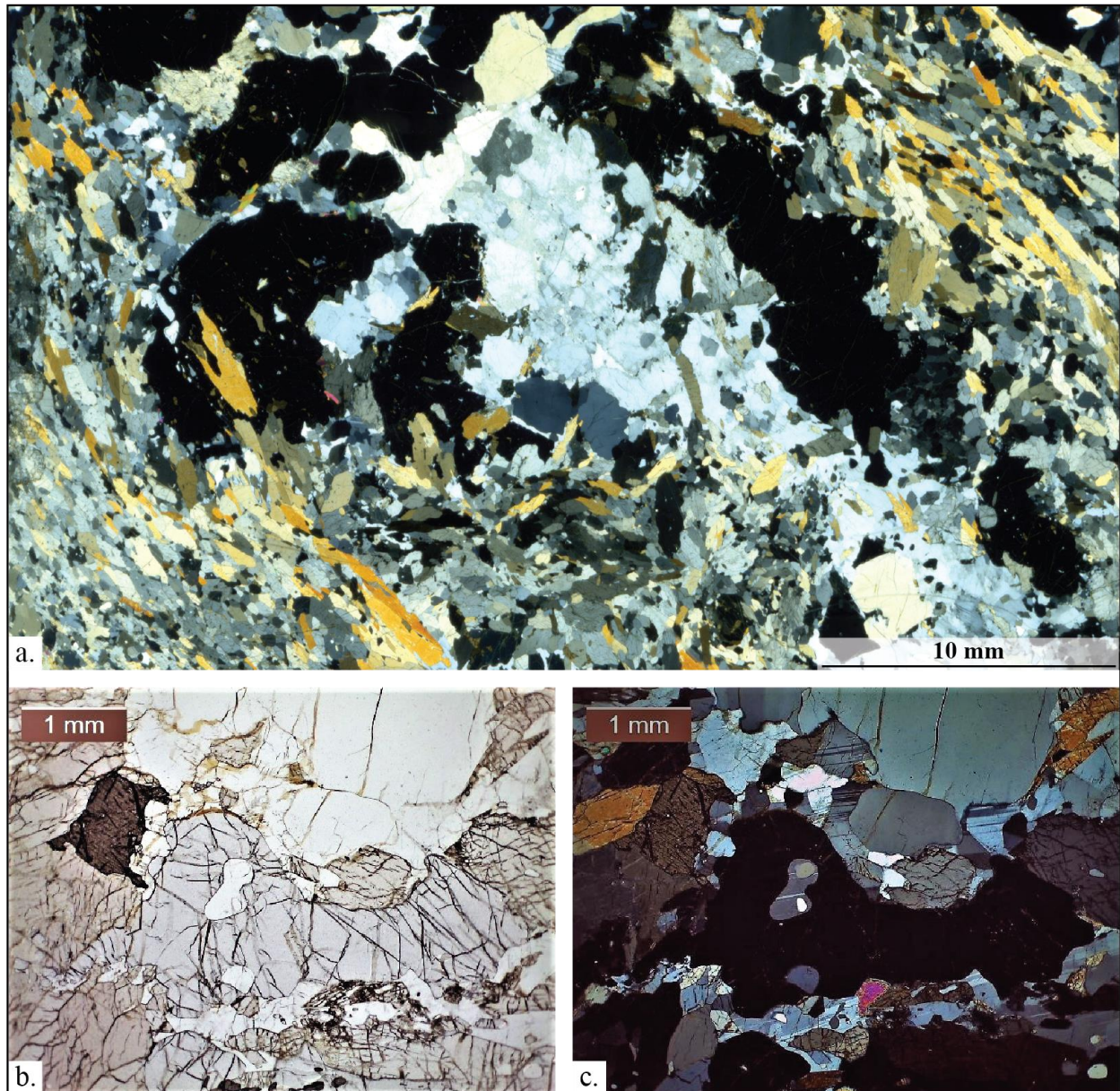
Figure 20. Photomicrographs of MR-BC-03a from the Ennis Lake locality in the Madison Range.

the thin section, plagioclase can be seen forming partial coronas around garnet (Figure 21). The

inclusions observed within garnet are rutile, quartz, plagioclase, gedrite, kyanite, and apatite.

They are oriented with respect to the foliation, suggesting post-kinematic growth.
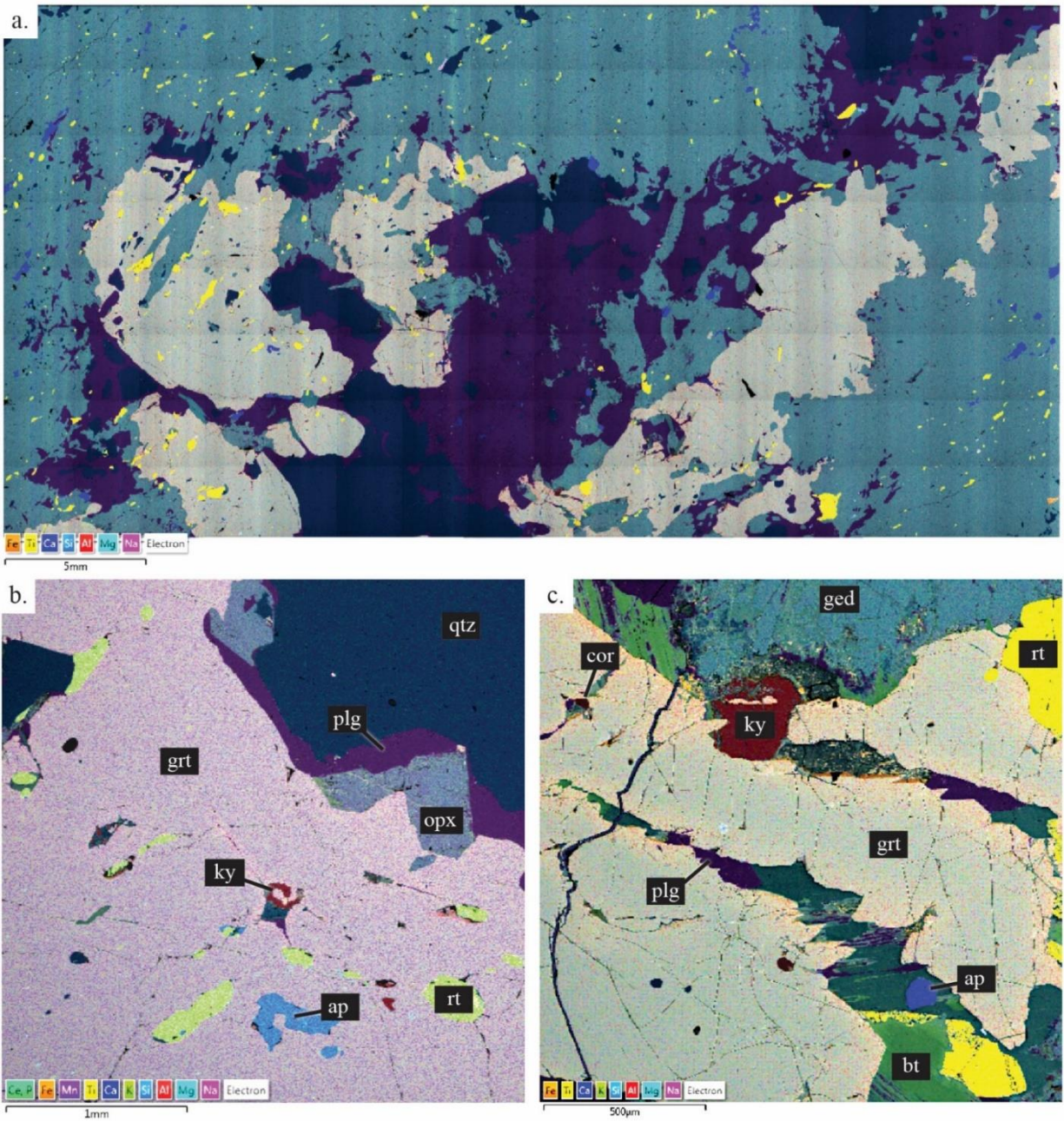
Figure 21. SEM and EDS images of MR-BC-03a showing the full section scan (a) that has a groundmass of gedrite with a leucosome containing garnet, plagioclase, and quartz going diagonally across the sample. Partial rims of plagioclase exist around the garnets (b), which tend to have inclusions of kyanite, rutile, and apatite (b and c).

Gravelly Range

20-JB-14

20-JB-14 is a fine-grained orthoamphibole gneiss with garnet, plagioclase, quartz, rutile, and ilmenite (Figure 22). Weathering can give the sample an overall orange tint. Dark brown to black orthoamphibole blades, 1-3 mm in length, define the foliation. Discrete (<1 mm) layers of plagioclase are interspersed throughout the sample parallel to foliation. In thin section, subhedral garnets (1-2.5 mm) show indications of synkinematic growth.
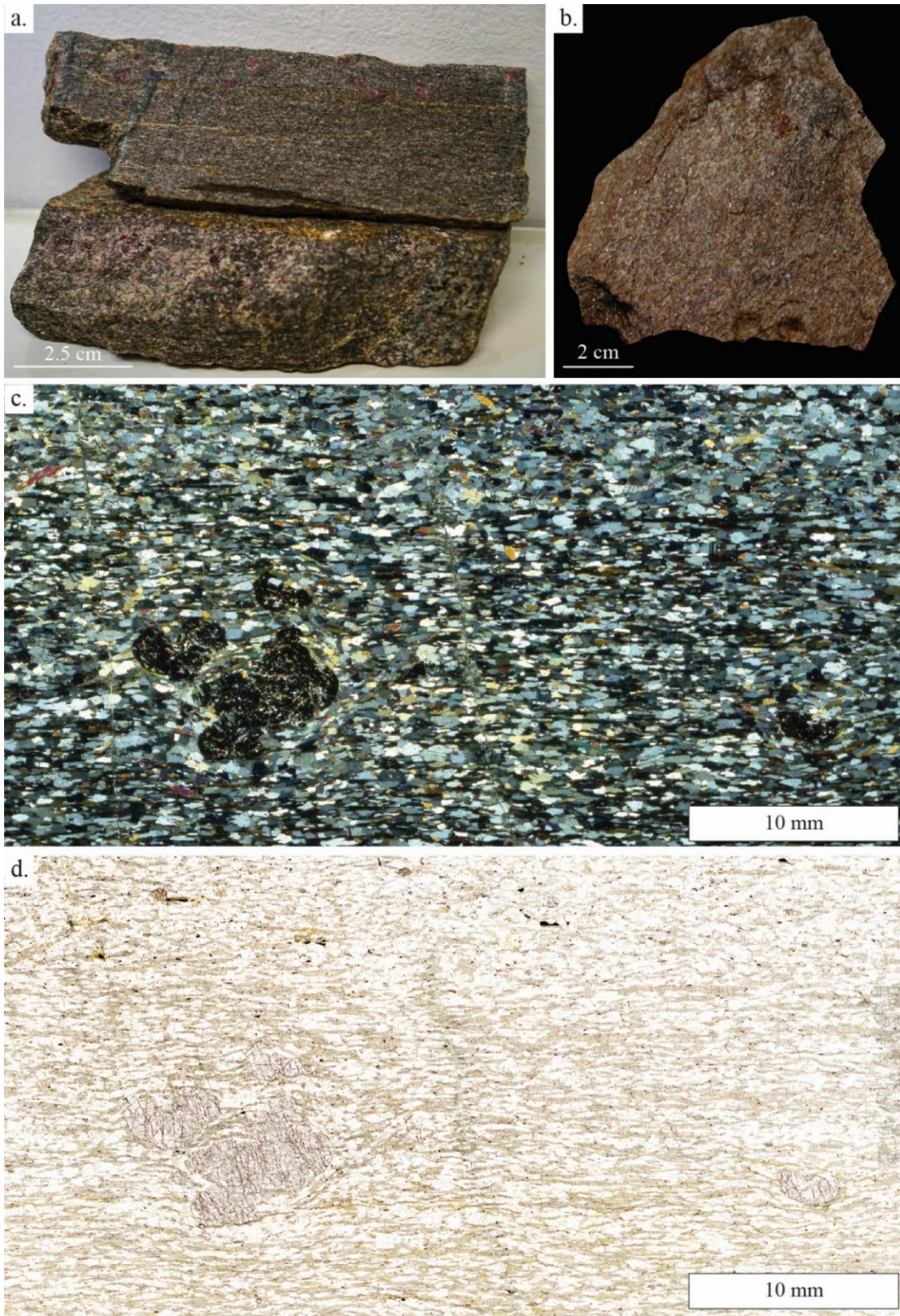
Figure 22. Hand sample images (a and b) and photomicrographs (b and c) of 20-JB-14 from the Gravelly Range.

4.3 Bulk rock chemistry and protolith classification

The XRF bulk rock geochemistry and ICP-MS trace element datasets were used in the software Geochemical Data Toolkit (Janoušek et al., 2006) to categorize the likely protolith material of COG. Among the samples selected, 9 were from the Ruby Range and 7 were from the Highland Mountains. In light of the comprehensive geochemical study done on COG from the Tobacco Roots by Burger et al., 2004, which includes 29 samples, only 3 samples from this study were used to supplement that overall data set. One representative sample was chosen from the Madison Range (MR-BC-03a). Notably, the bulk geochemistry for this sample was calculated from the spectrum of a full section SEM-EDS analysis instead of XRD. The results of these analyses can be seen in Tables 2-3. Using this data for tectonic discriminatory diagrams, major element classification diagrams, and REE plots allowed for a more comprehensive look into the likely petrogenetic origins of COG.

Sample	SiO$_2$	TiO$_2$	Al$_2$O$_3$	FeO	MnO	MgO	CaO	Na$_2$O	K$_2$O	P$_2$O$_5$
RR-BC-03a	55.09	1.55	13.87	16.38	0.05	11.38	0.74	0.51	0.27	0.16
RR-BC-03b	57.00	2.08	10.72	12.80	0.28	10.60	4.31	0.52	1.54	0.16
RR-BC-04a	51.05	1.65	14.83	14.45	0.06	15.41	0.68	0.95	0.72	0.20
RR-BC-05a	60.24	1.66	11.03	15.37	0.09	10.01	0.28	1.11	0.02	0.19
RR-BC-05b	60.93	1.41	12.09	13.72	0.05	10.25	0.33	0.98	0.02	0.22
RR-BC-05c	46.64	3.02	8.90	24.44	0.19	15.45	0.37	0.83	0.01	0.16
RR-BC-05d	53.90	2.53	4.09	20.21	0.16	17.66	0.68	0.37	0.00	0.39
RR-BC-06a2	59.53	1.58	12.62	15.05	0.08	9.72	0.47	0.64	0.01	0.30
17-SS-18	56.06	0.92	8.86	11.85	0.15	15.32	5.71	0.67	0.44	0.02
HM-BC-01a	58.16	0.67	13.99	11.09	0.11	13.64	1.15	1.07	0.02	0.09
HM-BC-01b	50.06	1.53	14.32	14.65	0.25	6.53	10.84	1.12	0.58	0.12
HM-BC-01c	56.83	0.63	13.45	10.57	0.17	9.28	7.72	1.12	0.14	0.09
HM-BC-02d	56.87	1.33	14.68	15.72	0.26	6.63	2.74	1.45	0.11	0.23
HM-BC-03a	58.10	1.79	14.48	14.68	0.21	6.40	2.15	1.93	0.17	0.10
18-HM-01	50.11	0.69	14.99	12.69	0.18	18.10	1.76	1.31	0.08	0.08
NP04	53.22	1.73	15.74	17.14	0.35	7.19	2.96	1.30	0.11	0.27
18-TR-01a	59.18	0.68	14.20	10.95	0.16	11.90	1.18	1.31	0.33	0.10
18-TR-06-1	61.86	0.58	13.14	10.39	0.10	11.44	0.41	0.40	1.64	0.05
18-TR-06-2	52.26	0.68	13.50	13.25	0.10	18.32	0.33	1.21	0.30	0.04
MR-BC-03a	54.80	1.30	17.80	13.50	-	11.10	0.80	3.30	0.10	-

Table 2. Normalized XRF bulk chemistry of major elements, expressed as a weight % oxide and normalized on a volatile-free basis, where Fe is expressed as FeO.

Sample	La	Ce	Pr	Nd	Sm	Eu	Gd	Tb	Dy	Ho	Er	Tm	Yb	Lu	Ta	Cs	Sc
RR-BC-03a	31.01	59.14	6.90	26.56	5.59	1.73	5.67	0.97	6.02	1.24	3.35	0.47	2.81	0.43	0.62	0.49	29.17
RR-BC-03b	16.90	34.43	4.40	18.38	4.63	2.12	4.94	0.82	5.08	1.02	2.72	0.38	2.33	0.36	0.58	0.22	27.22
RR-BC-04a	9.16	21.59	3.04	14.37	4.34	1.54	5.30	0.97	6.32	1.34	3.73	0.53	3.33	0.51	0.43	0.35	39.24
RR-BC-05a	37.25	71.45	8.34	32.32	7.33	1.72	7.89	1.49	9.57	1.93	5.14	0.71	4.20	0.62	0.63	0.10	29.93
RR-BC-05b	27.55	54.11	6.34	24.77	5.55	1.12	5.78	1.00	6.32	1.33	3.72	0.54	3.47	0.53	0.72	0.16	27.02
RR-BC-05c	60.84	113.59	13.17	50.80	11.07	1.72	10.95	1.81	10.75	2.16	5.53	0.78	4.83	0.72	0.75	0.06	45.96
RR-BC-05d	209.19	401.71	41.49	152.57	25.76	3.09	19.14	2.22	9.80	1.55	3.35	0.41	2.30	0.35	3.22	0.07	32.44
RR-BC-06a2	32.23	63.71	7.57	29.28	6.83	1.69	7.32	1.24	7.61	1.53	4.23	0.61	3.78	0.59	0.73	0.08	28.93
17-SS-18	14.76	42.68	6.33	27.71	7.04	2.22	6.11	0.89	4.85	0.88	2.23	0.31	1.82	0.26	1.10	0.15	18.44
HM-BC-01a	16.05	30.17	3.56	13.77	3.07	0.86	3.52	0.66	4.77	1.09	3.23	0.49	3.08	0.48	0.33	0.16	40.62
HM-BC-01b	7.95	18.00	2.73	12.84	3.83	1.35	4.80	0.84	5.47	1.14	3.03	0.44	2.69	0.40	0.28	0.08	44.35
HM-BC-01c	12.25	25.44	3.06	12.10	2.81	1.05	2.98	0.56	3.59	0.75	2.16	0.32	2.07	0.32	0.29	0.07	32.51
HM-BC-02d	20.56	40.78	4.93	19.97	4.80	1.34	6.16	1.07	6.31	1.25	3.21	0.44	2.68	0.40	0.39	0.14	33.96
HM-BC-03a	9.11	19.01	2.37	9.81	3.08	1.09	5.67	1.10	7.38	1.53	4.19	0.59	3.66	0.56	0.84	0.29	42.27
18-HM-01	11.99	25.92	3.24	12.88	3.47	0.84	4.27	0.73	4.36	0.88	2.48	0.38	2.44	0.40	0.31	0.21	52.08
NP04	22.56	47.98	6.12	25.19	6.00	1.87	6.68	1.18	7.12	1.39	3.61	0.49	2.89	0.43	0.62	0.20	33.73
18-TR-01a	13.11	25.74	3.04	11.65	2.77	0.77	3.29	0.68	4.85	1.09	3.21	0.49	3.15	0.48	0.47	0.59	31.67
18-TR-06-1	55.30	105.14	11.85	43.96	8.63	1.16	6.15	0.86	5.10	1.07	2.99	0.41	2.54	0.39	0.33	4.36	27.31
18-TR-06-2	15.70	30.09	3.43	13.08	2.71	0.35	2.71	0.43	2.75	0.62	1.84	0.28	1.79	0.29	0.46	0.83	34.77

Table 3. Rare earth element ICP-MS analyses expressed in ppm.

Due to the general absence of any fabric and the associated lithologies that COG is found interbedded with across the MMT, it is suspected to be igneous in origin and to have undergone late-stage hydrothermal alteration. To assess the effects of this in Precambrian volcanic rocks, COG was plotted using the Jensen cation plot (Jensen, 1976). This plotting scheme uses Fe, Ti, Al, and Mg instead of alkali elements or Ca, so that the effects of late-stage hydrothermal alteration can be negated. COG from the MMT show a bimodal distribution between tholeiitic and komatiitic compositions. Most of the samples from the Ruby Range fall under komatiitic while most of the samples from the Highlands are tholeiitic; although, there is a considerable portion of the Highlands data that fall under Komatiite as well (Figure 23). The Tobacco Roots
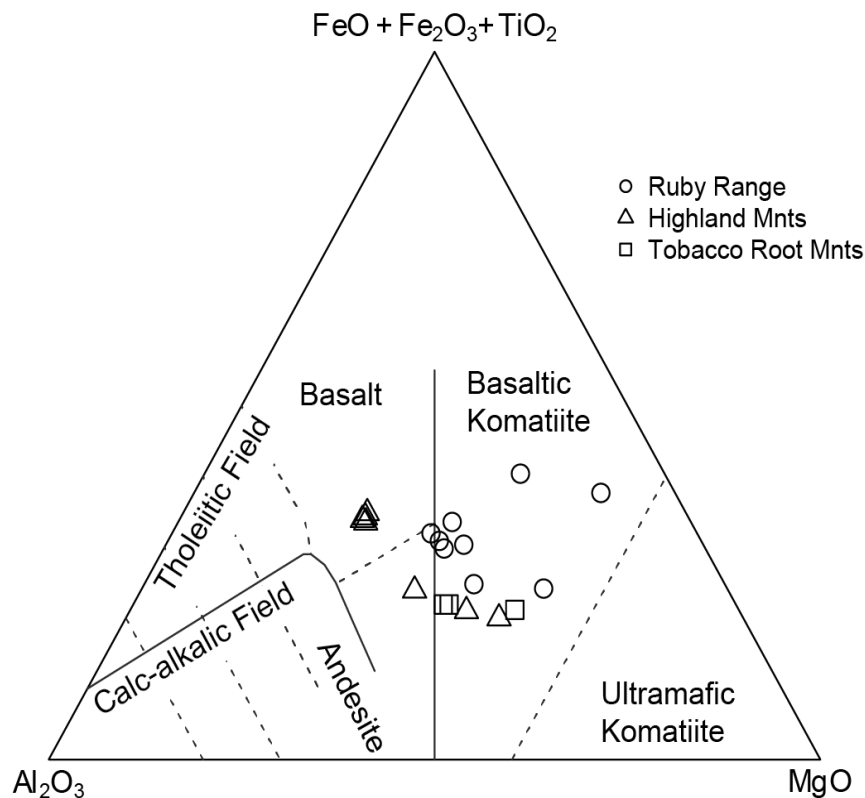
Figure 23. Cation plot for classifying subalkalic volcanic rocks by Jensen (1976).

samples from this study fall under the komatiite composition. However, only 3 of the 29 data points from the Burger study (Burger et al., 2004) plot in the komatiite field while the other 26 fall under tholeiitic. This is caused by slightly varying amounts of MgO content. For example, samples from the Ruby Range tend to have marginally higher amounts of MgO and slightly less Al_2O_3. However, in the case of the Tobacco Roots samples, including the Burger study, the cause of the disparity observed is attributed to the heterogeneity of the representative samples chosen.

One of the tectonic discriminatory diagrams used to examine COG is a ternary of MnO-TiO_2-P_2O_5 (Mullen, 1983), which is typically used to differentiate among basaltic rocks of oceanic environments. Notably, this plotting scheme filters data through a SiO_2 threshold of 45-55% which has excluded a considerable number of data points from the overall data set. However, the Tobacco Root and Highland Mountains samples both distinctly fall under island arc tholeiite. Two-thirds of the Ruby Range samples plot as either seamount tholeiites or seamount alkalic rocks, while the remaining third plots slightly into the mid-ocean ridge basalt field (Figure 24).

In the basaltic classification scheme that utilizes Zr-Ti ratios (Pearce, 1982), 88% of the samples from the Ruby Range classify as within-plate lavas and 100% of the Tobacco Root samples classify as island arc lavas (Figure 25). Interestingly, the Highland Mountains samples show an equal distribution across island arc lavas, MORB's, and within plate lavas (Figure 25).
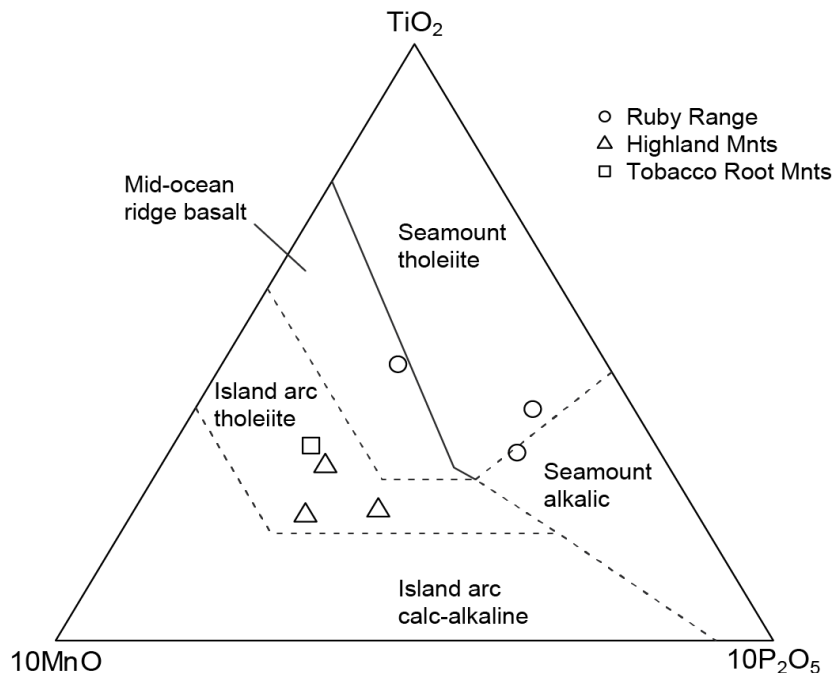
Figure 24. MnO-TiO2-P2O5 after Mullen (1983) for discriminating types of basaltic rocks from oceanic environments.
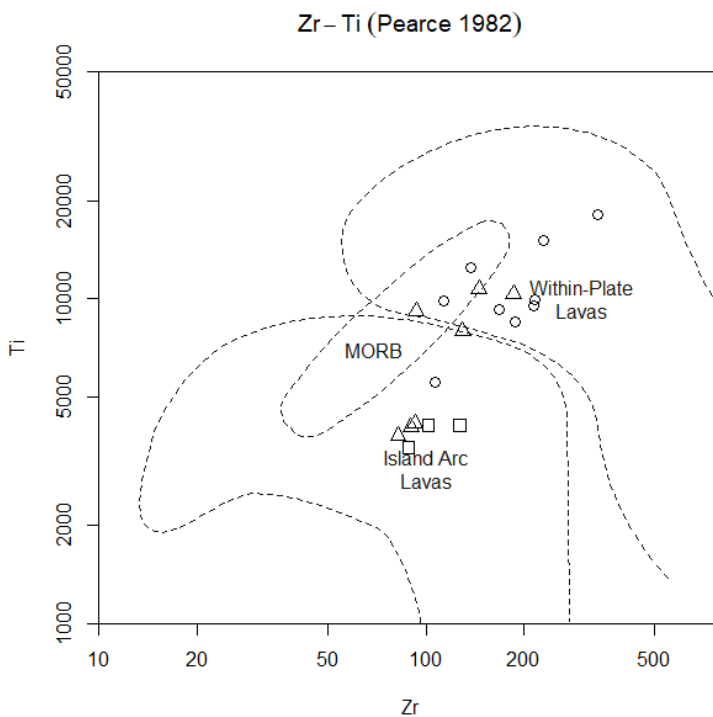
Figure 25. Basaltic protolith classification scheme by Pearce (1982) comparing Zr-Ti ratios.

Using a Ta/Yb-Th/Yb ratio plot devised by Pearce (Pearce, 1983) overlain with modern basalt fields (Condie, 1990), it can be seen that 14 out the 17 data points categorize as calc-alkaline basalts from a continental margin arc setting (Figure 26). Two of the three remaining data points have a slightly more enriched Th/Yb ratio which causes them to fall marginally outside of this boundary. The remaining "outlier" is from the Highlands and it slightly overlaps the fields between calc-alkaline basalts from continental margin arcs and within-plate basalts.
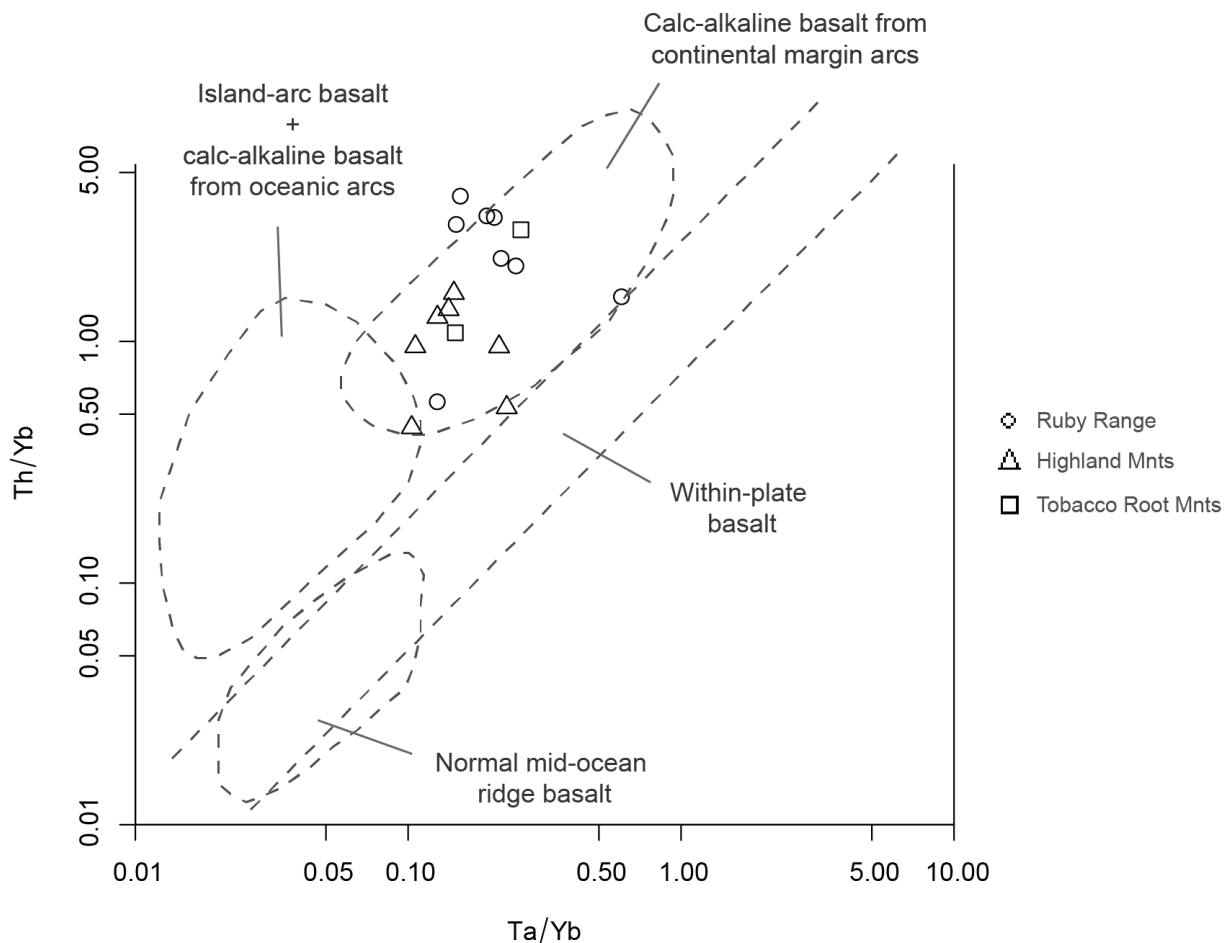
Figure 26. Basaltic protolith classification scheme by Pearce (1983) comparing Ta/Yb vs Th/Yb overlain with modern basalt fields (Condie 1990), where the majority of samples plot as continental margin arc basalts.

Figure 27 shows Mg/((Al + Na + K)/2) versus Ca/((Al + Na + K)/2) (Schumacher, 1988) and it projects the compositions of diopside, plagioclase, orthopyroxene, and olivine. A normal amphibolite composition plots as a mixture between plagioclase, diopside, and ferromagnesian minerals with no Ca. Using the amphibolite data from the Burger study (Burger et al., 2004), an average composition was calculated and is represented by the solid black data
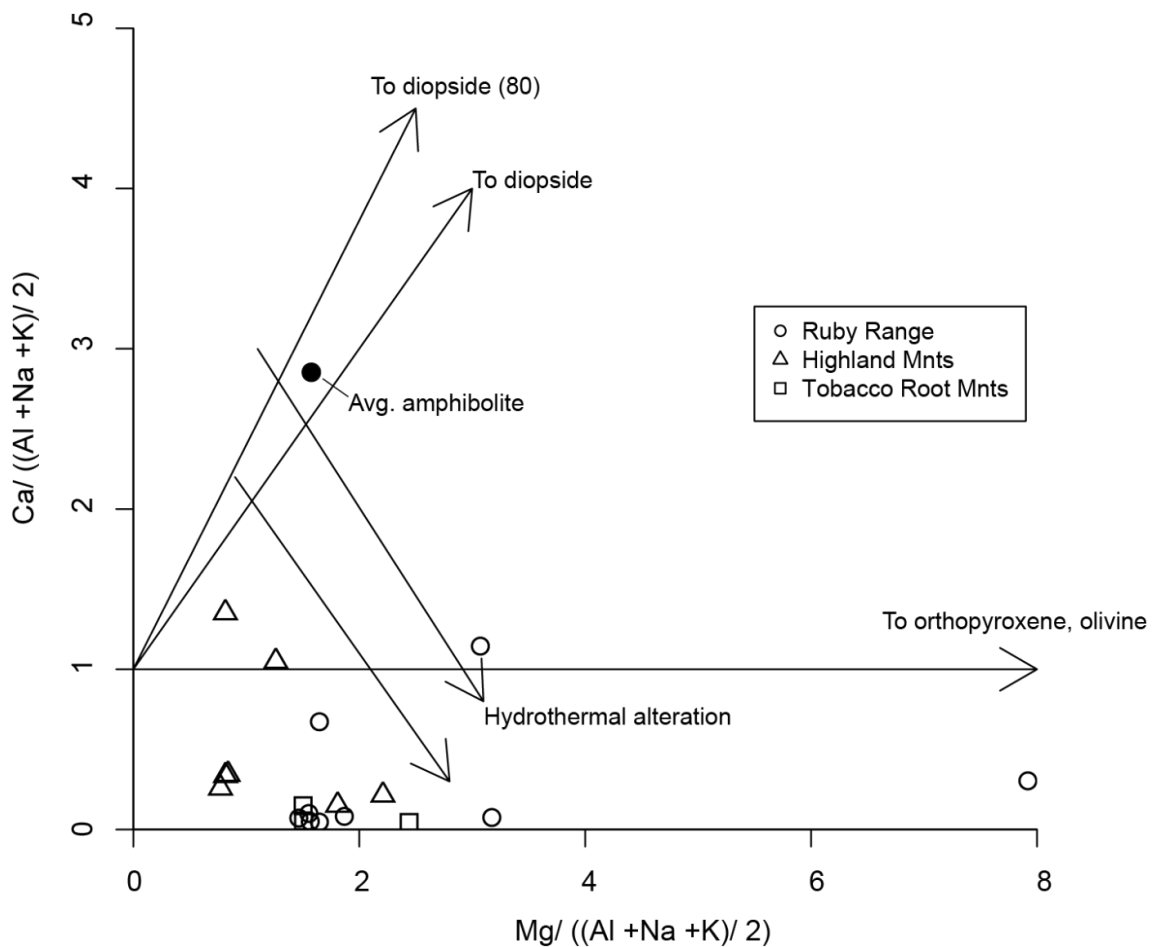
Figure 27. Major element diagram showing an average amphibolite sample from the Tobacco Root Mountains (data from Burger et al., 2004). It's consistent with mixtures of pyroxenes (i.e. diopside), plagioclase, and olivine. COG samples have noticeably lower Ca and higher Mg content, which is consistent with hydrothermal alteration of the protolith by seawater.

point. 84% of the COG samples plot below the plagioclase-orthopyroxene+olivine mixing line, with the remaining 16% falling right above this boundary. This is consistent with Ca depletion (by plagioclase dissolution) and precipitation of Al- and Mg-rich minerals during hydrothermal alteration of COG's protolith.

An additional geochemical trend that distinguishes COG from "normal" amphibolites is the correlation between the Ca depletion and Sr content, as amphibolites typically have compositions enriched in both Ca and Sr while COG does not. The Ca-Sr ratio of >300 is commonly representative of an intermediate plagioclase composition, which is assumed to be in the protolith of COG (Smith, 1974). However, approximately 90% of COG samples have a lower Ca-Sr ratio than this (Figure 28). The processes involved in hydrothermal alteration of a phase with a constant Ca-Sr ratio would cause data points to migrate closer to the origin of this figure. This is shown by the two primary mechanisms assumed to drive Ca depletion in COG, which can be seen illustrated on Figure 28. The first mechanism being the dissolution of clinopyroxenes, groundmass phases, and glass in the protolith and the second being the dissolution of plagioclase. In some rocks, these latter phases are exhausted before the dissolution of plagioclase is complete and this consequently causes them to plot close to the Ca/Sr ≈ 300 line. The position at which the data falls upon this line, away from the origin, thus indicates how much plagioclase is still remaining.
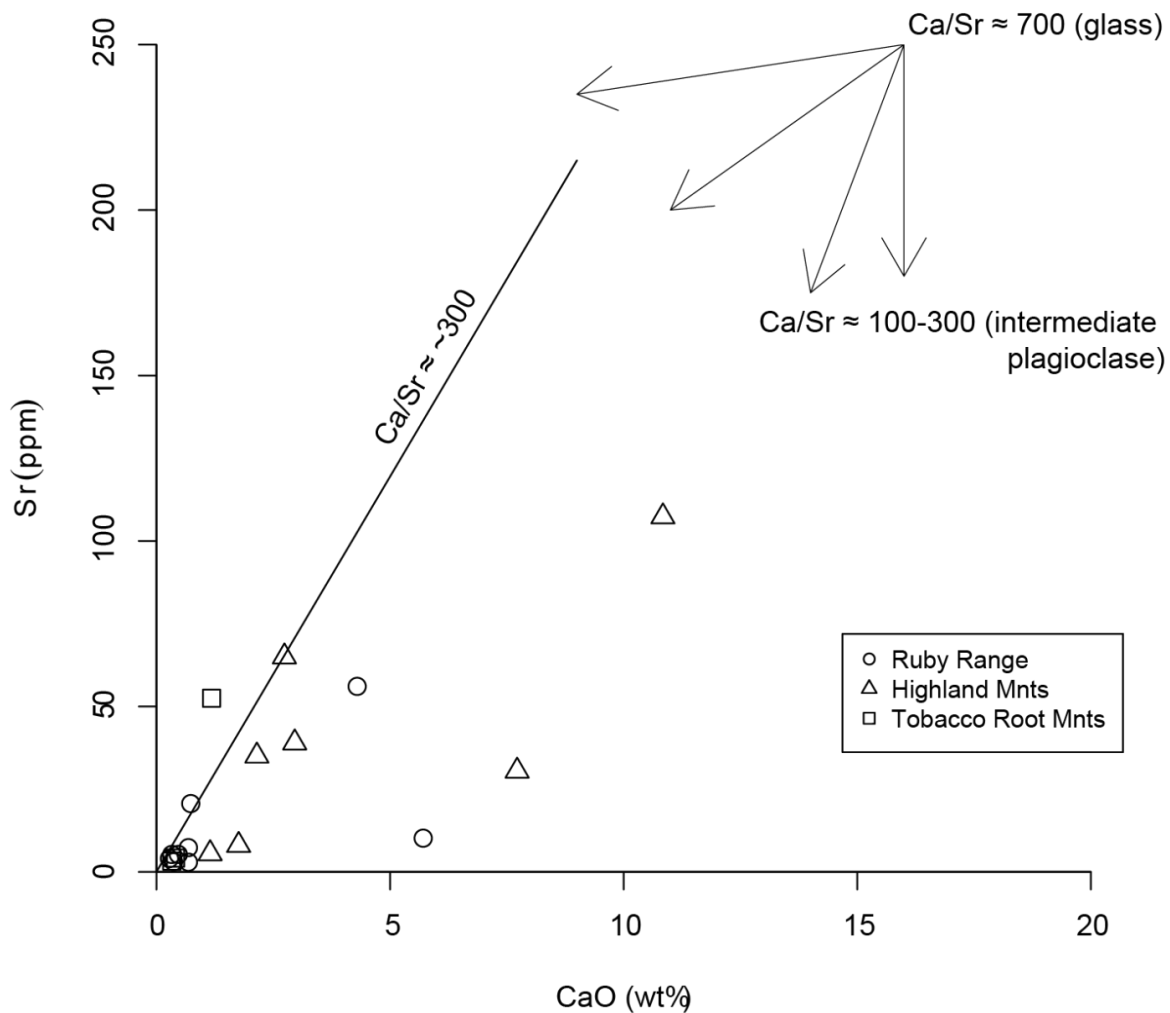
Figure 28. CaO (wt %) and Sr (ppm) diagram for COG samples. Dissolution of plagioclase, glass, or other groundmass phases during hydrothermal alteration of the protolith would cause rocks to move towards the origin point (0,0) of this diagram.

Overall, COG has considerably more mobile elements and MgO as compared to the associated amphibolites. Chondrite-normalized REE diagrams of COG display LREE enrichment and flat HREE to MREE profiles (Figure 29). There is also a prominent negative Eu anomaly, which is a characteristic identified in the REE profiles of other cordierite-orthoamphibole rocks around the world. This is a feature that has been attributed to plagioclase dissolution. Interestingly however, the associated amphibolites that COG is found interbedded with do not
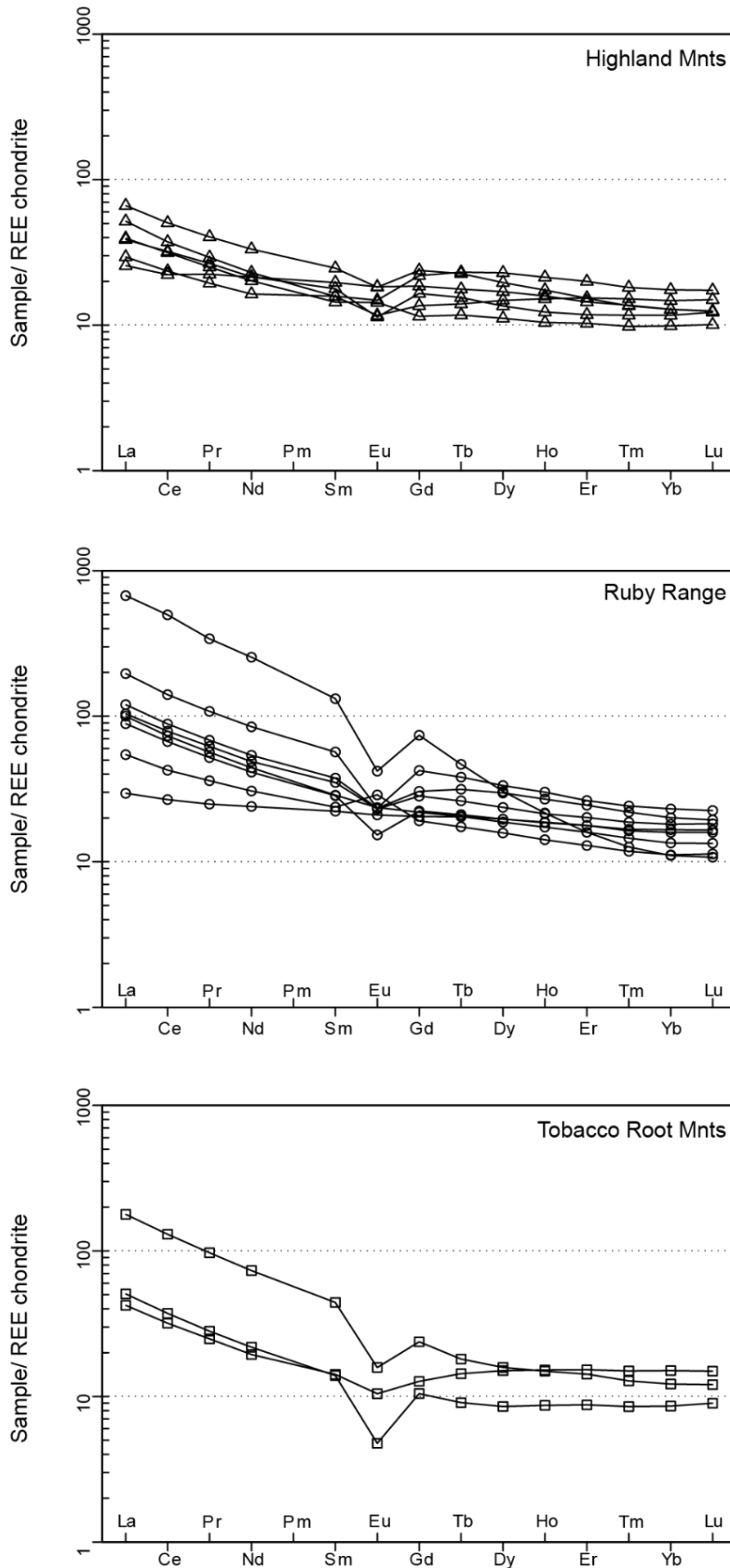
Figure 29. Chondrite-normalized rare earth element diagrams of COG showing prominent negative Eu anomalies. This is a characteristic that is not identified in the associated amphibolites that COG is found interbedded with, however the REE profiles of other cordierite orthoamphibole rocks around the world do display it. Chondrite concentrations from Boynton (1984).

display this. Samples with the lowest CaO content also show the largest negative Eu anomalies, which suggests the likely mechanism of depletion was plagioclase dissolution.

In summary, the majority of the geochemical trends point to COG having a basaltic protolith that is most likely a calc-alkaline basalt from an island arc setting. There is also strong evidence for dissolution processes and metasomatic alteration taking place given the negative Eu anomalies, the Ca-Sr values, and the geochemical comparison of COG with "normal" amphibolites.

4.4 Mineral chemistry

Representative mineral chemistry for samples RR-BC-03a, 18-TR-06, MR-BC-03a, and HM-BC-01a can be seen in Tables 4-9, where:

$X_{Fe} = Fe^{2+}/(Fe^{2+} + Mg)$

$X_{Mg} = Mg/(Fe^{2+} + Mg)$

$X_{Ca} = Ca/(Ca + Mg + Fe^{2+})$

$X_{An} = Ca/(Ca + Na + K)$

$X_{Ab} = Na/(Ca + Na + K)$

$X_{Al} = Al/(Al + Si)$

Sample Setting	18-TR-06 Core	18-TR-06 Rim	HM-BC-01a Core	HM-BC-01a Rim	MR-BC-03a Core	MR-BC-03a Rim	RR-BC-03a Core	RR-BC-03a Rim
SiO_2	40.20	41.17	38.48	37.86	39.16	39.30	39.86	38.51
TiO_2	0.00	0.00	0.00	0.00	0.00	0.00	0.00	0.00
Al_2O_3	22.82	23.47	21.71	21.42	22.43	22.63	22.64	21.78
Cr_2O_3	0.11	0.00	0.08	0.10	-0.04	0.02	0.01	0.01
FeO	20.54	24.29	28.79	29.91	26.40	27.95	27.70	30.73
MnO	0.25	0.33	1.23	0.78	0.34	0.42	0.09	0.16
MgO	13.82	12.41	6.61	6.38	10.50	9.73	9.92	7.34
CaO	0.99	1.13	2.53	1.68	0.66	0.66	0.64	0.70
Σ	98.73	102.80	99.43	98.13	99.45	100.71	100.86	99.23
Si	3.03	3.02	3.02	3.02	3.00	3.00	3.03	3.03
Ti	0.00	0.00	0.00	0.00	0.00	0.00	0.00	0.00
Al	2.03	2.03	2.01	2.02	2.03	2.03	2.03	2.02
Cr	0.01	0.00	0.00	0.01	0.00	0.00	0.00	0.00
Fe^{2+}	1.29	1.49	1.89	2.00	1.69	1.78	1.76	2.02
Mn	0.02	0.02	0.08	0.05	0.02	0.03	0.01	0.01
Mg	1.55	1.36	0.77	0.76	1.20	1.11	1.12	0.86
Ca	0.08	0.09	0.21	0.14	0.05	0.05	0.05	0.06
X_{Fe}	0.45	0.52	0.71	0.72	0.59	0.62	0.61	0.70
X_{Alm}	43.99	50.40	63.89	67.63	57.01	60.02	59.83	68.48
X_{Prp}	52.76	45.90	26.15	25.72	40.42	37.25	38.20	29.16
X_{Grs}	2.72	3.00	7.19	4.87	1.83	1.82	1.77	2.00
X_{Sps}	0.54	0.69	2.76	1.79	0.74	0.91	0.20	0.36

Table 4. Representative garnet SEM-EDS analyses.

Sample	18-TR-06	18-TR-06	HM-BC-01a	HM-BC-01a	MR-BC-03a	MR-BC-03a
Setting	near grt	near grt	sill corona	matrix	near grt	matrix
SiO$_2$	62.44	61.26	56.58	60.16	66.72	66.35
Al$_2$O$_3$	24.86	24.71	26.41	25.99	22.01	22.06
CaO	5.39	5.69	8.47	7.22	2.22	2.37
NaO	9.14	8.74	6.78	8.05	11.13	11.04
Σ	101.83	100.40	98.24	101.42	102.09	101.81
Si	2.71	2.70	2.57	2.64	2.86	2.85
Al	1.27	1.28	1.42	1.34	1.11	1.12
Ca	0.25	0.27	0.41	0.34	0.10	0.11
Na	0.77	0.75	0.60	0.68	0.93	0.92
X$_{An}$	24.58	26.46	40.84	33.14	9.93	10.60
X$_{Ab}$	75.42	73.54	59.16	66.86	90.07	89.40

Table 5. Representative plagioclase SEM-EDS analyses.

Sample	18-TR-06	18-TR-06	MR-BC-03a	MR-BC-03a
Setting	matrix	near grt	near grt	near grt
SiO_2	39.45	42.17	39.56	39.52
TiO_2	3.12	3.14	2.19	2.00
Al_2O_3	17.78	19.27	18.84	19.20
FeO	7.69	7.26	9.66	8.87
MnO	0.00	0.00	0.01	0.00
MgO	18.11	19.93	17.56	18.01
K_2O	8.75	9.39	8.89	8.75
CaO	0.00	0.00	0.07	0.04
Σ	94.90	101.16	96.71	96.35
Si	5.63	5.63	5.59	5.58
Ti	0.34	0.32	0.23	0.77
Al	2.99	3.03	3.14	3.19
Fe^{2+}	0.92	0.81	1.14	1.05
Mn	0.00	0.00	0.00	0.00
Mg	3.86	3.96	3.70	3.79
K	1.59	1.60	1.60	1.58
Ca	0.00	0.00	0.01	0.01
X_{Fe}	0.19	0.17	0.24	0.22

Table 6. Representative biotite SEM-EDS analyses.

Sample Setting	HM-BC-01a matrix	HM-BC-01a matrix	MR-BC-03a near grt	MR-BC-03a matrix
SiO_2	48.41	47.97	44.04	46.08
TiO_2	0.24	0.22	0.53	0.55
Al_2O_3	14.45	15.56	19.09	16.51
Cr_2O_3	0.11	0.13	0.00	0.01
FeO	12.62	13.58	17.26	17.15
MnO	0.08	0.10	0.10	0.11
MgO	19.78	19.40	16.20	17.07
CaO	0.55	0.51	0.16	0.17
Na_2O	1.23	1.37	2.02	1.76
Σ	97.47	98.84	99.40	99.41
Si	1.79	1.74	1.61	1.68
Ti	0.01	0.01	0.01	0.02
Al	0.62	0.67	0.82	0.71
Cr	0.00	0.00	0.00	0.00
Fe^{2+}	0.39	0.41	0.44	0.51
Mn	0.00	0.00	0.00	0.00
Mg	1.08	1.05	0.88	0.93
Ca	0.02	0.02	0.01	0.01
Na	0.09	0.10	0.14	0.12
X_{Fe}	0.26	0.28	0.37	0.36

Table 7. Representative orthopyroxene SEM-EDS analyses.

Sample	HM-BC-01a	HM-BC-01a	RR-BC-03a	RR-BC-03a
Setting	grt corona	grt corona	grt corona	grt corona
SiO_2	48.85	48.74	49.72	50.00
Al_2O_3	33.15	33.00	33.16	33.42
FeO	3.46	3.52	5.02	4.57
MgO	10.72	10.74	10.04	10.24
CaO	0.06	0.05	0.06	0.04
Na_2O	0.09	0.07	0.25	0.26
K_2O	0.04	0.05	0.06	0.05
Σ	96.37	96.17	98.31	98.58
Si	5.01	5.02	5.04	5.04
Al	4.01	4.00	3.96	3.97
Fe^{2+}	0.30	0.30	0.43	0.39
Mg	1.64	1.65	1.52	1.54
Ca	0.01	0.01	0.01	0.00
Na	0.02	0.01	0.05	0.05
K	0.01	0.01	0.01	0.01
X_{Fe}	0.85	0.84	0.78	0.80

Table 8. Representative cordierite SEM-EDS analyses.

Sample	18-TR-06	18-TR-06	HM-BC-01a	HM-BC-01a	MR-BC-03a	MR-BC-03a	RR-BC-03a	RR-BC-03a
Setting	matrix	near grt	matrix	near grt	within grt	matrix	matrix	within grt
SiO_2	49.44	47.46	48.35	49.17	45.34	46.59	48.41	48.42
TiO_2	0.43	0.39	0.28	0.12	0.54	0.56	0	0
Al_2O_3	14.68	16.68	15.65	13.68	17.33	16.43	12.96	16.12
Cr_2O_3	0.16	0.14	0.14	0.09	0	0	0.03	0
FeO	12.89	12.85	13.15	18.11	16.45	16.48	17.92	16.3
MnO	0.06	0.09	0.11	0.27	0.12	0.11	0.04	0.04
MgO	20.64	19.55	19.49	17.7	17.01	17.26	16.99	18
Na_2O	1.40	1.65	1.38	1.13	1.82	1.8	1.25	1.45
CaO	0.24	0.17	0.37	0.4	0.16	0.15	0.27	0.2
Σ	99.94	98.98	98.92	100.67	98.77	99.38	97.87	100.53
Si	6.733	6.547	6.666	6.809	6.387	6.512	6.889	6.651
Ti	0.044	0.04	0.029	0.012	0.057	0.059	0	0
Al	2.356	2.712	2.543	2.232	2.877	2.706	2.174	1.26
Cr	0.017	0.015	0.015	0.01	0	0	0.003	0
Fe^{2+}	1.468	1.482	1.516	2.097	1.938	1.923	2.133	1.872
Mn	0.007	0.011	0.013	0.032	0.014	0.013	0.005	0.005
Mg	4.191	4.02	4.006	3.654	3.572	3.597	3.605	3.686
Na	0.37	0.374	0.369	0.303	0.497	0.488	0.345	0.386
Ca	0.035	0.035	0.055	0.059	0.024	0.022	0.041	0.029
X_{Fe}	0.259	0.269	0.274	0.364	0.351	0.348	0.371	0.336

Table 9. Representative orthoamphibole SEM-EDS analyses.

Garnet in RR-BC-03a is $Alm_{0.59-0.68}Prp_{0.29-0.38}Grs_{0.01-0.02}Sps_{<0.01}$. There is a slight

enrichment of Fe and Mn towards the rim, where X_{Fe} ranges from 0.61 (core) to 0.7 (rim). X_{Mg}

decreases from core to rim, ranging from 0.39 (core) to 0.30 (rim) and there is no zoning or

change observed in X_{Ca}. There is a high Al content in the orthoamphibole present, with X_{Al} that

ranges from 0.16-0.24, which suggests the orthoamphibole end-member present is gedrite. The

composition of the gedrite found as inclusions in garnet is considerably more enriched in Mg,

with X_{Mg}= 0.53 (avg), while for the gedrite found in the matrix X_{Mg} =0.45 (avg).

Garnet in 18-TR-06 is $Alm_{0.44-0.50}Prp_{0.45-0.52}Grs_{0.02-0.03}Sps_{0.01}$. X_{Fe} increases from core to

rim ranging from 0.45-0.52. There is no zoning or change observed in X_{Ca}. X_{Mg} decreases from

core to rim, going from 0.55 to 0.48. Biotite in the matrix shows slightly elevated X_{Fe} content at

0.30 whereas biotite adjacent to, or included in, garnets has X_{Fe}= 0.25. The orthoamphibole

present is gedrite and shows no significant chemical variations dependent on setting, with a

range of X_{Mg} = 0.60-0.62. The plagioclase present, which is almost entirely associated with

zones that have reaction textures and moats involving garnet, is X_{An} = 0.38 and X_{Ab} = 0.61.

The garnet in HM-BC-01a is $Alm_{0.49-0.67}Prp_{0.25-0.40}Grs_{0.04-0.12}Sps_{0.01-0.04}$. X_{Ca} shows a slight

decrease from core to rim, ranging from 0.13 (core) to 0.05 (rim). The orthoamphibole end-

member present is gedrite. X_{Mg} values for gedrite associated with garnet have a composition of

X_{Mg}= 0.49-0.52, while the gedrite found in the groundmass is X_{Mg}= 0.58-0.60. The grains in the

groundmass are X_{Fe}= 0.40 (avg), the ones in the cracks of the garnet are X_{Fe}= 0.45 (avg), and the

grains associated with the garnet coronas are X_{Fe}= 0.49 (avg). The gedrite within the cracks of

garnet show significant Al zoning from one end of the grain to the other. In the posterior part of

the gedrite grain which is closer to the interior of the garnet, X_{Al} = 0.35, which suggests a

composition that borders anthophyllite. Then within the exterior portion of the gedrite grain

which is more proximal to the edges of the garnet, $X_{Al} = 0.43$. This gedrite within the moats also shows a significant reduction in Ti content as compared to that of the groundmass, where Ti= 0.14 on average (moats) and 0.29 on average for those in the groundmass. The composition of the plagioclase that forms coronas around sillimanite is $X_{An} = 0.55$ and $X_{Ab} = 0.45$, on average. The composition of plagioclase in the groundmass is $X_{An} = 0.51$ and $X_{Ab} = 0.50$, on average. The X_{Fe} of the orthopyroxene in the sample is 0.40 on average and 0.23 on average for the cordierite.

The garnet of MR-BC-03a is $Alm_{0.56-0.60}Prp_{0.37-0.41}Grs_{0.01-0.02}Sps_{<1}$. There are no significant compositional zoning trends exhibited in the garnet. The orthoamphibole end-member present is gedrite, with $X_{Fe} = 0.48-0.49$ and $X_{Mg} = 0.50-0.51$. The plagioclase in the sample is mostly albite with an overall average of $X_{An} = 0.17$ and $X_{Ab} = 0.83$. The X_{Fe} is 0.51 on average for orthopyroxene present. The biotite in the sample shows a notable decrease in Ti content and increase in Fe content within grains that are inclusions in garnet as compared to grains in the groundmass. Ti content decreases from 2.21 to 1.42 and Fe increases from 8.87 to 11.89. $X_{Fe} = 0.33$ for the groundmass biotite and increases to 0.41 for the inclusions in garnet.

4.5 Phase equilibria modeling

Samples RR-BC-03a, 18-TR-06, HM-BC-01a, and MR-BC-03a were modeled with the bulk rock chemistry using Theriak-Domino (De Capitani and Petrakakis, 2010). Two influential aspects of the modeling process which have the potential to greatly affect the accuracy of the output and should be considered when examining the resulting pseudosections are water content and melt loss. In order to calculate the pseudosections, the water content had to be adjusted to reflect the water content of the rock during metamorphism. Thus, with the bulk chemistry of any given sample, iterative calculations were run with continually adjusted values

for the water content until the resulting section was stable. The resulting pseudosections and associated isopleths can be seen in Figures 30-37.

T-X_{H2O} diagrams were used to guide the adjustments in lieu of the LOI data from the XRF analysis. The overall H_2O content in XRF analyses represents the structural water in the sample and it also incorporates other elements such as fluorine and chlorine from micas, for example. Moreover, it represents the remaining water content of the rock after it has potentially undergone melting, melt loss, and post-cooling recrystallization. The rock during prograde metamorphism, before partial melting and melt-loss, would have had a higher water content. This causes the model in Theriak-Domino to require more water in order to run than the LOI values report.

RR-BC-03a

The peak assemblage of this sample is anth + grt + bt + opx + ky + ru + qtz and occurs over 6.0-7.5 kbar and 560-615 °C (Figure 30). The mol fraction almandine isopleths, referred to as Grt (alm) on the diagrams, range from 0.59-0.63 within this field which is consistent with the observed mineral chemistry values of 0.59-0.68 (Figure 31). The X_{Mg} content in the orthoamphibole present, referred to as Oamp (#Mg) on the diagrams, ranges from 0.43-0.53 and is slightly lower than the isopleth range of 0.62-0.66. The absence of plagioclase in this sample is also consistent with the isopleth projections. The percent almandine composition observed in the rim of garnet is 0.68, on average, which aids in defining retrograde path conditions to roughly 5.0-6 kbar and 550-600 °C. In summary, these results suggest a clockwise

P-T path with peak conditions of 6.0-7.5 kbar and 560-615 °C with retrograde conditions of

approximately 5.0-6.0 kbar and 550-600 °C.

Figure 30. Pseudosection for RR-BC-03a, showing the max P-T field corresponding to the samples assemblage highlighted in orange.
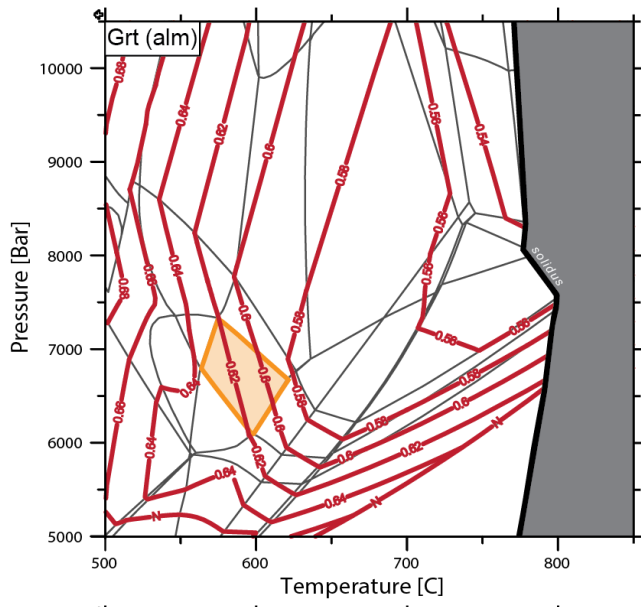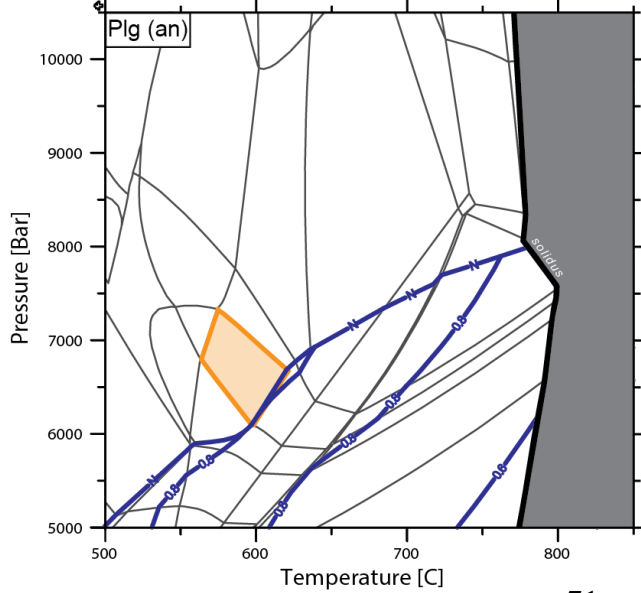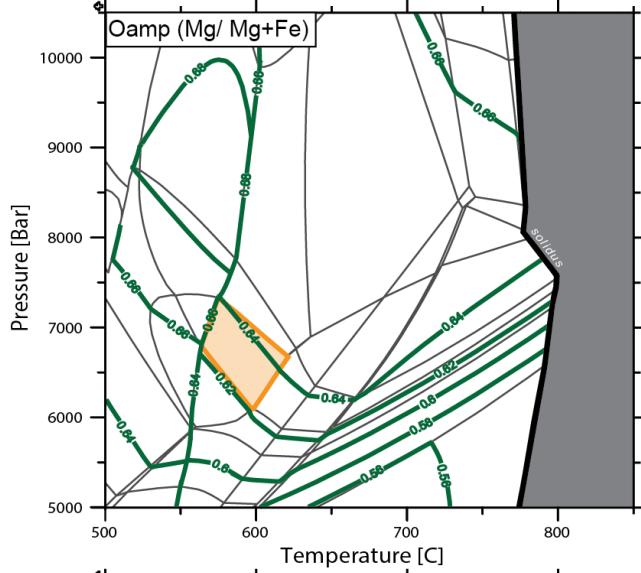
Figure 31. Isopleths for RR-BC-03a based on SEM-EDS sourced mineral chemistry.

18-TR-06

The peak assemblage is anth + grt + opx + plg + bt + ru + qtz and occurs from 8.6-10.5 kbar and 715-830 °C (Figure 32). The percent almandine isopleth ranges from 0.39- 0.42 which is slightly lower than the mineral chemistry that ranges from 0.45-0.52 (Figure 33). The X_{Mg} content in the orthoamphibole ranges from 0.60-0.62 which is slightly lower than the modeled isopleth range of 0.72-0.75. The plagioclase mineral chemistry and isopleth values show considerable difference in this section. The composition of the observed mineral chemistry is $X_{An} = 0.37$-0.39 which is much higher than the isopleths which range from 0.1-0.2. Since there are no isopleths that directly align with the observed mineral chemistry, constraining the retrograde conditions cannot be done with accuracy. In summary, these results suggest peak P-T conditions of 8.6-10.5 kbar and 715-830 °C for the Tobacco Roots.

HM-BC-01a

The peak assemblage for this sample is anth + grt + opx + plg + sill + bt + ru + qtz and occurs from 7.8-8.9 kbar and 700-775 °C (Figure 34). The percent almandine isopleth ranges from 0.41-0.48 which is very close to the mineral chemistry that ranges from 0.49-0.67 (Figure 35). The X_{Mg} content in the orthoamphibole ranges from 0.40-0.60 which is slightly lower than the modeled isopleth range of 0.70-0.74. The plagioclase composition from the mineral chemistry is $X_{An} = 0.47$-0.56, which is consistent with the modeled isopleths that range from 0.5-0.7. In summary, these results suggest peak P-T conditions of 7.8-8.9 kbar and 700-775 °C for the Highland Mountains.

Figure 32. Pseudosection for 18-TR-06, showing the max P-T field corresponding to the samples assemblage highlighted in orange.

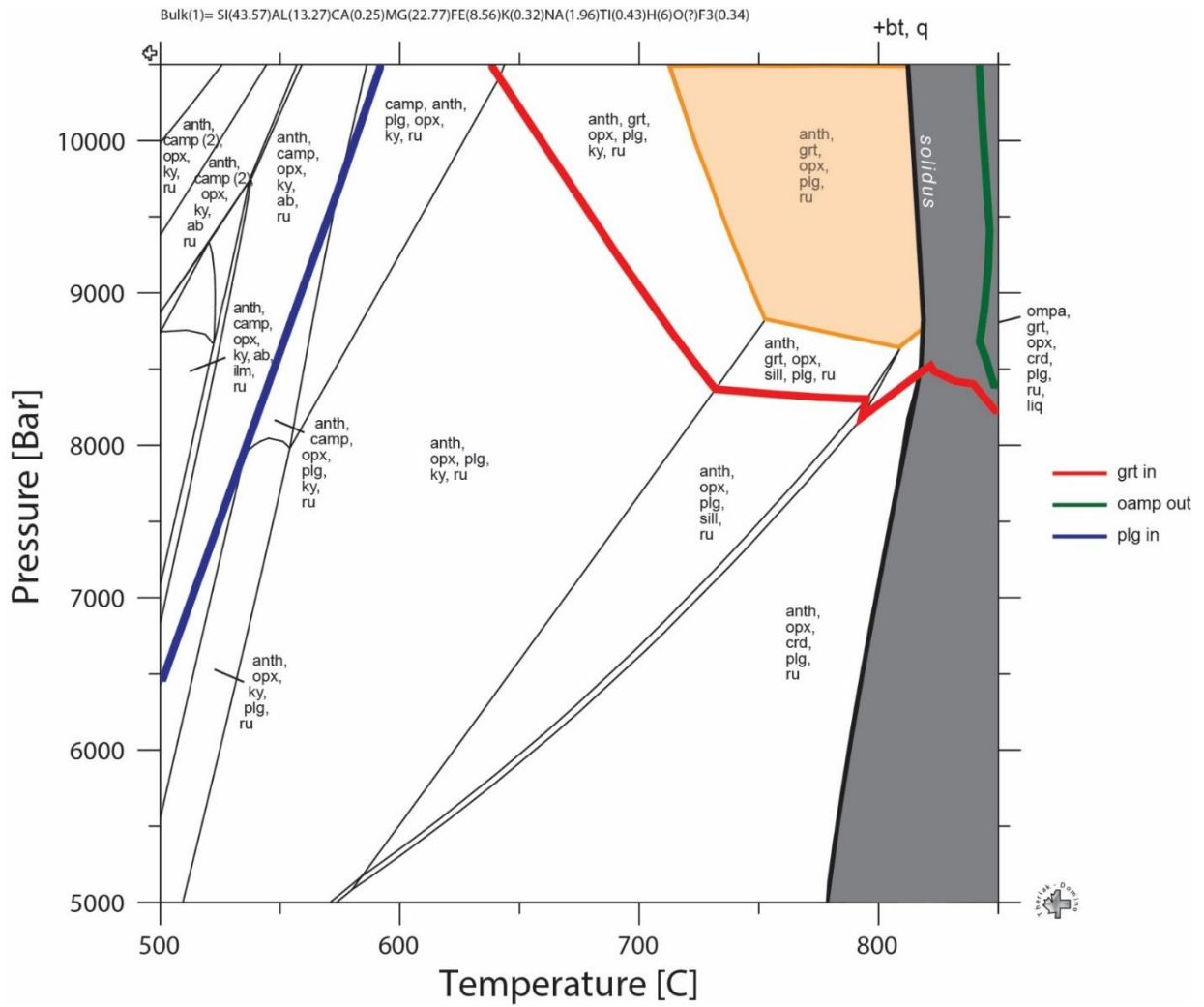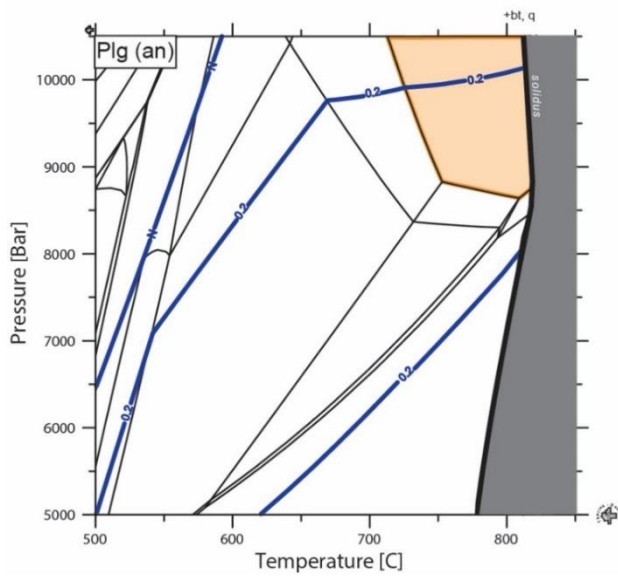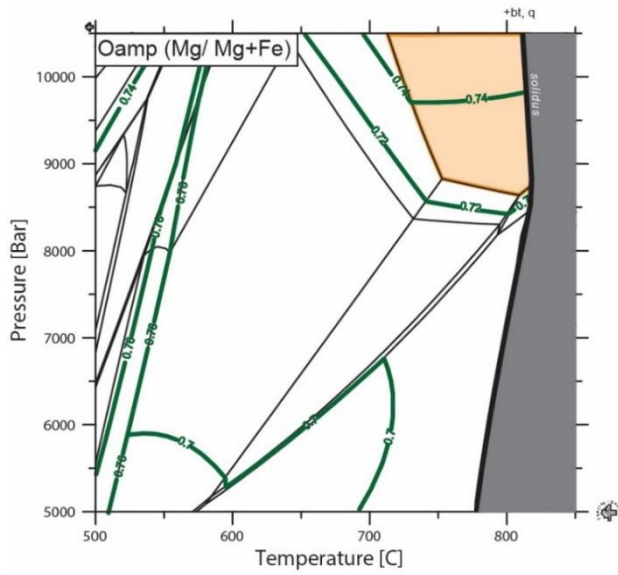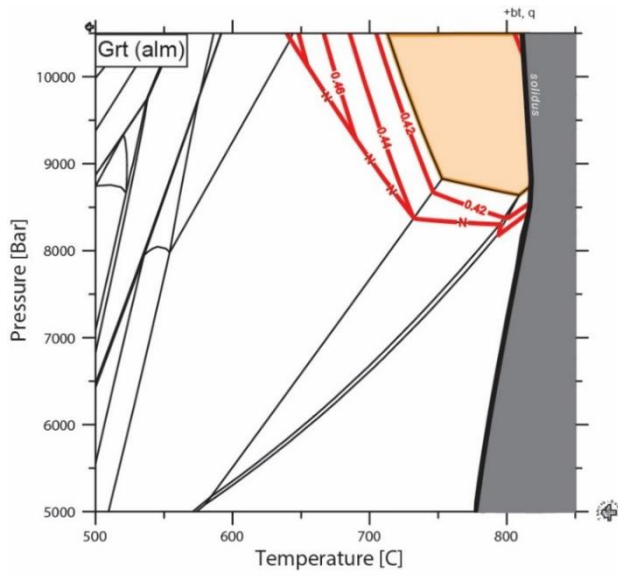Figure 33. Isopleths 18-TR-06 based on SEM-EDS sourced mineral chemistry.

74

Figure 34. Pseudosection for HM-BC-01a, showing the max P-T field corresponding to the samples assemblage highlighted in orange.

Figure 35. Isopleths HM-BC-01a based on SEM-EDS sourced mineral chemistry.
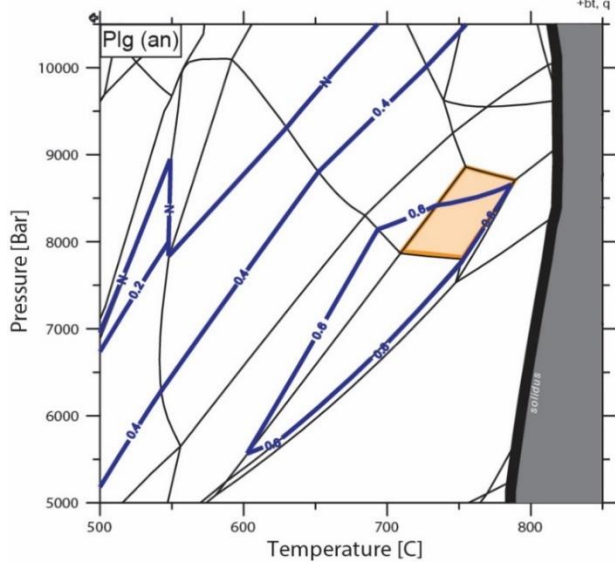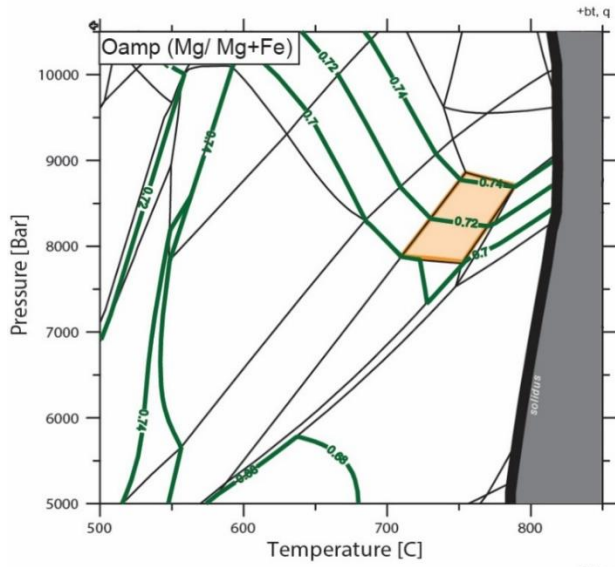
MR-BC-03a

The peak assemblage for this sample is anth + grt + bt + opx + plg + ru + qtz and occurs from 6.6-8.6 kbar and 625-760 °C (Figure 36). The percent almandine mineral chemistry is very close to the modeled isopleth range. It ranges from 0.56-0.60 whereas the isopleth compositions range from 0.51-0.54 (Figure 37). There is no clear zoning in the garnet that can be used to further constrain the P-T range. The orthoamphibole mineral chemistry yields a composition of $X_{Mg} = 0.40$-0.60 which is slightly less than the modeled isopleth range of $X_{Mg} = 0.63$-0.66. The plagioclase mineral chemistry for this section also closely resembles the isopleths, with the mineral chemistry composition being $X_{An} = 0.16$-0.17 and the isopleths being $X_{An} = 0.14$-0.16. These results propose peak P-T conditions of 6.6-8.6 kbar and 625-760 °C for the northern Madison Range.
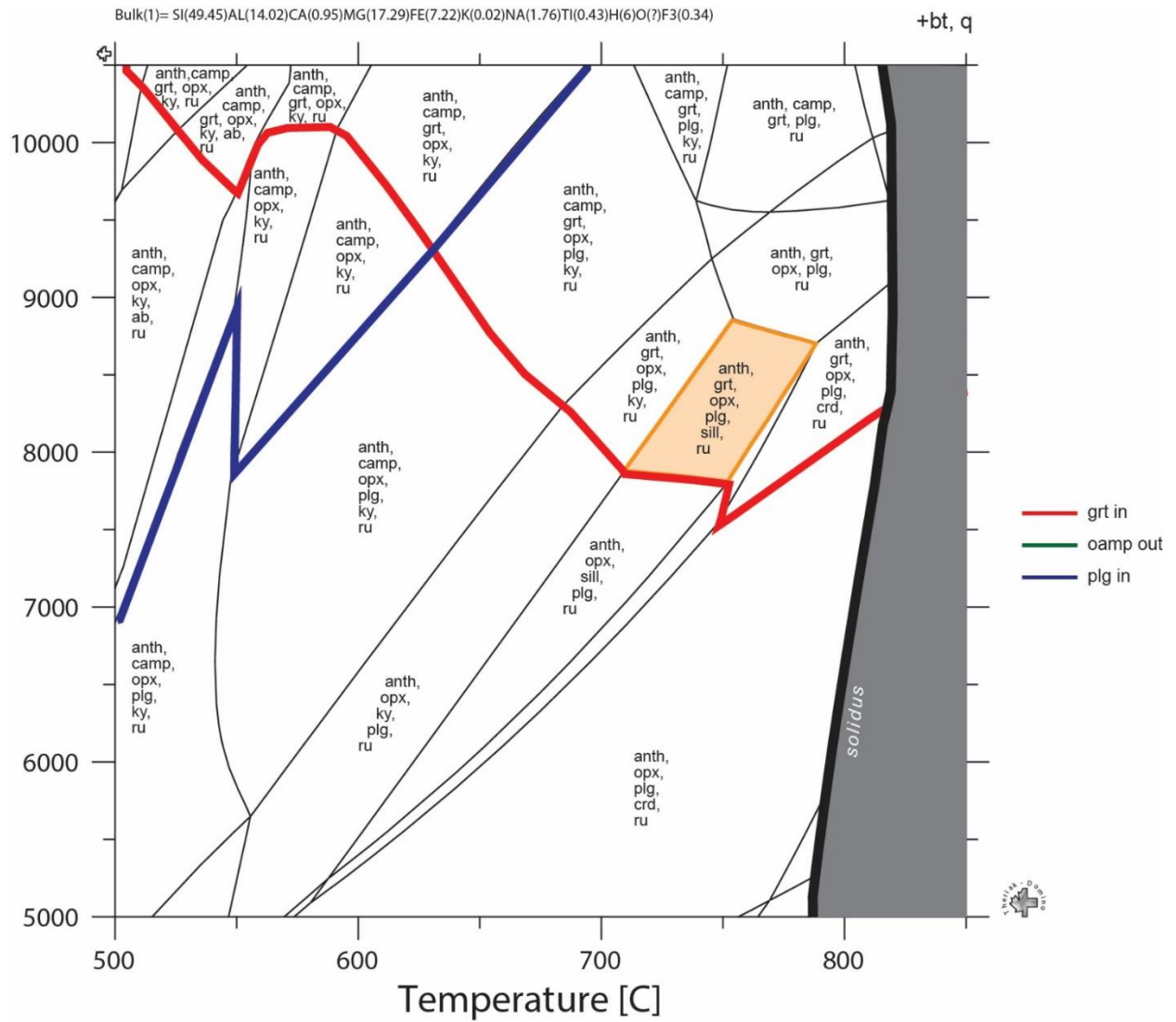
Figure 36. Pseudosection for MR-BC-03a, showing the max P-T field corresponding to the samples assemblage highlighted in orange.

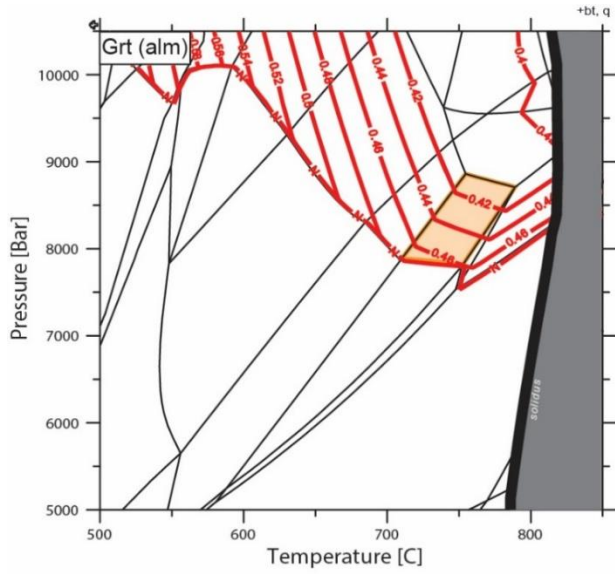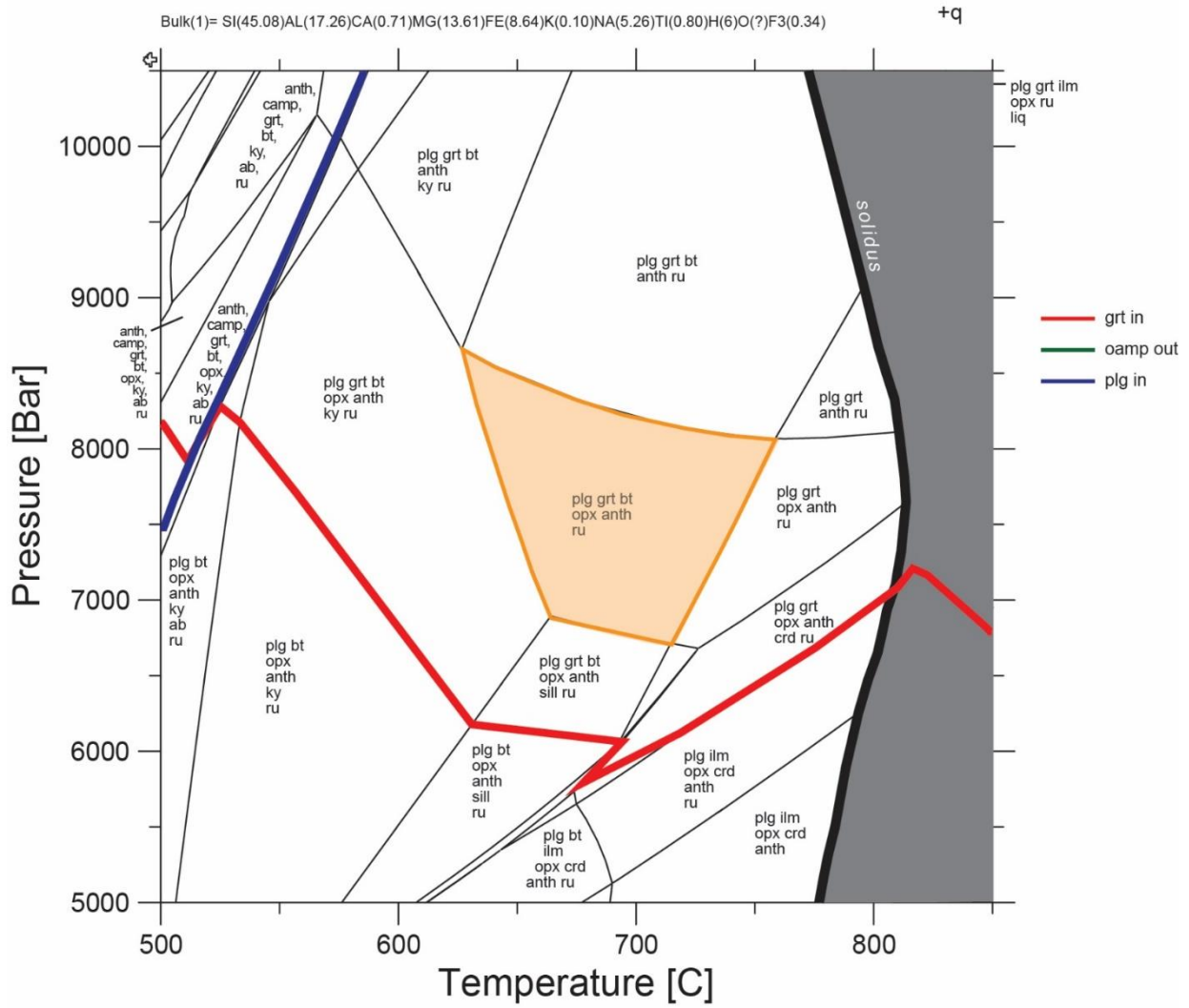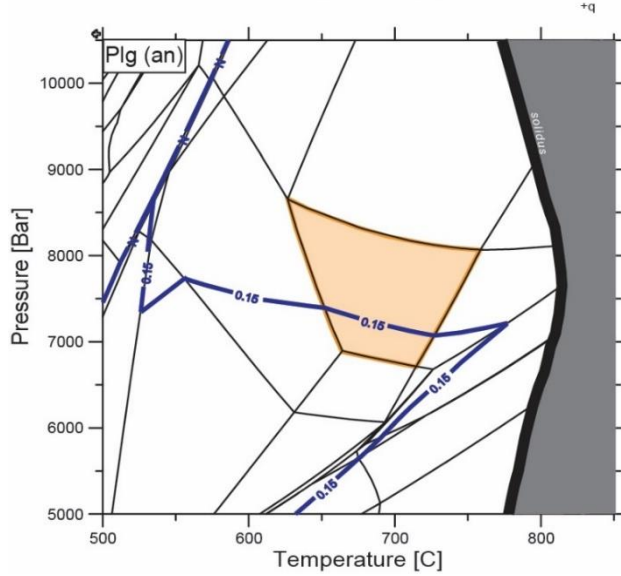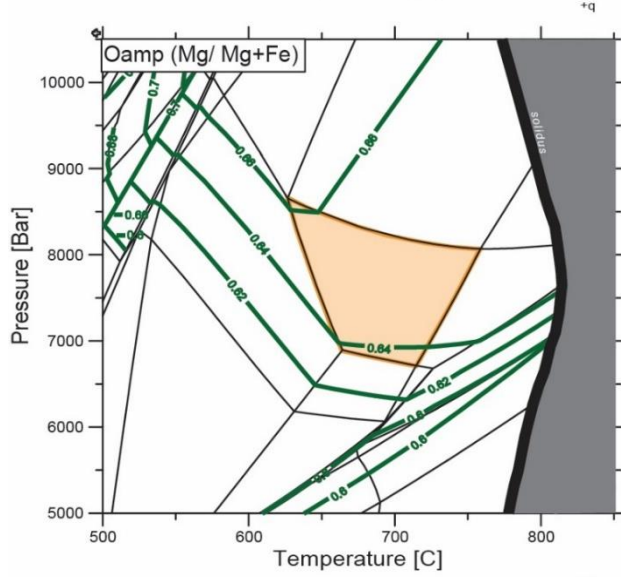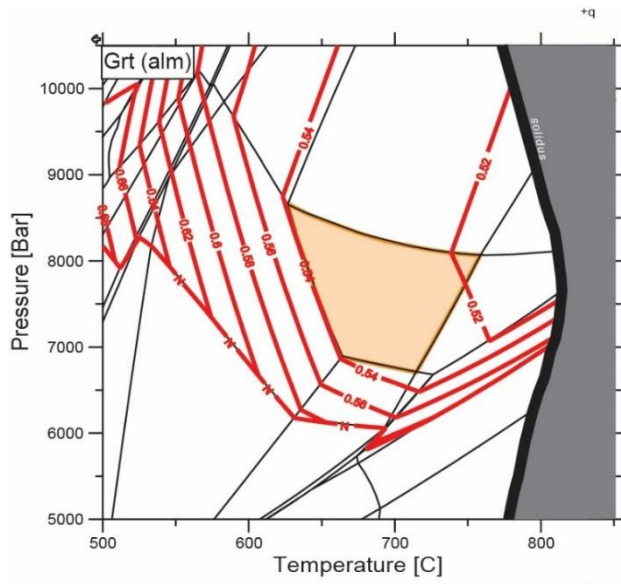Figure 37. Isopleths MR-BC-03a based on SEM-EDS sourced mineral chemistry.

Cumulatively, the various phase equilibria models show that the Ruby Range, Highland Mountains, and northern Madison Range were metamorphosed to upper amphibolite facies conditions. The lowest P-T conditions were recorded in the Ruby Range, while the Highland Mountains and northern Madison Range have slightly higher metamorphic conditions that could, respectively, be considered about the same. The highest P-T conditions were recorded in the Tobacco Roots, which the phase equilibria models suggest experienced granulite facies conditions. All the samples remained under subsolidus conditions during maximum pressures and temperatures.

5. Discussion

COG has served as a keystone for understanding the geologic environment and conditions of Proterozoic metamorphism within the MMT. It is unique due to the multi-faceted and intricate reaction textures that it preserves which involve a wide-variety of diagnostic minerals. The complexity of these features promote the lithology as a valuable tool for placing constraints on *P-T* conditions and paths regionally; such as COG in the Tobacco Root Mountains that contain coarse grained kyanite and orthopyroxene, which has specifically defined the upper limits of metamorphism for the Big Sky Orogeny. In addition to this, COG has attracted the attention of metamorphic petrologists and economic geologists for decades due to its unusual composition, implications for its origin, and for its common association with economic sulphide deposits.

COG is characteristically depleted in Ca and alkali elements, while enriched in Mg, Fe, and Al. The unusual bulk chemistry of rocks like COG have caused the nature of the protolith to be a historically debated topic across the world. The four petrogenetic models that have been proposed from previous studies include partial melting of a metavolcanic in which COG represents the residuum after extraction of granitic melt (Grant, 1968; Hoffer and Grant, 1980),

syn-metamorphic metasomatism brought on by introducing Fe and Mg via diffusion or through infiltration of a hydrothermal fluid into a range of rock types (Eskola, 1914; Irving and Ashley, 1976), metamorphism of a particular sedimentary facies, such as a pelitic evaporite or paleosol horizon (Gable et al., 1970; Young, 1973; Reinhardt and Cook, 1987), and that COG represents a volcanic rock that was hydrothermally altered prior to metamorphism (Vallance, 1967; Schumacher, 1988; Smith et al., 1992; Peck and Smith, 2005).

Studies that have conducted research on COG in the northern Rocky Mountains reflect this lack of consensus as well. The Thor-Odin dome, in the regionally proximal Shuswap metamorphic core complex of British Columbia, contains COG that are arguably identical to the COG rocks in the MMT. They occur as mafic boudins interlayered with metapelitic gneisses and orthogneiss, and they contain high temperature assemblages such as gedrite + garnet + cordierite + spinel + corundum + kyanite/sillimanite + sapphirine + staurolite. They also retain similar reaction textures, including cordierite coronas around garnet, replacement of kyanite with sillimanite, and partial to complete replacement of kyanite with corundum, spinel, and sapphirine symplectites. However, one difference that should be taken into account between COG of the Thor-Odin dome and the MMT is the contrasting age. The overall geology of the Thor-Odin region is a product of terrane accretion onto western North America that occurred during the Cordilleran Orogeny, which is Mesozoic to early Cenozoic in age. Despite the regional geology being well understood though, and the thorough documentation that has been gathered on COG, there are still vastly opposing arguments made pertaining to the protolith material. COG of the Thor-Odin dome have been postulated on one hand to be a result of partial melting that occurred via decompression in the Cordilleran orogeny (Norlander et al., 2002). This line of thinking is supported by the frequent occurrence of COG in highly migmatitic terranes that have abundant

markers for a high percentage of melt being present. Additionally, the complex reaction textures (i.e. symplectites) and *P-T* models of the samples all indicate a period of decompression that is potentially related to tectonic unroofing. Dehydration-melting reactions have a positive slope in *P-T* space, thus they can occur either from an increase in temperature (e.g. heating due to burial) or a decrease in pressure (e.g. from tectonic unroofing). However, H_2O saturated melting can occur during heating due to burial as well.

The other hypothesis concerning COG of the Thor-Odin dome is that they reflect a basaltic protolith that likely underwent hydrothermal alteration prior to metamorphism (Hinchey and Carr, 2007). This conclusion is largely supported by looking at the geochemical data. Firstly, it is known that metasomatism via sea water on basaltic rocks generally results in the loss of Ca and gain of Mg, which COG are consistent with (Smith et al., 1992; Peck and Smith, 2005). However, the bulk composition alone could be a reflection of the hydrothermally altered protolith material, or the original protolith material. Looking at HFSE, transitional element, REE, and trace element data sets are critical for gaining an accurate depiction of the original protolith composition because they are considered relatively immobile during most secondary processes, and as such would not be as altered by metasomatic processes. Using discriminatory diagrams with this data, COG of the Thor-Odin dome have been shown to consistently plot as basaltic to andesitic in composition (Hinchey and Carr, 2007). Their REE element profiles also show slightly negative Eu anomalies, which is a signature characteristic of basalts or andesites. Additionally, the geochemical data of the amphibolites that COG is interbedded with indicates they are basaltic in origin. These interpretations, however, should be considered in light of the factors that could potentially influence the observed effects of hydrothermal alteration. These

factors include, but are not limited to, fluid temperature, initial composition of the protolith, and water content.

The COG rocks of the MMT are also interpreted to be hydrothermally altered mafic volcanic rocks; moreover, they are believed to represent Proterozoic oceanic crust that underwent metasomatic chemical changes prior to, or during, metamorphism. Similar to the Thor-Odin dome, COG in the MMT are found as discontinuous, boudinaged lenses intercalated within amphibolite that has been notably unaffected by the metasomatic processes observed in COG. There are two mechanisms to explain this disparity, which depend on whether the amphibolites are interpreted to have been part of the original package alongside COG or if they represent a younger suite of rocks. Hydrothermal fluids, likely seawater, would have select entry points to penetrate the rock along faults which would justify the localized alteration of specifically COG. However, the discontinuous and boudinaged nature of COG could also be explained if the amphibolites represent a younger series of mafic dikes that juxtapose COG after it was already altered. There were also markers at each site that indicated a moderate to high amount of melt involved, such as hydrothermal veins or migmatitic structures.

The association of COG with amphibolites, quartzofeldspathic gneiss, and marble was observed at all the field sites, which is consistent with the interpretation of an ocean basin setting. Large ultramafic bodies were found in close proximity to all of the field sites and these rocks occur in a considerably analogous manner to COG, as dismembered, tectonically-emplaced lenses. The ultramafic bodies are distributed throughout the MMT as distinct, elongate pods parallel to the regional foliation. In addition to the discontinuous way in which both of these lithologies occur, they are commonly found within, or near, the crest of isoclinal folds. The exact petrogenetic origins for the ultramafic bodies has also been highly subject to debate (Reinhardt

and Cook, 1987). The range of ideas concerning the petrogenetic origins of the ultramafics include: 1) it was a cumulate of a differentiating basaltic magma that was emplaced in a solid state (Tendall, 1978; Johnson et al., 2004), 2) it was a forcibly emplaced body of hydrous peridotitic magma (Heinrich, 1963), 3) it was a tectonically emplaced ultramafic body that was serpentinized prior to metamorphism (Desmarais, 1981), 4) it was a sliver of oceanic crust generated during ensialic basin development (Cummings and McCulloch, 1993), or 5) it represents metamorphosed komatiite lavas (Johnson et al., 1996; MacFarlane, 1996). Generally though, all of the theories agree that the protolith is a mafic igneous rock that may or may not have been subjected to specific metasomatic processes. Furthermore, this consensus supports the interpretation of the GFTZ as a suture zone which potentially records ocean basin closure and allows COG to be emplaced in that setting as well.

The different expressions of COG found across the mountain ranges of the MMT show significant variations in physical attributes. Since it is believed that all the varieties of COG in this study came from the same protolith material, the differing physical attributes are then considered to be a result of the local *P-T* histories. In the Gravelly Range, COG is much finer-grained and does not display any reaction textures such as coronas or symplectites. It also does not preserve as high grade an assemblage as the other ranges. In the Highland Mountains, COG is dominated by tabular megacrysts of gedrite and typically has large garnets and blades of sillimanite that have reaction rims of cordierite or plagioclase. COG in the Ruby Range have notably more prismatic, dark colored, and elongate blades of anthophyllite alongside smaller sized garnets. COG of the Ruby Range also have a more encompassing assemblage (kyanite, staurolite, sapphirine, spinel, and corundum, etc.) that often exhibits symplectites. In the Tobacco Roots, the physical attributes of COG at the Thompson Peak exposure are considerably different

than at the Granite Creek location. The Thompson Peak variety has more tabular blades of gedrite, the highest grade assemblage, and displays more complex reaction textures than any other site. This includes the samples from the Granite Creek locality, which contain more prismatic, dark colored orthoamphibole blades that are segregated from "melty" leucosomes that incorporate garnet and kyanite. Lastly, COG in the northern Madison Range are essentially identical to the samples at Granite Creek. However, despite these varying attributes, the major components of the mineral assemblage at each site remained consistent and COG was also associated with, or interbedded within, the same lithologies at each site. Therefore it is still believed that all the variants of COG found across the MMT originated from the same hydrothermally altered basaltic protolith material.

The tectonic discriminatory diagrams further substantiate this interpretation. For example, Figure 26 (Basaltic protolith classification scheme by Pearce (1983)) and Figure 23 (Cation plot for classifying subalkalic volcanic rocks by Jensen (1976)) both show that COG samples from all of the various mountain ranges plot as subalkalic basalts which are likely from a continental margin arc setting. Overall, the tectonic discriminatory diagrams and classification plots based on the bulk and trace element geochemistry of COG confirm that it is most likely from a basaltic protolith. Additionally, there is strong evidence for the protolith having undergone metasomatic alteration prior to metamorphism. The identification of COG's protolith material and likely depositional setting provides invaluable context to the *P-T* conditions and metamorphic history it records.

Prior to the terminal collision that resulted in the Big Sky Orogeny, sediments were being shed off the Wyoming Province into the surrounding epicontinental sea. Subsequently, as the collision occurred, these sediments and associated basement rocks were buried to varying depths.

After this depositional sequence was metamorphosed, it would have comprised what is now

postulated as the high grade metamorphic core of the Big Sky Orogeny (Harms et al., 2004).

Based on the pseudosections and petrographic textures found in each mountain range, a general

trend emerges that has implications for the architecture of the core of the orogeny.

The phase equilibria modeling of COG suggests that the highest peak metamorphic

conditions occurred in the Tobacco Roots, which suggests the Tobacco Roots were the

structurally deepest mountain range. The northern Madison Range shows conditions that are

marginally decreased from those of the Tobacco Roots, making it the second structurally

deepest. Slightly to the west of the Tobacco Roots, the *P-T* conditions in the Highland Mountains

are roughly approximate to those found in the northern Madison Range, yet petrographic textures

suggest that despite the high temperatures, the Highland Mountains experienced a much different

pressure regime. The reaction textures observed in COG, such as the coronas and symplectites,

have been interpreted across the Rocky Mountains as products of nearly isothermal

decompression (Heimann et al., 2006; Hinchey and Carr, 2007). Within the MMT specifically,

reaction textures such as the replacement of sillimanite and garnet by cordierite are believed to

have been generated via orogenic collapse from regional tectonic unroofing following peak

metamorphism (Cramer, 2015; Stotter, 2019). Rocks types associated with COG, such as certain

pelitic lithologies found in the Ruby Range and Tobacco Roots, have been found to record these

textures as well (Cramer, 2015; Stotter, 2019). However, symplectites are notably less abundant,

if present at all, in the Highland Mountains. This implies that the presence of Highland

Mountains within the system of the Big Sky Orogeny was such that it was excluded from

experiencing the same decompressional unroofing phase as the Tobacco Roots and Ruby Range.

This notion has been proposed in a previous study done in the Highland Mountains and was

founded on the basis of the lack of cordierite coronas observed around garnets (Reioux, 2014). This reasoning is found to be extremely problematic though, since amphibolite associated with COG in O'Neill's gulch was found to have an abundance of cordierite coronas around garnet (Figure 7d). Despite this fallible evidence, it is still believed that the Highlands did not experience the drastic pressure reduction brought on via orogenic collapse that the other localities were exposed to. To explain this, the Highland Mountains are proposed to represent island-arc terrain that was accreted onto the margin of the Wyoming Province during subduction, instead of being part of the orogenic core. The proximal location to the GTFZ and the lithologic suite of rocks which have both sedimentary and igneous protoliths, support this theory as they suggest it is an amalgamation of ocean basin sediments and basaltic crust.

The lowest *P-T* conditions preserved in this study were from the Ruby Range, however, previous *P-T* work in the Ruby Range has shown that some localities record much lower metamorphic conditions than others due a thermal gradient that is increasingly sensitive to structural depth. For example, at the Stone Creek location, peak conditions of the Big Sky Orogeny were estimated to be ~6.5 kbar and 760 °C while conditions at the Elk Gulch locality were estimated to have reached ~9 kbar and 780 °C (Cramer, 2015). This is due to the fact that the Elk Gulch rocks belong to a suite which is interpreted to be structurally deeper than the rocks of the Christiansen Ranch Metasedimentary Suite, in which the Stone Creek locality belongs to (Stotter, 2019). The higher *P-T* conditions reported from Elk Gulch combined with the abundant symplectites found in the rocks at Stone Creek, the Ruby Range is considered to have undergone similar uplift rates as the Tobacco Roots, which are interpreted to be caused by orogenic collapse. Therefore, the Ruby Range is considered to represent a deeper structural level than the Highlands, but not as deep as the Tobacco Roots.

Lastly, *P-T* studies conducted in the northern Gravelly Range have described the peak

metamorphic conditions there for the Big Sky Orogeny to be around the andalusite-kyanite-

sillimanite triple point, which is of significantly lower metamorphic grade than all the other

localities (Green et al., 2007). This is supported by the petrographic observations which do not

document any high grade minerals present (kyanite, corundum, etc.) and implies that the

Gravelly Range either resided on the flanks of the orogenic core or was located closer to the

center of the Wyoming Province during collision and was thus not as affected. However, it

should also be taken into consideration that this locality is very close to a zone of thermal

resetting collectively referred to as Giletti's line (Giletti, 1966). K-Ar and Rb-Sr ages are what

initially indicated the presence of Giletti's line, which demarcates where the basement rocks

have been thermally reset, but more recent studies have expanded upon this and attribute it to a

regional ~1.6 Ga thermal resetting event (Stotter, 2019).

In summary, the tectonic discriminatory diagrams and associated lithologies identify a

basaltic protolith for COG that underwent metasomatic alteration, likely via seawater, prior to

metamorphism. Moreover, COG represents remnant pieces of basaltic crust which originated

from the epicontinental sea adjacent to the Wyoming Province. The petrography and *P-T* history

that this lithology records across multiple mountain ranges, documents the closure of the ocean

basin, the collision between the Wyoming Province and Medicine Hat Block in the Big Sky

Orogeny, and the subsequent orogenic collapse and unroofing that followed. The trend of

metamorphic conditions across the MMT show the highest peak conditions occur at localities

closest to the GFTZ (Figure 38). Although this does not include the Highland Mountains, which

are interpreted to represent island arc terrane that was accreted onto the margin of the Wyoming

Province during the collision. The architecture of the orogenic core that can be interpreted from these results is summarized in Figure 38.

6. Conclusions

Based off the geochemical analyses and subsequent tectonic discriminatory diagrams, the likely protolith of COG in the MMT is a basalt that existed as part of the epicontinental sea and island arc environment adjacent to the Wyoming Province during the Paleoproterozoic. Furthermore, it is believed that COG was hydrothermally altered, likely by sea water, prior to metamorphism. The associated lithologies observed in the field such as marbles, quartzites, and amphibolites, promote an interpretation of the geologic setting that coincides with the proposed petrogenetic model for COG. The metamorphic history recorded by COG documents ocean basin closure and subsequent collision across the MMT that occurred during the Big Sky Orogeny (ca. 1.78-1.72 Ga). The phase equilibria models display an overall trend of metamorphic conditions being the highest in the Tobacco Root Mountains and decreasing in grade with closer proximity to the zone of thermal resetting that is known as Giletti's line (Figure 38). The Highland Mountains are excluded from this trend however, as the range is interpreted to be resultant of island arc terrane that was accreted onto the margin of the province during ocean basin closure.
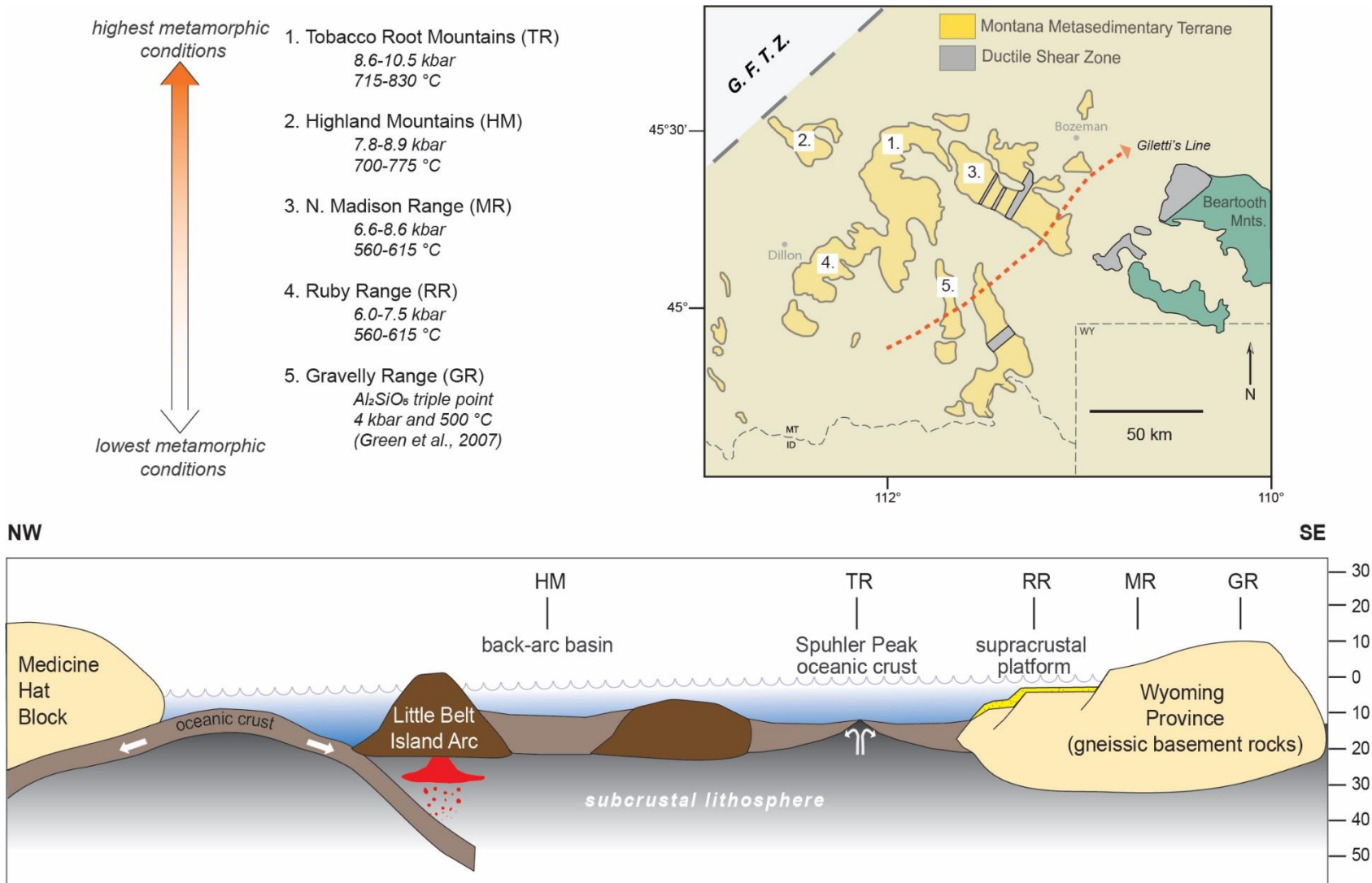
Figure 38. Summary diagram showing the interpreted architecture of the orogenic core based off the P-T and petrography results of this study.

7. References

Beeson, R., 1978, The geochemistry of orthoamphiboles and coexisting cordierites and phlogopites from South Norway: Contributions to Mineralogy and Petrology, v. 66, p. 5–14, doi:10.1007/BF00376080.

Burger, H.R. et al., 2004, Geology and geochemistry of the Spuhler peak metamorphic suite: Special Paper of the Geological Society of America, v. 377, p. 47–70, doi:10.1130/0-8137-2377-9.47.

De Capitani, C., and Petrakakis, K., 2010, The computation of equilibrium assemblage diagrams with Theriak/Domino software: American Mineralogist, v. 95, p. 1006–1016, doi:10.2138/am.2010.3354.

Chamberlain, K.R., 1998, Medicine Bow orogeny: Timing of deformation and model of crustal structure produced during continent-arc collision, ca. 1.78 Ga, southeastern Wyoming: Rocky Mountain Geology, v. 33, p. 259–277, doi:10.2113/33.2.259.

Chamberlain, K.R., Frost, C.D., and Frost, B.R., 2003, Early Archean to Mesoproterozoic evolution of the Wyoming Province: Archean origins to modern lithospheric architecture: Canadian Journal of Earth Sciences, v. 40, p. 1357–1374, doi:10.1139/e03-054.

Cheney, J.T. et al., 2004, Proterozoic metamorphism of the Tobacco Root Mountains, Montana: Special Paper of the Geological Society of America, v. 377, p. 105–129, doi:10.1130/0-8137-2377-9.105.

Condie, K.C., 1990, Geochemical characteristics of Precambrian basaltic greenstones: Early Precambrian basic magmatism, doi:10.1007/978-94-009-0399-9_3.

Condit, C.B., Mahan, K.H., Curtis, K.C., and Möller, A., 2018, Dating metasomatism: Monazite and zircon growth during amphibolite facies albitization: Minerals, v. 8, p. 1–30, doi:10.3390/min8050187.

Cramer, M., 2015, Proterozoic tectonometamorphic evolution of the Ruby Range, SW Montana, USA: Insights from phase equilibria modeling and in situ monazite petrochronology: , p. 120.

Cummings, M.L., and McCulloch, W.R., 1993, Geochemistry and origin of amphibolite and ultramafic rocks, Branham Lakes area, Tobacco Root Mountains, southwestern Montana: Basement tectonics 8, p. 323–340, doi:10.1007/978-94-011-1614-5_22.

Dahl, P.S., Hamilton, M.A., Wooden, J.L., Tracy, R.J., Loehn, C.W., Jones, C.L., and Foland, K.A., 2004, Do 2450-2480 mineral ages from Wyoming cratonic margins (USA) indicate incipient breakup of supercontinet Kenorland? Geological Society of America Annual Meeting, v. 36, p. 340.

Dahl, P.S., Holm, D.K., Gardner, E.T., Hubacher, F.A., and Foland, K.A., 1999, New constraints on the timing of Early Proterozoic tectonism in the Black Hills (South Dakota), with

implications for docking of the Wyoming province with Laurentia: Bulletin of the Geological Society of America, v. 111, p. 1335–1349, doi:10.1130/0016-7606(1999)111<1335:NCOTTO>2.3.CO;2.

Desmarais, N.R.., 1981, Metamorphosed Precambrian ultramafic rocks in the Ruby Range, Montana: Precambrian Research, v. 16, p. 67–101.

Diener, J.F.A., and Powell, R., 2012, Revised activity-composition models for clinopyroxene and amphibole: Journal of Metamorphic Geology, v. 30, p. 131–142, doi:10.1111/j.1525-1314.2011.00959.x.

Diener, J.F.A., Powell, R., and White, R.W., 2008, Quantitative phase petrology of cordierite-orthoamphibole gneisses and related rocks: Journal of Metamorphic Geology, v. 26, p. 795–814, doi:10.1111/j.1525-1314.2008.00791.x.

Eskola, P., 1914, On the Petrology of the Orijarvi Region in Southwestern Finland, *in* Printing office of the imperial Senate, p. 277.

Foster, D.A., Mueller, P.A., Mogk, D.W., Wooden, J.L., and Vogl, J.J., 2006, Proterozoic evolution of the western margin of the Wyoming craton: Implications for the tectonic and magmatic evolution of the northern Rocky Mountains: Canadian Journal of Earth Sciences, v. 43, p. 1601–1619, doi:10.1139/E06-052.

Gable, D.J., Sims, P.K., and Weiblen, P.W., 1970, Thermal Metamorphism of Cordierite-Garnet-Biotite Gneiss, Front Range, Colorado: The Journal of Geology, v. 78, p. 661–685.

Giletti, B., 1966, Isotopic ages from southwestern Montana: Journal of Geophysical Research, v. 71, p. 4029–4036.

Goodsmith, M.S., 2015, Symplectic Kyanite , Garnet , and Cordierite in Orthoamphibolites from the Ruby Range , Southwestern Montana.

Gorman, A.R. et al., 2002, Deep probe: Imaging the roots of western North America: Canadian Journal of Earth Sciences, v. 39, p. 375–398, doi:10.1139/e01-064.

Grant, J.A., 1968, Partial melting of common rocks as a possible source of cordierite-anthophyllite bearing assemblages: American Journal of Science, v. 266, p. 908–931, doi:10.2475/ajs.266.10.908.

Green, E., Holland, T., and Powell, R., 2007, An order-disorder model for omphacitic pyroxenes in the system jadeite-diopside-hedenbergite-acmite, with applications to eclogitic rocks: American Mineralogist, v. 92, p. 1181–1189, doi:10.2138/am.2007.2401.

Hamelin, C., 2015, Petrology, geothermobarometry & metamorphic history of metapelites from the central Ruby Range, southwest Montana: Smith College, 196 p.

Harms, T.A., Brady, J.B., Burger, H.R., and Cheney, J.T., 2004, Advances in the geology of the Tobacco Root Mountains, Montana, and their implications for the history of the northern Wyoming province: Special Paper of the Geological Society of America, v. 377, p. 227–243, doi:10.1130/0-8137-2377-9.227.

Heimann, A., Spry, P.G., Teale, G.S., and Jacobson, C.E., 2006, Coronas, symplectitic textures,

and reactions involving aluminous minerals in gedrite - Cordierite - Garnet gneiss from Evergreen, Front Range, Colorado: Canadian Mineralogist, v. 44, p. 1025–1044, doi:10.2113/gscanmin.44.5.1025.

Heinrich, E.W., 1963, Paragenesis of clinohumite and associated minerals from Wolf Creek, Montana: The American Mineralogist, v. 48, p. 597–613.

Hinchey, A.M., and Carr, S.D., 2007, Protolith composition of cordierite-gedrite basement rocks and garnet amphibolite of the bearpaw lake area of the Thor-Odin dome, Monashee complex, British Columbia, Canada: Canadian Mineralogist, v. 45, p. 607–629, doi:10.2113/gscanmin.45.3.607.

Hoffer, E., and Grant, J.A., 1980, Experimental investigation of the formation of cordierite-orthopyroxene parageneses in pelitic rocks: Contributions to Mineralogy and Petrology, v. 73, p. 15–22, doi:10.1007/BF00376257.

Hoffman, P.F., 1988, United plates of America, the birth of a craton: Early Proterozoic assembly and growth of Laurentia: Annual review of earth and planetary sciences. Vol. 16, p. 543–603, doi:10.1146/annurev.earth.16.1.543.

Irving, A.J., and Ashley, P.M., 1976, Amphibole-olivine-spinel, cordierite-anthophyllite and related hornfelses associated with metamorphosed serpentinites in the goobarragandra district, near tumut, New South Wales: Journal of the Geological Society of Australia, v. 23, p. 19–43, doi:10.1080/00167617608728919.

Janoušek, V., Farrow, C.M., and Erban, V., 2006, Interpretation of whole-rock geochemical data in igneous geochemistry: Introducing Geochemical Data Toolkit (GCDkit): Journal of Petrology, v. 47, p. 1255–1259, doi:10.1093/petrology/egl013.

Jensen, L.S., 1976, NEW CATION PLOT FOR CLASSIFYING SUBALKALIC VOLCANIC ROCKS.: Ont Div Mines Misc Pap,.

Johnson, K.E., Brady, J.B., MacFarlane, W.A., Thomas, R.B., Poulsen, C.J., and Sincock, M.J., 2004, Precambrian meta-ultramafic rocks from the Tobacco Root Mountains, Montana: Special Paper of the Geological Society of America, v. 377, p. 71–87, doi:10.1130/0-8137-2377-9.71.

Johnson, K.E., Burger, H.R., Brady, J.B., Cheney, J.T., and Harms, T.A., 1996, Archean meta-ultramafics in the Tobacco Root Mountains, S.W. Montana; an evaluation of the metamorphic history and protolith, *in* Geological Society of America, p. 493.

Jones, C.L., 2008, U-Pb geochronology of monazite and zircon in Precambrian metamorphic rocks from the Ruby Range, SW Montana: Deciphering geological events that shaped the NW Wyoming province: Master's Thesis, p. 131.

Kellogg, K.S., Snee, L.W., and Unruh, D.M., 2003, The mesoproterozoic Beaverhead impact structure and its tectonic setting, Montana-Idaho: 40Ar/39 and U-Pb isotopic constraints: Journal of Geology, v. 111, p. 639–652, doi:10.1086/378339.

MacFarlane, W.A., 1996, A geochemical and petrographic analysis of the meta-ultramafic rocks in the Tobacco Root Mountains, southwest Montana: Colorado College, 132 p.

Mogk, D.W., Mueller, P.A., and Wooden, J.L., 1992, The nature of Archean terrane boundaries: an example from the northern Wyoming Province:, doi:10.1016/0301-9268(92)90020-O.

Mueller, P.A., Burger, H.R., Wooden, J.L., Brady, J.B., Cheney, J.T., Hamrs, T.A., Heatherington, A.L., and Mogk, D.W., 2005, Paleoproterozoic metamorphism in the northern Wyoming province: Implications for the assembly of Laurentia: Journal of Geology, v. 113, p. 169–179, doi:10.1086/427667.

Mueller, P.A., and Frost, C.D., 2006, The Wyoming Province: A distinctive Archean craton in Laurentian North America: Canadian Journal of Earth Sciences, v. 43, p. 1391–1397, doi:10.1139/E06-075.

Mueller, P.A., Shuster, R.D., Wooden, J.L., Erslev, E.A., and Bowes, D.R., 1993, Age and composition of Archean crystalline rocks from the southern Madison Range, Montana: implications for crustal evolution in the Wyoming craton: Geological Society of America Bulletin, v. 105, p. 437–446, doi:10.1130/0016-7606(1993)105<0437:AACOAC>2.3.CO;2.

Mueller, P.A., Wooden, J.L., Nutman, A.P., and Mogk, D.W., 1998, Early Archean crust in the northern Wyoming province Evidence from U-Pb ages of detrital zircons: Precambrian Research, v. 91, p. 295–307, doi:10.1016/S0301-9268(98)00055-2.

Mullen, E.D., 1983, MnO/TiO2/P2O5: a minor element discriminant for basaltic rocks of oceanic environments and its implications for petrogenesis: Earth and Planetary Science Letters, doi:10.1016/0012-821X(83)90070-5.

Norlander, B.H., Whitney, D.L., Teyssier, C., and Vanderhaeghe, O., 2002, Partial melting and decompression of the Thor-Odin dome, Shuswap metamorphic core complex, Canadian Cordillera: Lithos, v. 61, p. 103–125, doi:10.1016/S0024-4937(02)00075-0.

Pamić, J., Balen, D., and Tibljaš, D., 2002, Petrology and geochemistry of orthoamphibolites from the Variscan metamorphic sequences of the South Tisia in Croatia - an overview with geodynamic implications: International Journal of Earth Sciences, v. 91, p. 787–798, doi:10.1007/s00531-002-0258-y.

Pearce, J.A., 1983, Role of the sub-continental lithosphere in magma genesis at active continental margins.: Continental Basalts and Mantle Xenoliths,.

Pearce, J.A., 1982, Trace element characteristics of lavas from destructive plate boundaries.: Andesites: Orogenic Andesites and Related Rocks,.

Peck, W.H., and Smith, M.S., 2005, Cordierite-gedrite rocks from the Central Metasedimentary Belt boundary thrust zone (Grenville Province, Ontario): Mesoproterozoic metavolcanic rocks with affinities to the Composite Arc Belt: Canadian Journal of Earth Sciences, v. 42, p. 1815–1828, doi:10.1139/e05-071.

Qian, J., Wei, C., Clarke, G.L., and Zhou, X., 2015, Metamorphic evolution and Zircon ages of Garnet-orthoamphibole rocks in southern Hengshan, North China craton: INSIGHTS into the regional Paleoproterozoic P-T-t history: Precambrian Research, v. 256, p. 223–240, doi:10.1016/j.precamres.2014.11.013.

Reinhardt, J., and Cook, J., 1987, <Reinhard_COR_sedimentary_origin.pdf>: , p. 451–472.

Reioux, D.A., 2014, Metamorphic Evolution of Precambrian Rocks in the Southern Highland Mountains: , p. 82.

Schumacher, J.C., 1988, Stratigraphy and geochemistry of the Ammonoosuc Volcanics, central Massachusetts and southwestern New Hampshire: American Journal of Science, doi:10.2475/ajs.288.6.619.

Smith, J. V., 1974, Feldspar Minerals:, doi:10.1007/978-3-642-96173-1.

Smith, M.S., Dymek, R.F., and Schneiderman, J.S., 1992, Implications of trace element geochemistry for the origin of cordierite-orthoamphibole rocks from Orijarvi, SW Finland: Journal of Geology, v. 100, p. 545–559, doi:10.1086/629607.

Stotter, S.V., 2019, Determining the Precambrian Structure and ermotectonic Evolution of the Central Ruby Range , southwest Montana:

Tendall, B.A., 1978, Mineralogy and petrology of Precambrian ultrmafic bodies from the Tobacco Root Mountains, Madison County, Montana: Indiana University, 127 p.

Vallance, T.G., 1967, Mafic rock alteration and isochemical development of some cordierite-anthophyllite rocks: Journal of Petrology, v. 8, p. 84–96, doi:10.1093/petrology/8.1.84.

White, R.W., Powell, R., and Clarke, G.L., 2002, The interpretation of reaction textures in Fe-rich metapelitic granulites of the Musgrave Block, Central Australia: Constraints from mineral equilibria calculations in the system: Journal of Metamorphic Geology, v. 20, p. 41–55, doi:10.1046/j.0263-4929.2001.00349.x.

White, R.W., Powell, R., and Holland, T.J.B., 2007, Progress relating to calculation of partial melting equilibria for metapelites: Journal of Metamorphic Geology, v. 25, p. 511–527, doi:10.1111/j.1525-1314.2007.00711.x.

Whitmeyer, S.J., and Karlstrom, K.E., 2007, Tectonic model for the Proterozoic growth of North America: Geosphere, v. 3, p. 220–259, doi:10.1130/GES00055.1.

Young, G.M., 1973, Tillites and aluminous quartzites as possible time markers for middle Precambrian (Aphebian) rocks of North America, *in* Huronian Stratigraphy and Sedimentation, Geological Association of Canada, p. 97–127.